



FP7-ICT Future Networks
SPECIFIC TARGETTED RESEARCH PROJECT
Project Deliverable

PHYDYAS Doc. Number	PHYDYAS_019
Project Number	ICT - 211887
Project Acronym+Title	PHYDYAS - PHYsical layer for DYnamic AccesS and cognitive radio
Deliverable Nature	Report
Deliverable Number	D6.2
Contractual Delivery Date	January 1st, 2010
Actual Delivery Date	February 5th, 2010
Title of Deliverable	Multiple access and cross-layer aspects
Contributing Work Package	WP6
Project starting date; Duration	01/01/2008; 30 months
Dissemination Level	PU
Author(s)	Leonardo Baltar, Qing Bai, Josef Nassek (TUM-WP6 leader); Nikos Passas (RA-CTI); Carlos Bader, Ismael Gutiérrez (CTTC); Michel Terré, Yahia Medjahdi (CNAM), Mario Tanda, Davide Mattera (UNINA)

Abstract: The continuation of the work on multiple access is reported with an evaluation of the impact of synchronization issues in the uplink of FBMC systems in the case of high frequency selective channels. We also continue the work on the crosslayer issues of separated optimization of resource allocation and scheduling and joint optimal resource allocation/scheduling.

Contents

1	Introduction	3
1.1	Scope	3
2	Multiple Access	4
2.1	Effects of timing and frequency offset in the up-link	4
2.1.1	Conclusions	17
2.2	Uplink Synchronization for FBMC Systems	17
2.2.1	Introduction	17
2.2.2	The adopted joint estimation algorithm for CP-OFDMA	18
2.2.3	Simulation results	20
2.2.4	Conclusions	34
3	Cross Layer Aspects	38
3.1	Introduction	38
3.2	Separated resource allocation and scheduling approach	38
3.2.1	Basic Procedure and System Structure	39
3.2.2	The Resource Allocator Design	40
3.2.3	Scheduler Design	55
3.3	Joint Resource Allocation and Scheduling	69
3.3.1	Introduction	69
3.3.2	Rectangular shaped bursts allocation	70
3.3.3	System description	71
3.3.4	Simulation Results	75
3.3.5	Conclusions from initial results	77
3.4	Conclusions	78
4	Conclusions	79

Chapter 1

Introduction

1.1 Scope

In this report the ongoing research conducted in work package 6 is described. The different topics in this work package, which are covered here, are:

- investigation of multiple access interference in the uplink: in extension of the results reported in D6.1 the effect of different equalization schemes and the impact on different subcarriers has been evaluated
- cross layer design has been extended to take into account carrier frequency offset (CFO) and show possible transmit power reduction with the FBMC approach.

Results on bandwidth allocation for feeding back channel state information from receiver to the transmitter has been published in [1] and is not repeated here.

Chapter 2

Multiple Access

2.1 Effects of timing and frequency offset in the up-link

We have compared the up-link performance of the FBMC system with that of a CP-OFDM system with the same bandwidth and, moreover, we have analyzed the performance degradation of both systems due to the presence of synchronization errors. We have considered two different allocation schemes: block-wise and interleaved. In particular, as illustrated in Figure 2.1, in the block-wise scheme groups of adjacent subcarriers are allocated to the same user while for the interleaved scheme groups of adjacent subcarriers are allocated to different users.

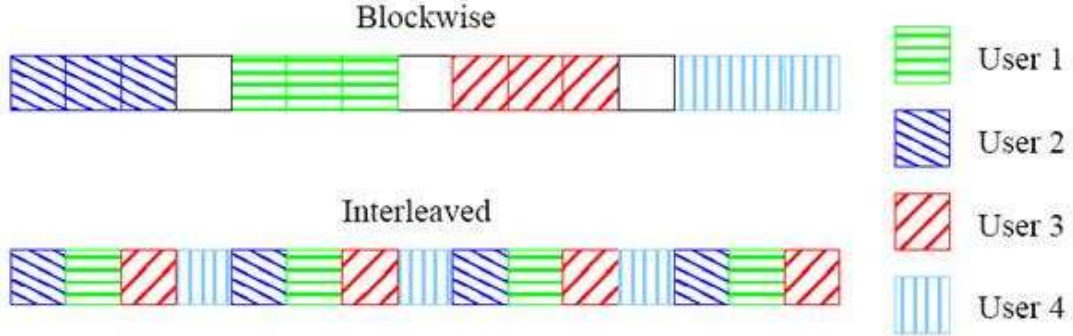


Figure 2.1: Sub-carriers allocation schemes

In our simulation analysis, we have compared the performance of the 1-tap sub-channel equalizer with perfect channel knowledge with that of the multi-tap equalizer based on the MMSE approach proposed by TUM [2] and that of the equalizer based on the frequency sampling (FS) approach proposed by CNAM [3]. Specifically, we have chosen the same equalizer length, 3, for both the MMSE and the FS sub-channel equalizers. The number of subcarriers for both systems is $M = 1024$. However, the number of used subcarriers,

evenly split between the users, is 912 for the FBMC system and 840 for the OFDM system. In the FBMC case the prototype filter of length $L = KM = 4096$ with a roll-off factor of one suggested by CNAM [4] has been used. For the block-wise allocation scheme the subcarriers to be equalized are the central subcarrier or the boundary subcarrier of the group allocated to the user of interest. We have analyzed the performance obtained in multipath fading ITU-Vehicular A and ITU-Vehicular B channels with 4-QAM and 64-QAM constellations taking into account in the OFDM case the energy loss due to the cyclic prefix. The first user has been considered as user of interest and, moreover, the other users have been assumed completely asynchronous with a timing offset uniformly distributed in the range $\{-(M/2)T_s, (M/2 - 1)T_s\}$, a carrier frequency offset normalized to the subcarrier spacing uniformly distributed in the range $[-0.125, 0.125]$, a carrier phase offset uniformly distributed in the range $[-\pi, \pi]$ and with a value of E_b/N_0 fixed at 16 dB. Figure 2.2 presents the BER obtained, in the case of perfect synchronization and block-wise allocation, for a 64-QAM constellation in multipath fading ITU-Vehicular A channel (solid lines) and ITU-Vehicular B channel (dashed lines). Specifically, the channel is fixed in each run but it is independent from one run to another.

Moreover, the subcarrier to be equalized is the last one of the group allocated to the first user. The results show that in Vehicular A channel all the considered sub-channel equalizers for the FBMC system assure nearly the same performance and clearly outperform the 1-tap sub-channel equalizer used for the OFDM system since, in this case, the last subcarrier is more affected by multiple-access interference. In Vehicular B channel both systems present a performance degradation, however, the MMSE and the FS sub-channel equalizers outperform the 1-tap sub-channel equalizer for the OFDM system in the whole range of considered values of E_b/N_0 . Figure 2.3 shows the BER obtained when the subcarrier to be equalized is the central one. In this case the multiple-access interference is negligible and, then, the performance gain of the FBMC system with respect the OFDM system in multipath channel A is reduced. However, in multipath channel B the MMSE equalizer clearly outperforms the other systems that present a floor. Specifically, also the OFDM system presents a floor since the CP has been assumed equal to $CP = M/8$.

If the interleaved scheme is adopted all the considered systems present a severe performance degradation (see Figure 2.4) due to the great amount of interference. For this reason in the following only results regarding the block-wise allocation are reported. Figures 2.5 and 2.6 show the BER degradation in the presence of a residual carrier frequency offset (RCFO) for the user of interest, for whom the residual timing offset (RTO) is zero, with the other users completely asynchronous. In particular the BER in Figure 2.5 has been obtained exploiting the boundary subcarrier while in Figure 2.6 the central subcarrier is considered, moreover, the value of E_b/N_0 for the user of interest is 20 dB. The results show that only the MMSE sub-channel equalizer can provide a satisfactory performance in both channel conditions and, moreover, an accuracy of $\pm 5\%$ of the subcarrier spacing can assure an acceptable performance degradation with respect to the case of perfect synchronization (RCFO = 0).

We have also analyzed the effect of the presence of a residual timing offset for the user of interest. The results reported in Figures 2.7 and 2.8 show that the FS sub-channel

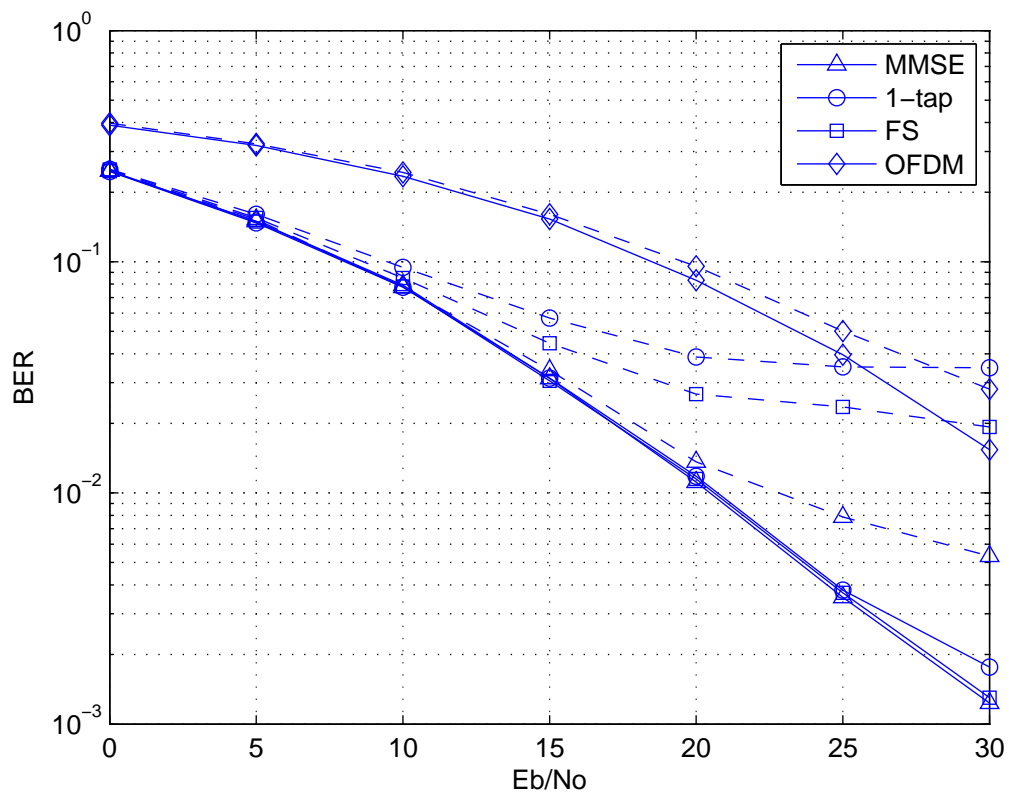


Figure 2.2: comparison between FBMC and OFDM in the absence of synchronization errors for the user of interest (64-QAM, block-wise allocation, boundary subcarrier, channel A solid lines, channel B dashed lines).

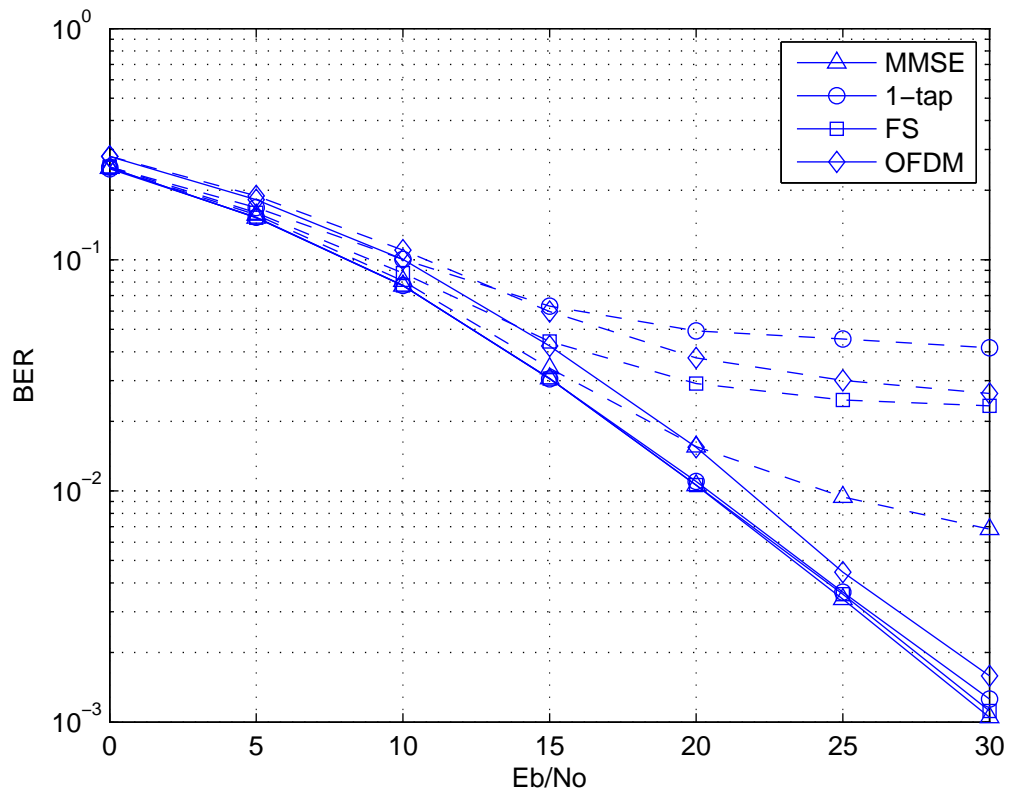


Figure 2.3: comparison between FBMC and OFDM in the absence of synchronization errors for the user of interest (64-QAM, block-wise allocation, central subcarrier, channel A solid lines, channel B dashed lines).

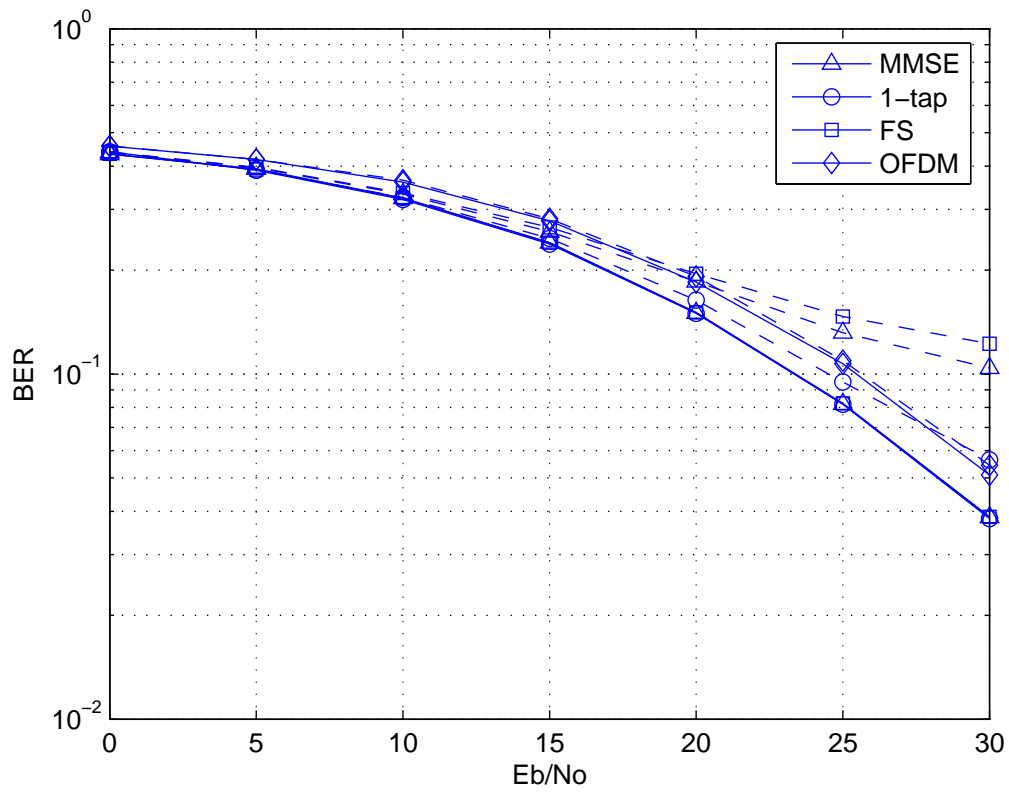


Figure 2.4: comparison between FBMC and OFDM in the absence of synchronization errors for the user of interest (64-QAM, interleaved allocation, channel A solid lines, channel B dashed lines).

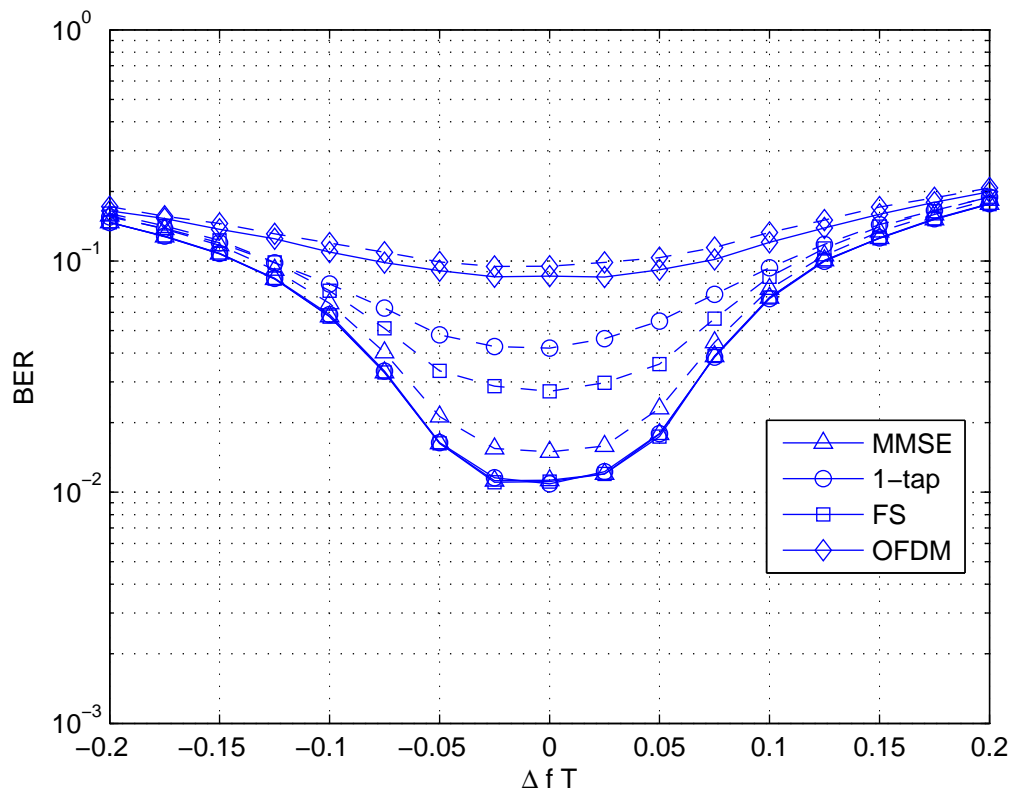


Figure 2.5: BER as a function of the RCFO normalized to the subcarrier spacing (64-QAM, block-wise allocation, boundary subcarrier, channel A solid lines, channel B dashed lines).

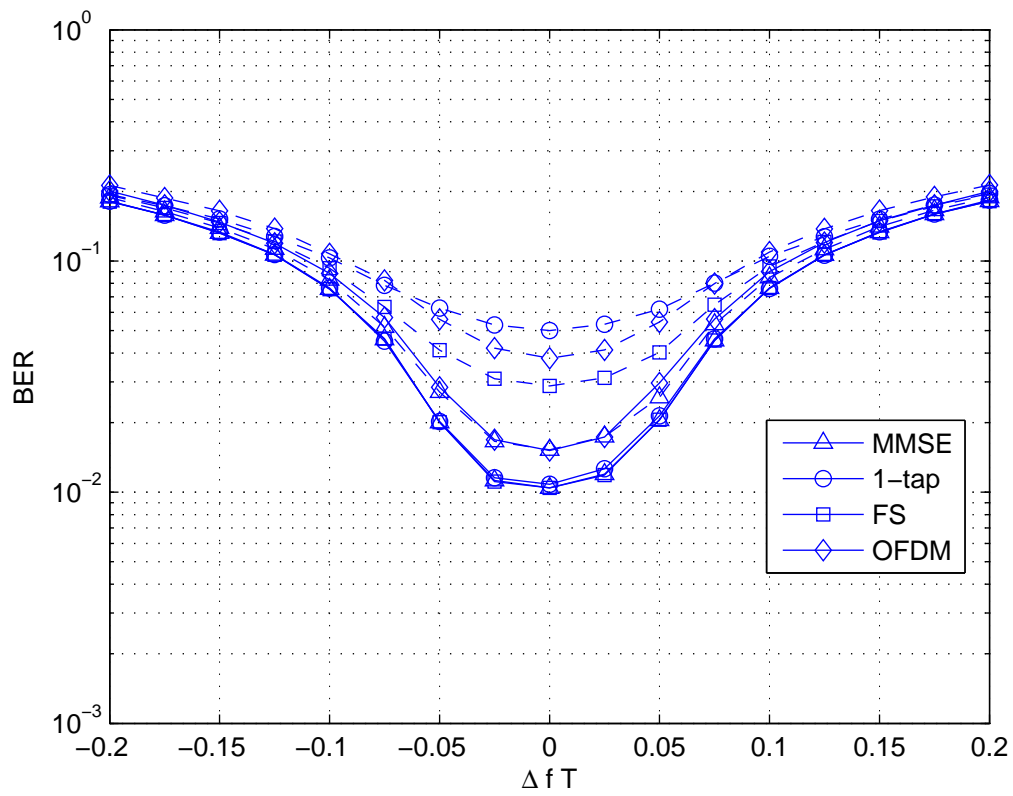


Figure 2.6: BER as a function of the RCFO normalized to the subcarrier spacing (64-QAM, block-wise allocation, central subcarrier, channel A solid lines, channel B dashed lines).

equalizer can assure in both channel conditions a lower sensitivity to the RTO with respect to the 1-tap equalizer, however, its performance presents a severe degradation when the RTO is greater than 15% of the FBMC symbol interval. On the other hand the MMSE sub-channel equalizer can be used also when the RTO is 50% of the FBMC symbol interval. The performance of the 1-tap sub-channel equalizer used for the OFDM system presents a severe degradation as the RTO becomes greater than the CP fixed at $M/8 = 128$.

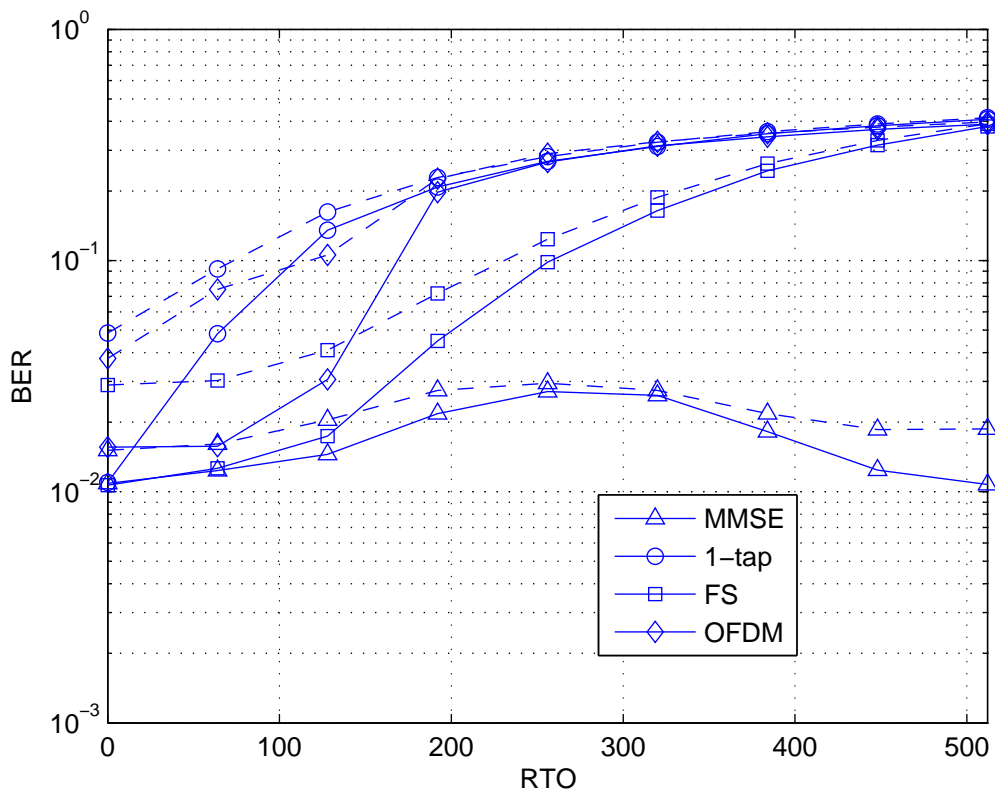


Figure 2.7: BER as a function of the RTO (64-QAM, block-wise allocation, central sub-carrier, channel A solid lines, channel B dashed lines).

Figures 2.9 and 2.10 present the BER obtained, in the case of perfect synchronization and block-wise allocation, for a 4-QAM constellation in multipath fading channel. Specifically, in Figure 2.9 the exploited sub-carrier is the central one while in Figure 2.10 the boundary sub-carrier is considered. The results show that with the adoption of this lower-dimensional constellation the MMSE equalizer assures nearly the same performance in both channel conditions and, moreover, it is the only structure that outperform the 1-tap sub-channel equalizer for OFDM system both in the absence and in the presence of multiple-access interference. Finally, Figures 2.11 and 2.12 show that the sensitivity to the RCFO and the RTO in the case of 4-QAM is reduced with respect to that observed with the higher-dimensional 64-QAM constellation.

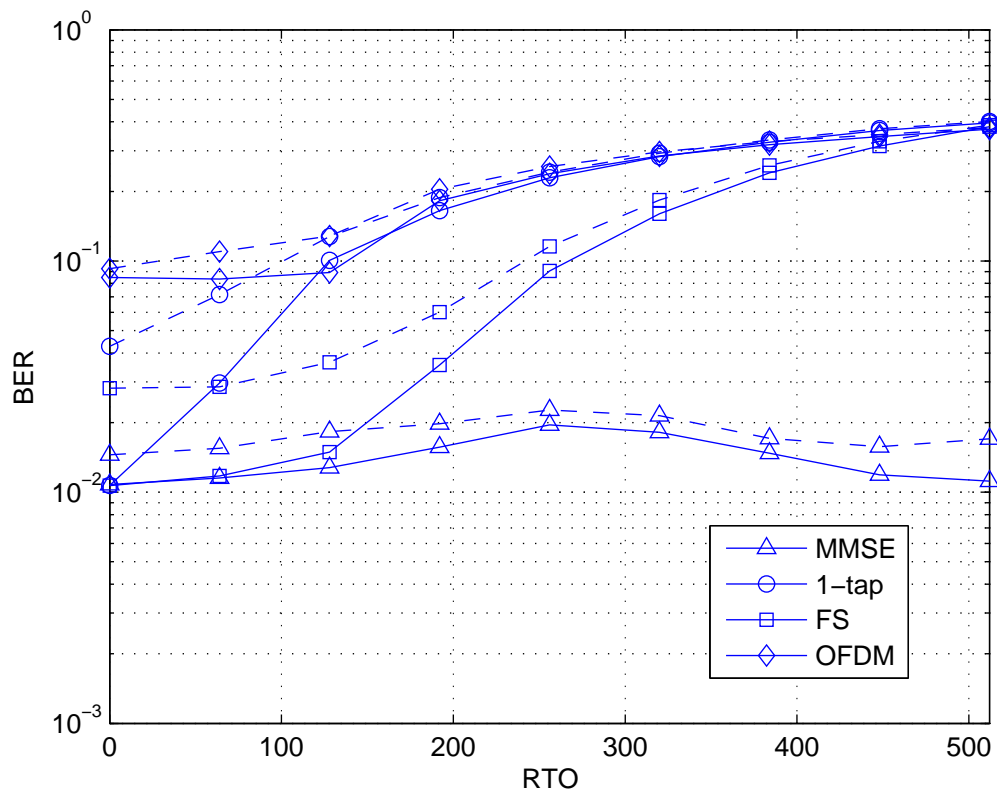


Figure 2.8: BER as a function of the RTO (64-QAM, block-wise allocation, boundary subcarrier, channel A solid lines, channel B dashed lines).

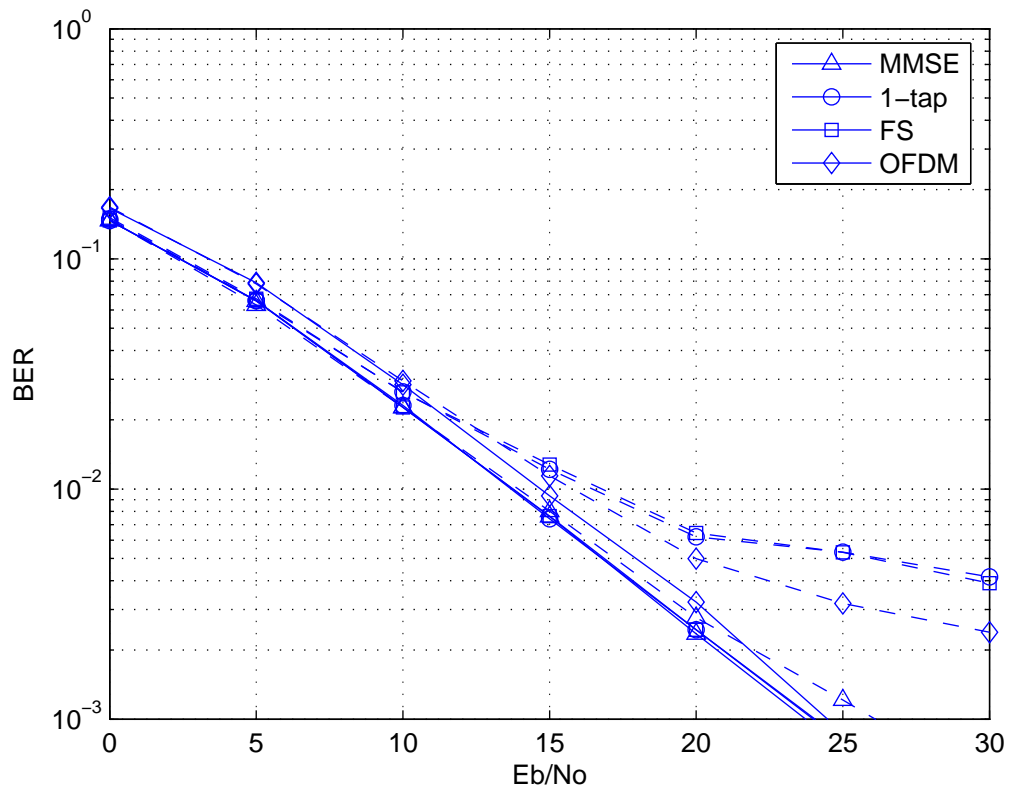


Figure 2.9: comparison between FBMC and OFDM in the absence of synchronization errors for the user of interest (4-QAM, block-wise allocation, central subcarrier, channel A solid lines, channel B dashed lines).

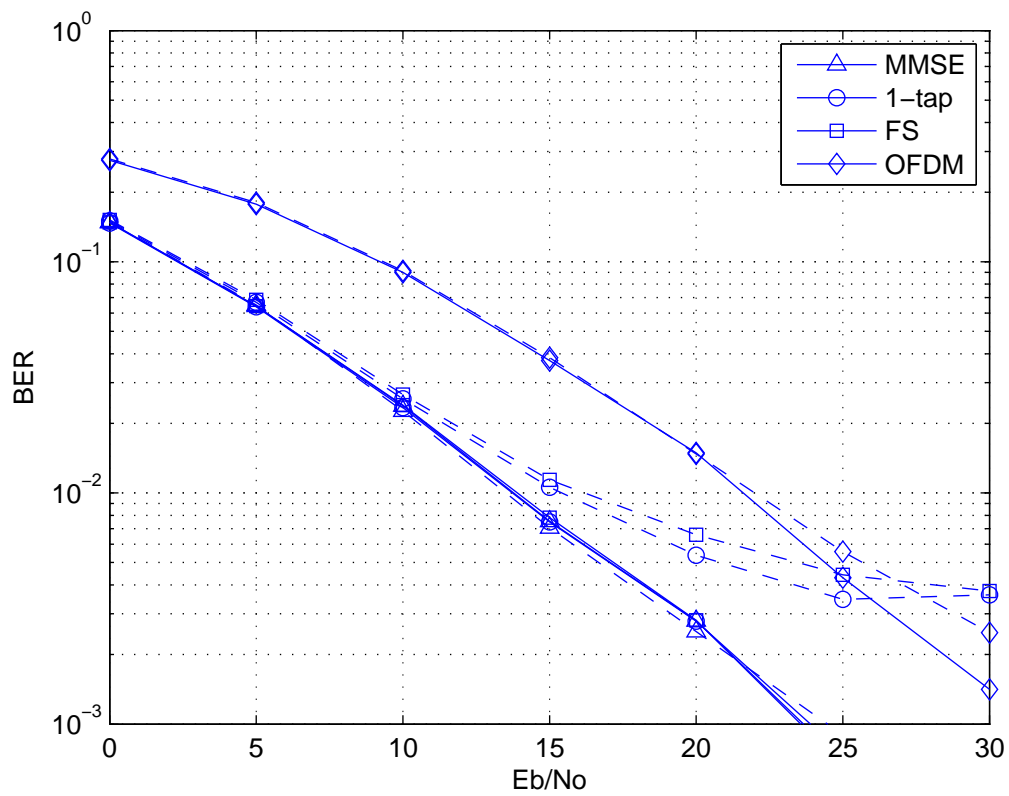


Figure 2.10: comparison between FBMC and OFDM in the absence of synchronization errors for the user of interest (4-QAM, block-wise allocation, boundary subcarrier, channel A solid lines, channel B dashed lines).

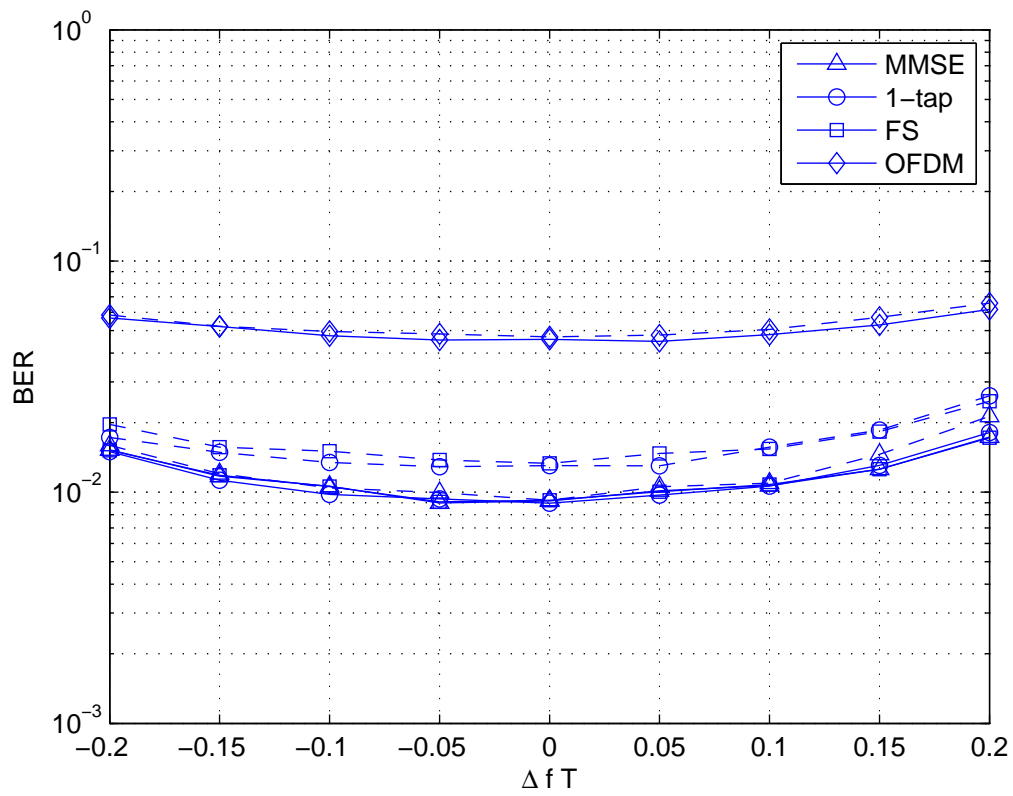


Figure 2.11: BER as a function of the RCFO normalized to the subcarrier spacing (4-QAM, block-wise allocation, boundary subcarrier, channel A solid lines, channel B dashed lines).

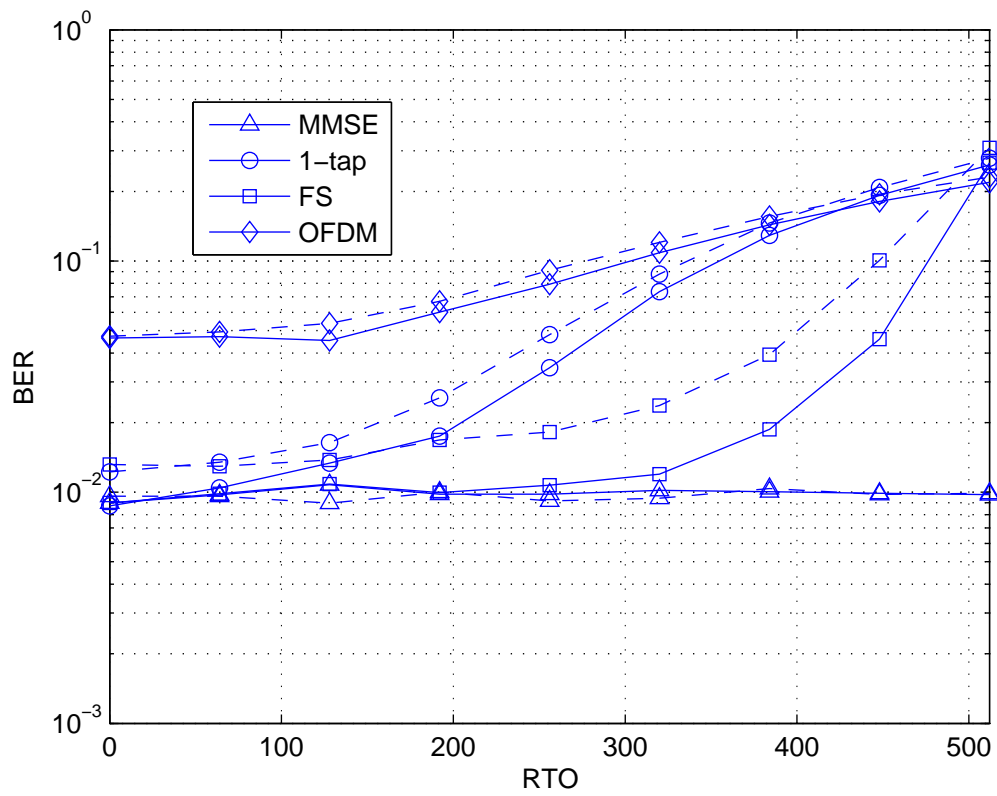


Figure 2.12: BER as a function of the RTO (4-QAM, block-wise allocation, boundary subcarrier, channel A solid lines, channel B dashed lines).

2.1.1 Conclusions

A comparison between the up-link performance of an FBMC and a CP-OFDM system has been made for two different allocation schemes: block-wise and interleaved. Specifically, the first user has been considered as user of interest and, the other users have been assumed completely asynchronous. Moreover, the performance degradation of both systems in the presence of synchronization errors for the user of interest has been analyzed. The multipath channel models ITU-Vehicular A and ITU-Vehicular B, and, moreover, 4-QAM and 64-QAM constellations, have been considered. The results have shown that, in the case of perfect synchronization for the user of interest and with the block-wise allocation scheme, boundary subcarriers of the CP-OFDM system are more affected by multiple-access interference. Moreover, with this allocation scheme and in channel B, only the MMSE sub-channel equalizer for the FBMC system provides a satisfactory performance. On the other hand, in the presence of the low frequency selective channel A, all the considered sub-channel equalizers for the FBMC system assure nearly the same performance, that is, no advantage is obtained using a multi-tap equalizer. Furthermore, in the case of perfect synchronization and with the interleaved allocation scheme, both CP-OFDM and FBMC systems present a severe performance degradation due to the great amount of interference. In the presence of a residual CFO for the user of interest, with block-wise allocation and for 64-QAM, only the MMSE sub-channel equalizer can provide a satisfactory performance in both channel conditions. Specifically, it assures an acceptable performance degradation, with respect to the case of perfect synchronization, when the RCFO is equal to $\pm 5\%$ of the sub-carrier spacing. Furthermore, in both channel conditions the MMSE sub-channel equalizer presents the lowest sensitivity to the RTO. Finally, the sensitivity of both systems to the RCFO and the RTO in the case of 4-QAM is reduced with respect to that observed with the higher-dimensional 64-QAM constellation.

2.2 Uplink Synchronization for FBMC Systems

2.2.1 Introduction

The multiple access technique used in a multicarrier system naturally is Frequency Division Multiple Access (FDMA). In the downlink, there is no carrier frequency offset (CFO) and no timing offset (TO) between the subcarriers dedicated to different users. Therefore, orthogonality between users is not destroyed. In the uplink the situation is quite different. Between users, there is CFO and TO and the BS cannot synchronize to all users simultaneously. In [5] the performance degradation due to these offsets has been investigated for different allocation schemes. Specifically, it has been shown that, in the case of a multi-user system in which the user of interest is perfectly synchronized to the base station (BS), FBMC-MA systems are more robust than CP-OFDMA systems with respect to misalignments between different users, assuring in the case of block-wise assignment a performance practically coincident with that obtained in the case of perfect synchronization. Moreover, it has been shown that, by exploiting the joint symbol timing and CFO estimation algo-

rithm for uplink synchronization described in [6] and [7], the FBMC system can assure a BER nearly equal to that obtained in the case of perfect synchronization. In particular, the performance has been evaluated both in AWGN and multipath channel A. In the last case one-tap equalization with perfect knowledge of the channel has been considered.

The multiple-access interference in the uplink in the case where the user of interest is perfectly synchronized and, moreover, the effect of a residual timing or frequency offset for the user of interest when different equalization schemes are adopted and the impact on the different subcarriers, have been investigated in [8].

In this report the performance of the FBMC system exploiting the joint ST and CFO estimator mentioned above is assessed via computer simulations and compared with that achieved by the CP-OFDM system equipped with an efficient synchronization procedure derived as an extension of that proposed for the FBMC system.

2.2.2 The adopted joint estimation algorithm for CP-OFDMA

Let us denote with $x(t)$ the OFDM transmitted signal; the received signal $r(t)$ over AWGN channel can be written as

$$r(t) = e^{j2\pi\Delta f_o t} x(t - \tau_o) + n(t). \quad (2.1)$$

The received signal is first sampled and, after removing the cyclic prefix, an input vector of dimension M undergoes FFT transform where M is the number of OFDM subcarriers. Let us denote with \mathbf{x}_1 the vector at the input of the FFT block in the $(k+1)$ th symbol interval at the receiver and with \mathbf{x}_2 the vector in the next symbol interval (the $(k+2)$ th). Note that, though not explicitly denoted, \mathbf{x}_1 and \mathbf{x}_2 depends on (a) the symbol vectors \mathbf{a}_1 and \mathbf{a}_2 , where \mathbf{a}_i denotes the transmitted symbol vector in the $(k+i)$ th symbol interval ($i = 1, 2$), (b) the additive disturbance in the two symbol intervals, and (c) the effects of the synchronization impairments ($\tau_o \neq 0$ and $\Delta f_o \neq 0$).

When (a) the same symbol vector is used in the two intervals ($\mathbf{a}_1 = \mathbf{a}_2$) and (b) the additive noise can be neglected, then the difference between \mathbf{x}_1 and \mathbf{x}_2 only depends on the synchronization parameters. We explicitly denote the dependence on the timing parameter of the two vectors $\mathbf{x}_1(\tau)$ and $\mathbf{x}_2(\tau)$ with τ denoting the timing advance introduced on the received signal to compensate for the channel delay τ_o . In fact, provided that τ is sufficiently close to τ_o (in particular, if $\tau_o - C_p T \leq \tau \leq \tau_o$ where $C_p T$ represents the duration of the cyclic prefix), the following relation holds

$$\mathbf{x}_2(\tau) = e^{j2\pi\Delta f T_O} \mathbf{x}_1(\tau) = e^{j2\pi\epsilon(1+C_p)} \mathbf{x}_1(\tau) \quad (2.2)$$

where $T_O = M(1+C_p)T_s = T(1+C_p)$ denotes the OFDM symbol period and $MC_p T_s = C_p T$ is the duration of the cyclic prefix.

2.2.2.1 Blind method

Relation (2.2) states that, when $\mathbf{a}_1 = \mathbf{a}_2$ and the noise is negligible, the vectors \mathbf{x}_1 and \mathbf{x}_2 are proportional provided that the timing advance τ is sufficiently close to the ideal value

τ_o . Therefore, the cosine $c(\mathbf{x}_1, \mathbf{x}_2)$ of the two vectors

$$c(\mathbf{x}_1, \mathbf{x}_2) \triangleq \frac{|\mathbf{x}_2^H(\tau)\mathbf{x}_1(\tau)|}{\|\mathbf{x}_2(\tau)\|\|\mathbf{x}_1(\tau)\|} \quad (2.3)$$

assumes the maximum value ($c(\mathbf{x}_1, \mathbf{x}_2) = 1$) when τ is sufficiently close to τ_o . In fact, when τ is not sufficiently close to τ_o , relation (2.2) is not guaranteed and the two vectors are not proportional in general; therefore, $c(\mathbf{x}_1, \mathbf{x}_2)$ is not equal to one in general any more.

Let us denote with $\hat{\tau}$ the estimated value of τ ; if $\hat{\tau}$ is sufficiently close to τ , relation (2.2) is valid for $\tau = \hat{\tau}$ and, consequently,

$$\frac{\mathbf{x}_1^H(\hat{\tau})\mathbf{x}_2(\hat{\tau})}{\|\mathbf{x}_1(\hat{\tau})\|^2} \simeq e^{j2\pi\varepsilon(1+C_p)} \quad (2.4)$$

and, therefore, the CFO can be estimated as follows:

$$\hat{\varepsilon} = \frac{1}{2\pi(1+C_p)} \angle (\mathbf{x}_1^H(\hat{\tau})\mathbf{x}_2(\hat{\tau})) . \quad (2.5)$$

The present method does not require to know the symbol vector \mathbf{a}_1 ; it requires to use in the preamble two symbol intervals to transmit the information required by a single symbol interval.

2.2.2.2 Known Symbol vector

When the symbol vector \mathbf{a}_1 is known, an improved procedure can be introduced. Let us denote with \mathbf{X}_i the FFT of \mathbf{x}_i ($i = 1, 2$); when relation (2.2) holds, the vectors \mathbf{X}_i are not only proportional among themselves

$$\mathbf{X}_2 = e^{j2\pi\varepsilon(1+C_p)}\mathbf{X}_1 \quad (2.6)$$

but they are also proportional to the vector \mathbf{a}_1 . Therefore, the following cost function

$$|\mathbf{a}_1^H \mathbf{X}_1| + |\mathbf{a}_1^H \mathbf{X}_2| \quad (2.7)$$

is independent of ε . Moreover, since (2.7) is maximum for \mathbf{X}_i proportional to \mathbf{a}_1 and in such a condition (2.7) is independent of ε , we can evaluate (2.7) for different values of τ without compensating the CFO and estimate $\hat{\tau}$ as the value of τ that maximizes (2.7).

After the timing advance has been estimated, we can estimate the normalized CFO ε on the basis of the relation (2.6):

$$\hat{\varepsilon} = \frac{1}{2\pi(1+C_p)} \angle ((\mathbf{a}_1^H \mathbf{X}_1)^* \mathbf{a}_1^H \mathbf{X}_2) \quad (2.8)$$

since from (2.6) it follows that

$$\mathbf{a}_1^H \mathbf{X}_2 = e^{j2\pi\varepsilon(1+C_p)} \mathbf{a}_1^H \mathbf{X}_1. \quad (2.9)$$

All the previous derivation refers to the case where $n(t)$ represents the background noise in the bandwidth of the useful signal; when multiple access is considered, the model here considered is still valid provided that $n(t)$ includes the components of the interfering signals in the signal bandwidth. Consequently, the derivation is still valid provided that interference powers in the signal bandwidth are negligible and this is a reasonable assumption when different subcarriers are assigned to different users and the channel introduces frequency shifts that are much smaller than intercarrier separation; such an approximation is much more reasonable when blockwise allocation is adopted at the transmitter side.

2.2.3 Simulation results

In this section the performance of the FBMC system exploiting the joint ST and CFO estimator presented in [6] and [7] is assessed via computer simulations and compared with that of the CP-OFDM system equipped with the synchronization procedure described in the previous section. Moreover, both systems exploit a one-tap subcarrier equalizer with perfect knowledge of the channel and of the residual synchronization errors. A number of 10^4 Monte Carlo trials has been performed under the following conditions (unless otherwise stated):

1. the considered FBMC system has a bandwidth $B = 1/T_s = 11.2$ MHz;
2. the preamble symbols are the real and imaginary part of QPSK symbols and, for each user on his subcarrier index set \mathcal{P} is satisfied the orthogonality condition (see eq. (2.22) of [9]) useful to improve synchronization performance;
3. the data symbols are the real and imaginary part of 4-QAM or 64-QAM symbols;
4. the overlap parameter β is fixed at $\beta = 4$;
5. the considered multipath fading channel model is the ITU Vehicular A;
6. the channel is fixed in each run but it is independent from one run to another;
7. to reduce the interference due to the data symbols, the useful data in the whole burst is delayed with respect to the preamble of the burst by one FBMC symbol interval;
8. the total number of subcarriers is $M \in \{512, 1024\}$ while the number of used subcarriers is $M_u \in \{456, 912\}$ for the FBMC system and $M_u \in \{420, 840\}$ for the OFDM system;
9. the blockwise allocation scheme is adopted;
10. the number of users is four and, the interfering users have a timing offset uniformly distributed within $\{-T/2, \dots, T/2\}$ and a normalized frequency offset uniformly distributed in the range $[-0.125, 0.125]$, moreover, unless otherwise stated, the SNR of the interfering users is set to 16 dB;

11. the relative length of the cyclic prefix is $C_p = 1/8$;
12. for the CP-OFDMA system the synchronization algorithm with known symbol vector \mathbf{a}_1 is used in the simulations.

In Fig. 2.13 the bit error ratio (BER) of the two systems is depicted for $M = 512$ and for 4-QAM constellation; we can notice that the performance of the FBMC system with estimated synchronization parameters (see curves labeled as pbfbmc (preamble-based estimation)) is equivalent to that of the FBMC system with perfectly known synchronization parameters (see curves labeled as psfbmc (perfect synchronization)). We can also notice that for CP-OFDM on multipath channel this is not true for large SNR (see curves labeled as psofdm and pbofdm). Note also that the single-tap equalizer in FBMC becomes suboptimum for large SNR; for such a reason, with perfectly known parameters, OFDM achieves the same performance of the FBMC system for large SNR. However, OFDM is more sensible to the errors in the estimation of the synchronization parameters; consequently, with estimated parameters, the performance advantage of the FBMC system is confirmed also for large SNR (at least 4 dB for BER equal to 10^{-3}).

Figs. 2.14, 2.15 and 2.16 confirm that it is the sensibility of OFDM to synchronization impairments the reason for poorer performance of OFDM in comparison with FBMC. In fact, Figs. 2.14 and 2.15 show that the performance of the CFO estimator for OFDM is superior to that for FBMC while the ST estimators for the two systems exhibit irrelevant performance differences. Moreover, Fig. 2.16 shows that also when the multiple-access interference (MAI) is contained (SNR of the interfering users equal to -10 dB) the difference between the performance of the OFDM system with estimated synchronization parameters and that of the same system with perfect synchronization is still evident as in Fig. 2.13, although the accuracy of the CFO estimates is improved (see Fig. 2.17).

Fig. 2.18 shows that also for $M = 1024$ subcarriers similar conclusions can be derived; the difference lies in the fact that the single-tap equalizer now exhibits in the case of the FBMC system a reduced floor effect at large SNR and, therefore, a slight performance loss of OFDM in comparison to FBMC for perfectly known parameters is present for large SNR; again, however, FBMC with proposed synchronization algorithms is perfectly equivalent both in AWGN and multipath to the FBMC with perfectly known synchronization parameters, while in OFDM this is true almost always but the case of SNR larger than 25 dB. However, figure 2.19 shows that for $M = 1024$ subcarriers when the MAI is negligible (SNR of the interfering users equal to -10 dB) the performance loss of the OFDM system due to the synchronization procedure is reduced with respect to the case of $M = 512$ subcarriers.

Figs. 2.20, 2.21, 2.22 and 2.23 show that when the 64-QAM constellation is employed, the FBMC system with estimated synchronization parameters can outperform the OFDM system with perfect synchronization in both considered MAI conditions only when $M = 1024$ subcarriers are used. Moreover, it is worthwhile to emphasize that, when the 64-QAM constellation is employed, in multipath channel and in the presence of MAI the SNR-loss of OFDM with respect to FBMC can be more significant than that observed in the case of 4-QAM constellation.

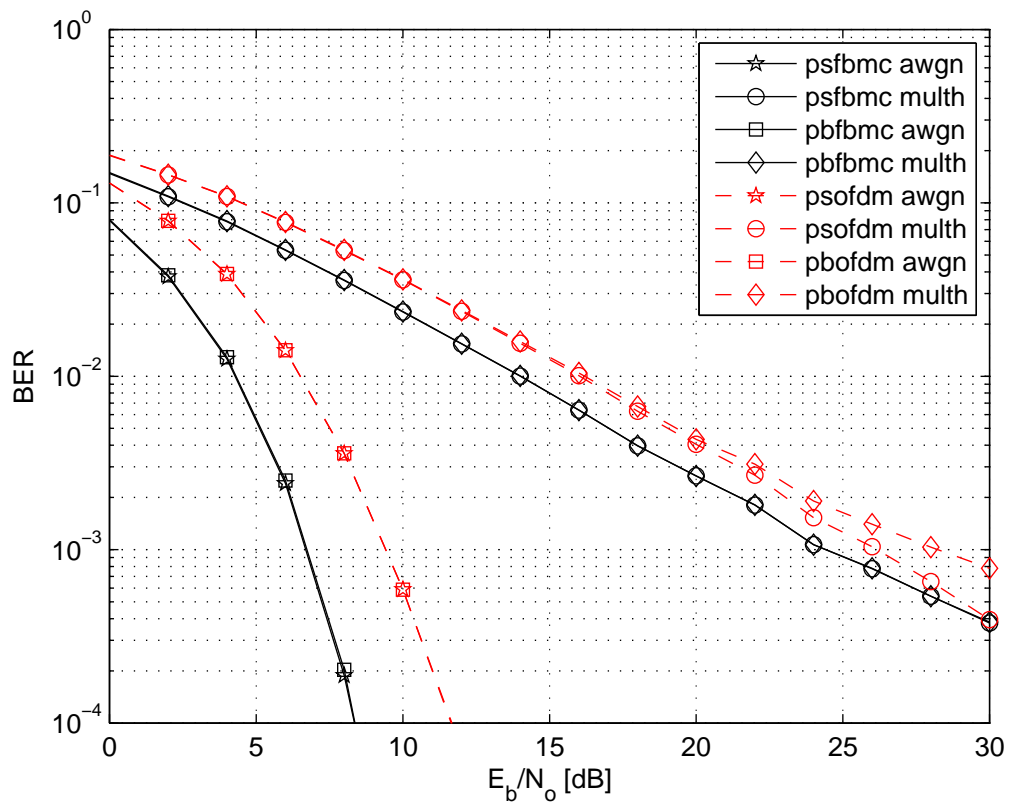


Figure 2.13: Performance of FBMC and OFDM systems in multipath and AWGN channels with perfectly known or estimated synchronization parameters for $M = 512$ subcarriers and 4-QAM constellation. The SNR of the interfering users is set to 16 dB.

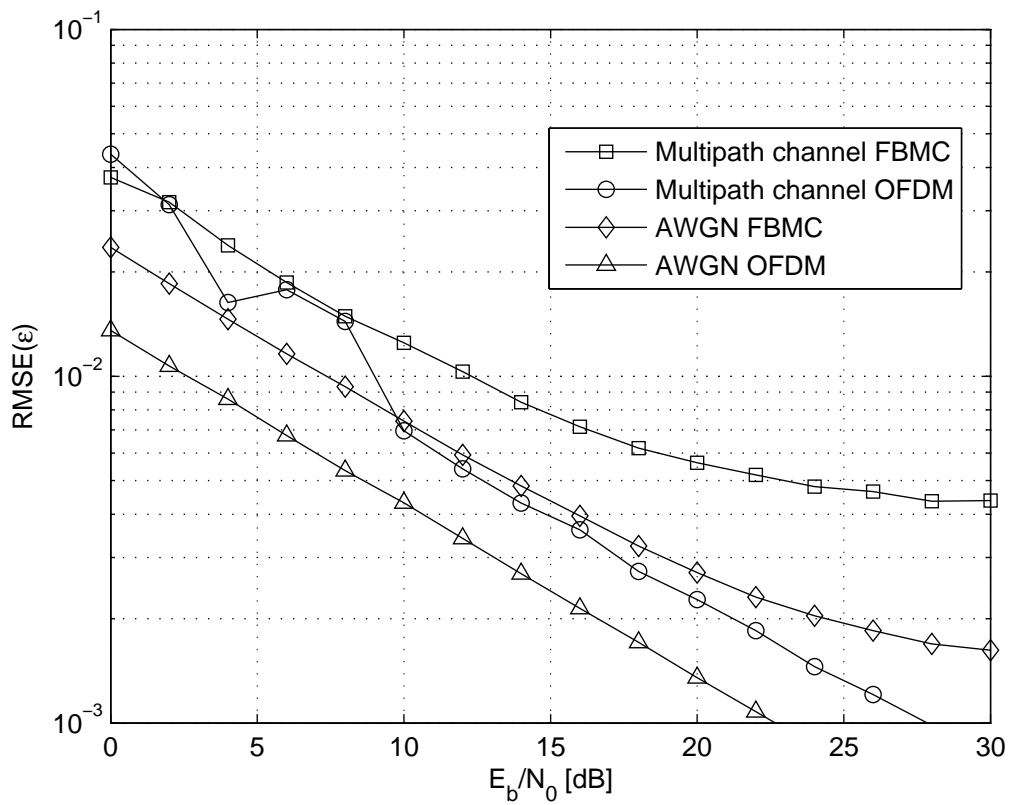


Figure 2.14: RMMSE of the CFO estimators for FBMC and OFDM systems in multipath and AWGN channels for $M = 512$ subcarriers and 4-QAM constellation. The SNR of the interfering users is set to 16 dB.

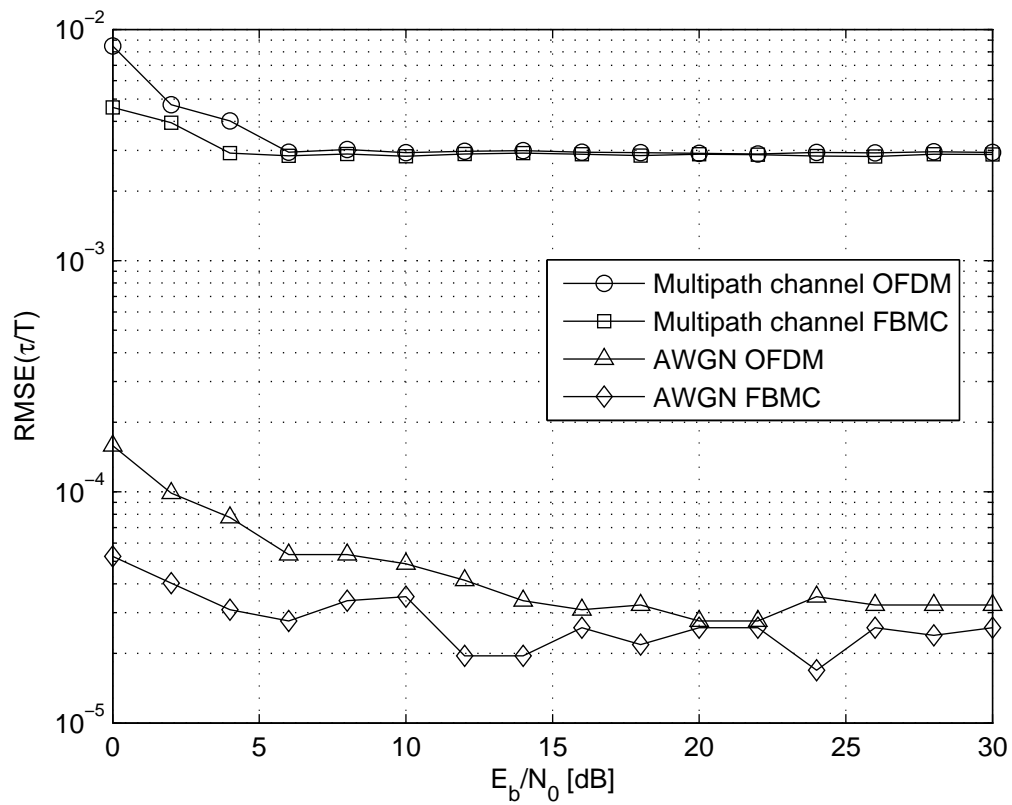


Figure 2.15: RMMSE of the ST estimators for FBMC and OFDM systems in multipath and AWGN channels for $M = 512$ subcarriers and 4-QAM constellation. The SNR of the interfering users is set to 16 dB.

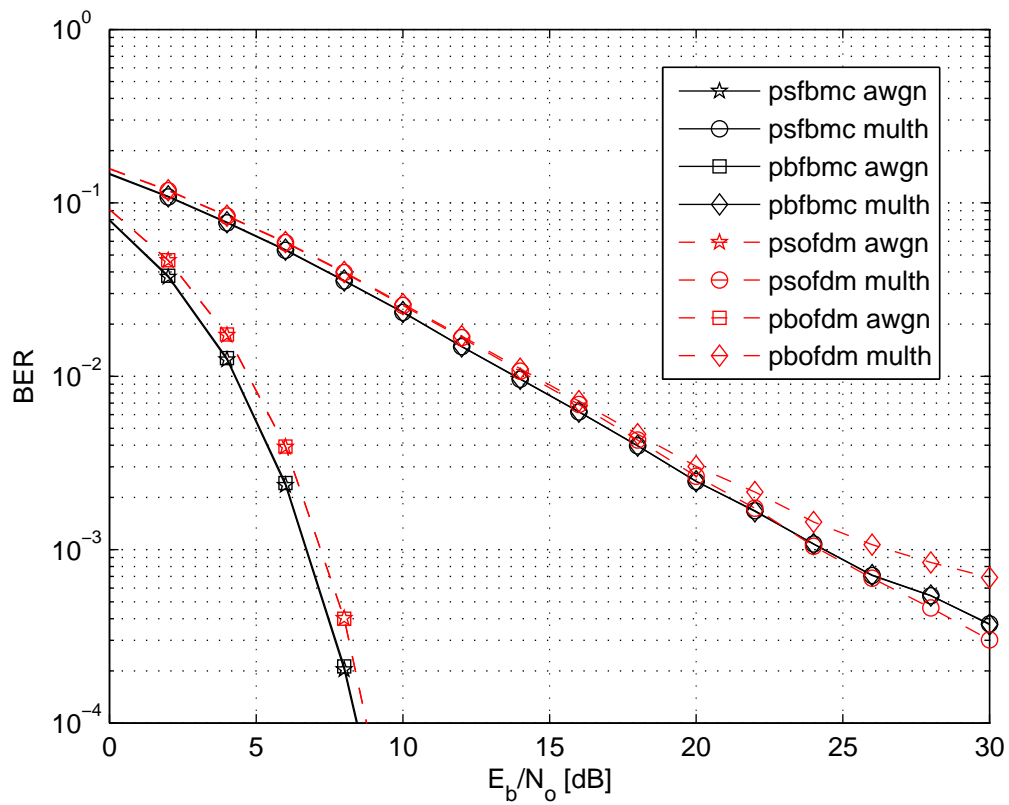


Figure 2.16: Performance of FBMC and OFDM systems in multipath and AWGN channels with perfectly known or estimated synchronization parameters for $M = 512$ subcarriers and 4-QAM constellation. The SNR of the interfering users is set to -10 dB.

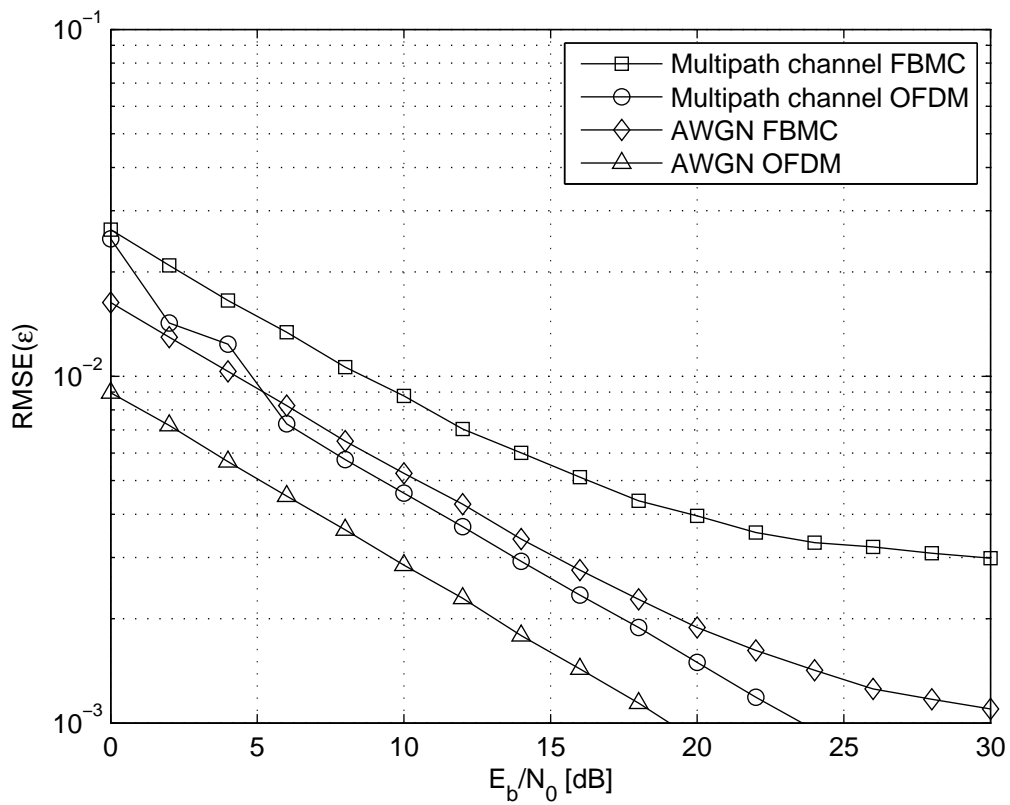


Figure 2.17: RMMSE of the CFO estimators for FBMC and OFDM systems in multipath and AWGN channels for $M = 512$ subcarriers and 4-QAM constellation. The SNR of the interfering users is set to -10 dB.

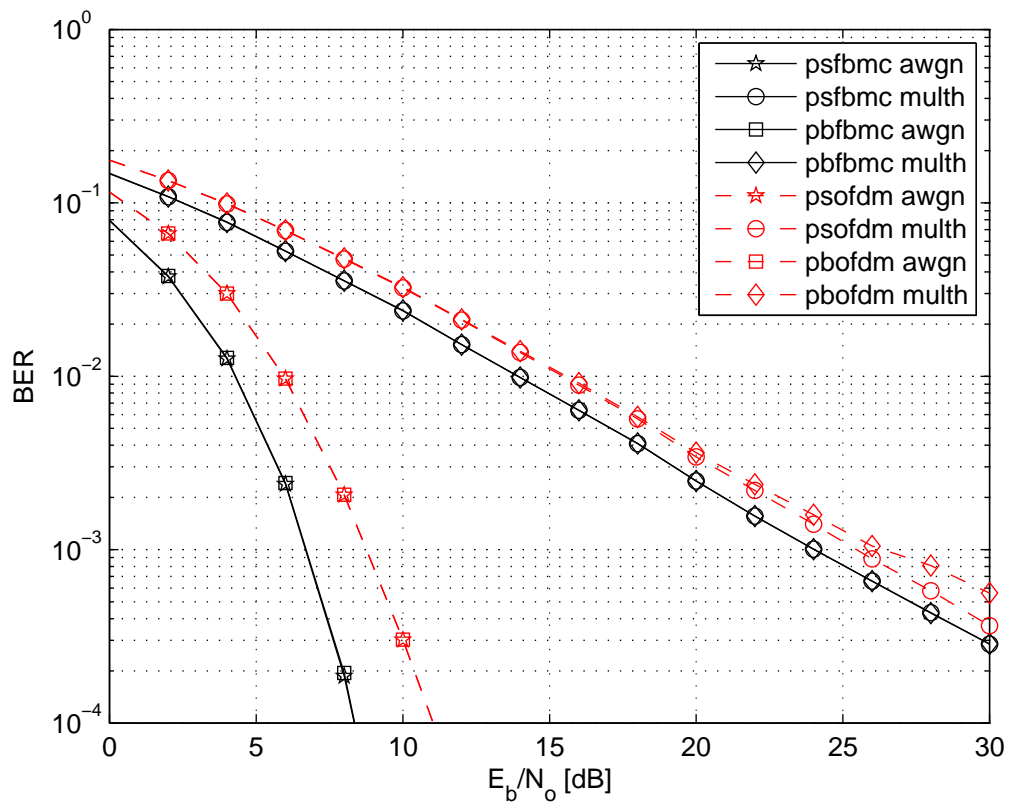


Figure 2.18: Performance of FBMC and OFDM systems in multipath and AWGN channels with perfectly known or estimated synchronization parameters for $M = 1024$ subcarriers and 4-QAM constellation. The SNR of the interfering users is set to 16 dB.

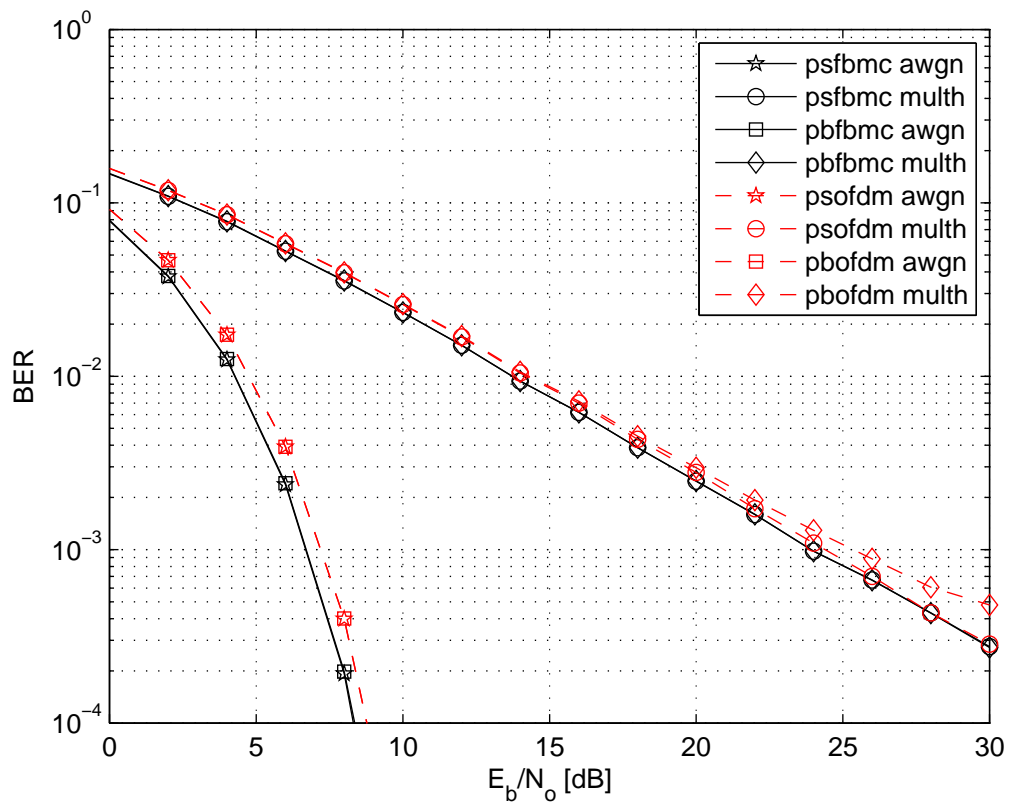


Figure 2.19: Performance of FBMC and OFDM systems in multipath and AWGN channels with perfectly known or estimated synchronization parameters for $M = 1024$ subcarriers and 4-QAM constellation. The SNR of the interfering users is set to -10 dB.

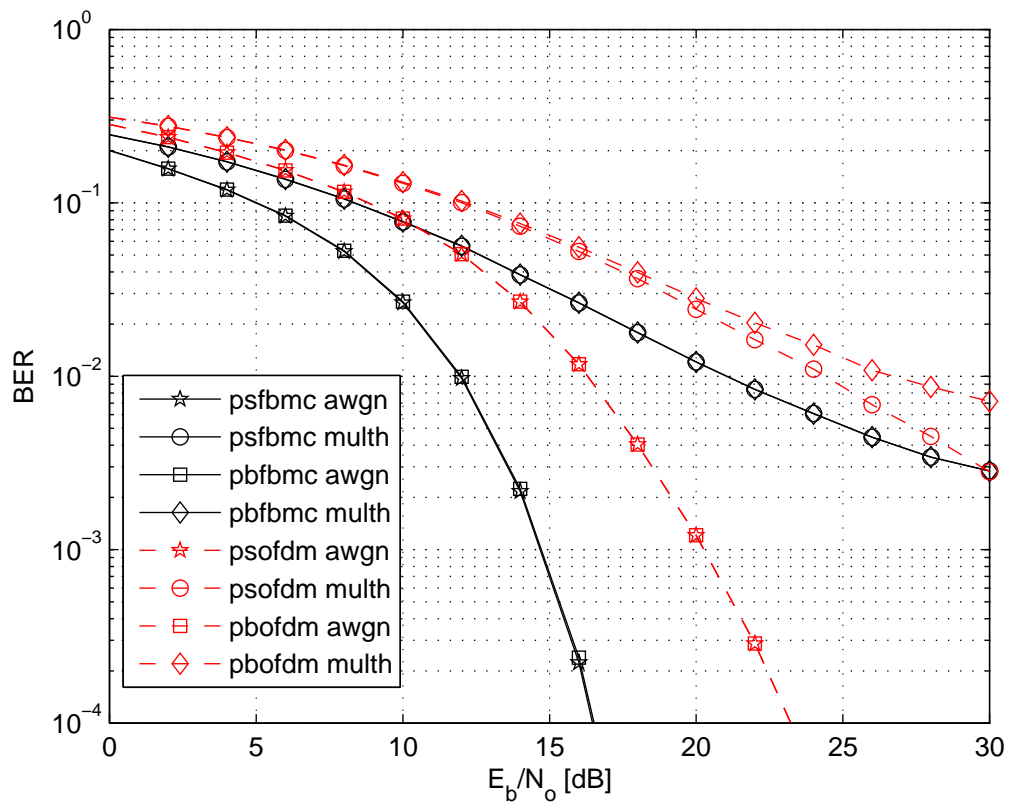


Figure 2.20: Performance analysis of FBMC and OFDM systems in multipath and AWGN channels with perfectly known or estimated synchronization parameters for $M = 512$ and 64-QAM constellation. The SNR of the interfering users is set to 16 dB.

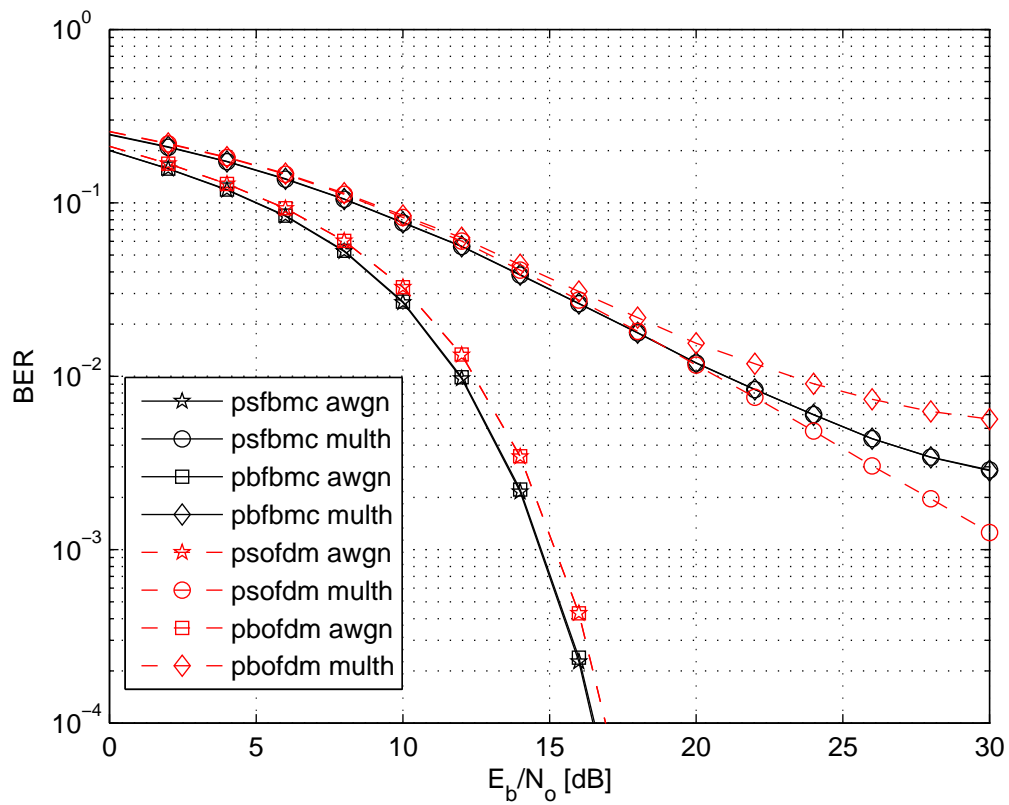


Figure 2.21: Performance of FBMC and OFDM systems in multipath and AWGN channels with perfectly known or estimated synchronization parameters for $M = 512$ and 64-QAM constellation. The SNR of the interfering users is set to -10 dB.

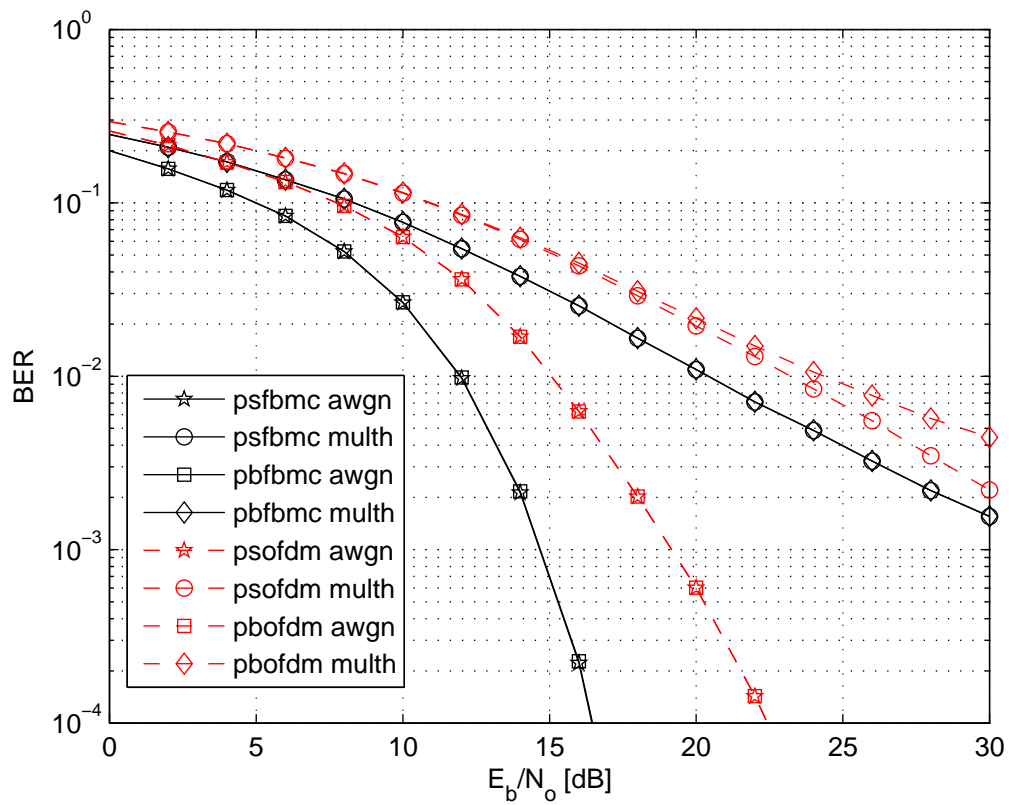


Figure 2.22: Performance of FBMC and OFDM systems in multipath and AWGN channels with perfectly known or estimated synchronization parameters for $M = 1024$ subcarriers and 64-QAM constellation. The SNR of the interfering users is set to 16 dB.

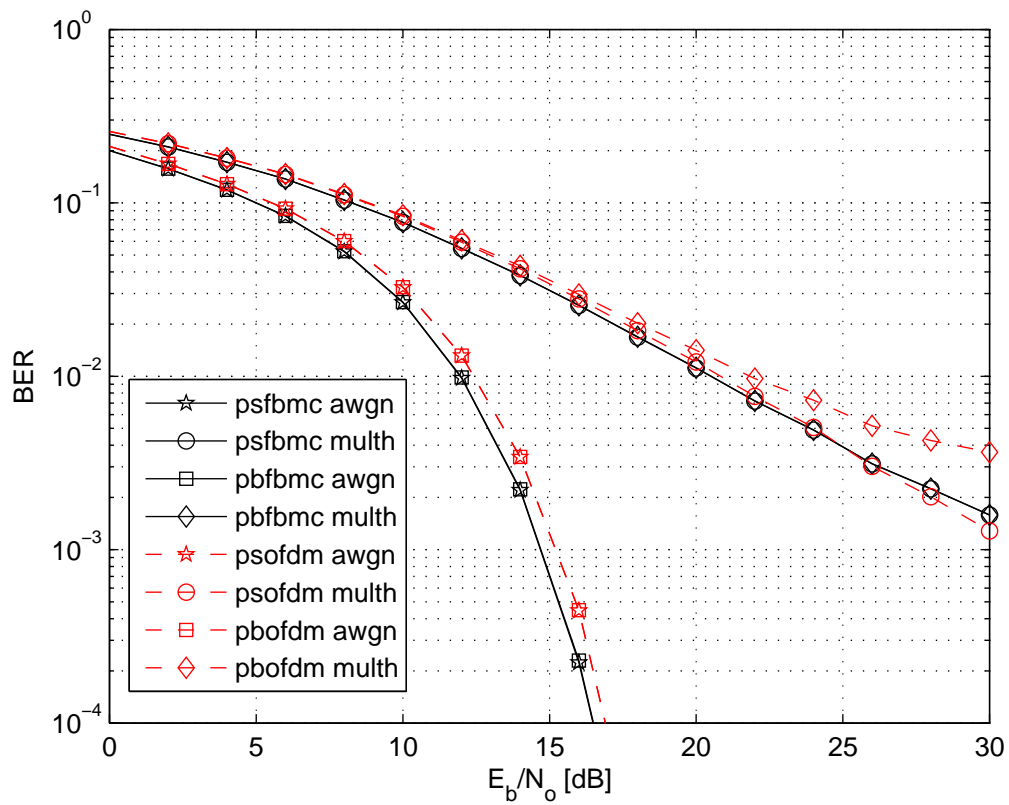


Figure 2.23: Performance of FBMC and OFDM systems in multipath and AWGN channels with perfectly known or estimated synchronization parameters for $M = 1024$ subcarriers and 64-QAM constellation. The SNR of the interfering users is set to -10 dB.

Fig. 2.24 shows that, for limited values of the normalized CFO, the RMMSE of the proposed CFO estimator for OFDM provides (both in AWGN and multipath channel) improved performance with respect to the proposed estimator for FBMC; however, it exhibits a narrower acquisition range.

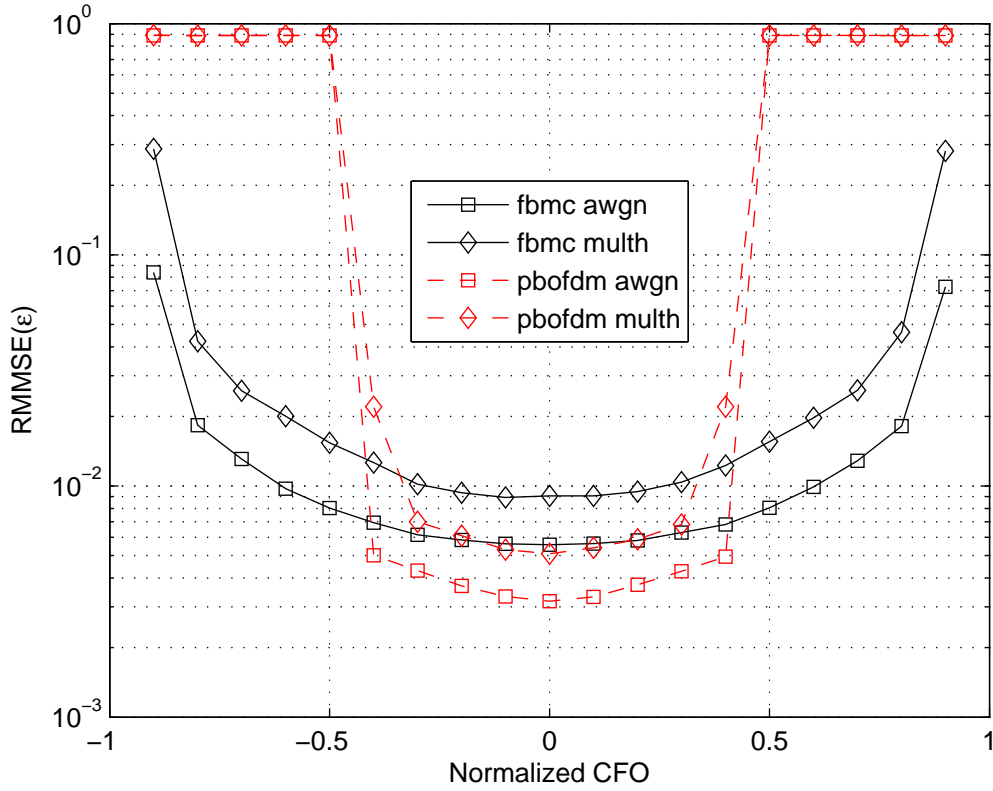


Figure 2.24: RMMSE of the CFO estimators for FBMC and OFDM systems in multipath and AWGN channels versus the actual values of the normalized frequency offset for $M = 1024$ subcarriers, $SNR = 4$ dB, and 64-QAM constellation. The SNR of the interfering users is set to 4 dB.

Fig. 2.25 shows the sensitivity of the two systems to the near-far effect by representing the behavior of the system BER with respect to the SNR of the interfering users for an SNR of the user of interest equal to 26 dB. The results show that the BER of FBMC is independent of SNR of the interfering users while it is significantly worsened by the increase of interfering user powers for OFDM. Moreover, note that also the performance of OFDM in AWGN channel starts to appear in the figure due to the severe degradation related to larger interference powers. Furthermore, Figures 2.26 and 2.27 show the ratio

$$R_i = \frac{n_i}{\sum_{i \in \mathbf{A}_1} n_i} \quad (2.10)$$

where n_i represents the number of wrong bit decisions on the i th subcarrier and \mathbf{A}_1 is the set of subcarriers allocated to the user of interest, that is, the first user. The results show that in FBMC all the subcarriers exhibit the same behavior while in OFDM the subcarriers more subject to the interferences of the other users exhibit a performance degradation as long as the SNR of the interfering users becomes larger. Therefore, the results of the experiments reported in Figs. 2.25, 2.26, and 2.27 confirm that, when equipped with the proposed synchronization procedures, not only MA-FBMC can work correctly without timing advance procedures but also without power control procedures.

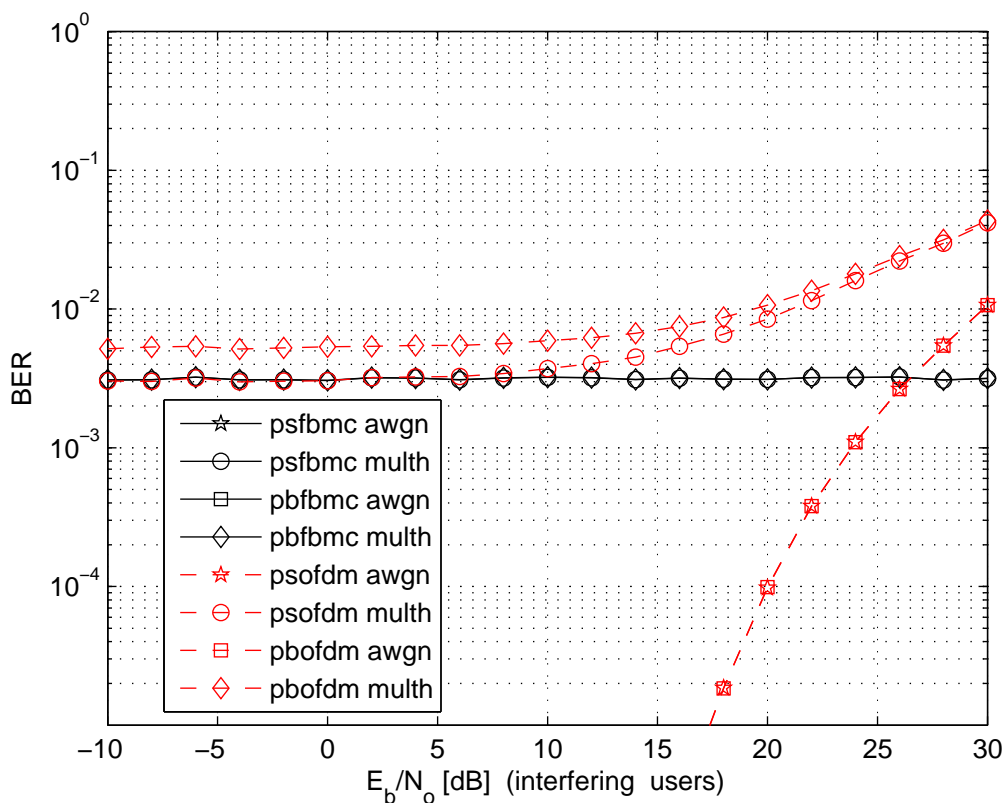


Figure 2.25: Performance of FBMC and OFDM systems in multipath and AWGN channels with perfectly known or estimated synchronization parameters versus the SNR of the interfering users for $N = 1024$ subcarriers, $SNR = 26$ dB and 64-QAM constellation. The SNR of the interfering users is set to 16 dB.

2.2.4 Conclusions

A comparison between the uplink performance of FBMC and CP-OFDM systems has been made for the blockwise allocation scheme. Specifically, the first user has been considered as user of interest while the other users have been assumed completely asynchronous. The

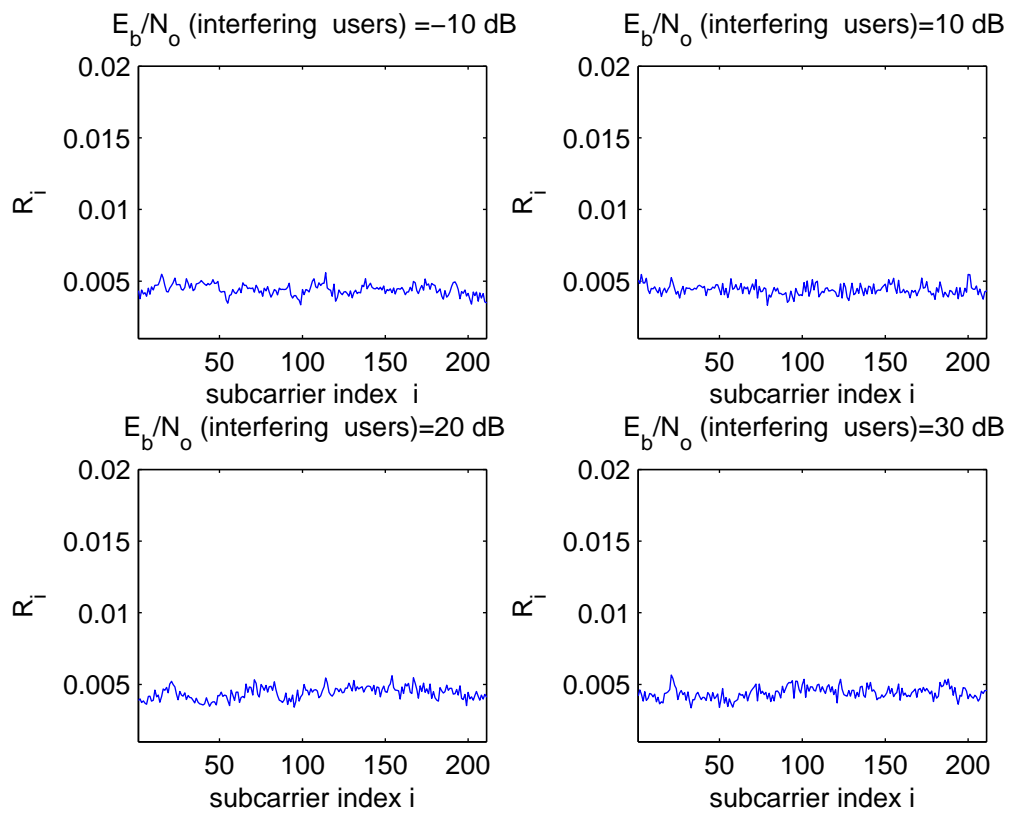


Figure 2.26: Performance of FBMC system in multipath channel with estimated synchronization parameters versus the subcarrier index for different values of the SNR of the interfering users and, for $M = 1024$ subcarriers, $SNR = 26$ dB and 64-QAM constellation. The SNR of the interfering users is set to 16 dB.

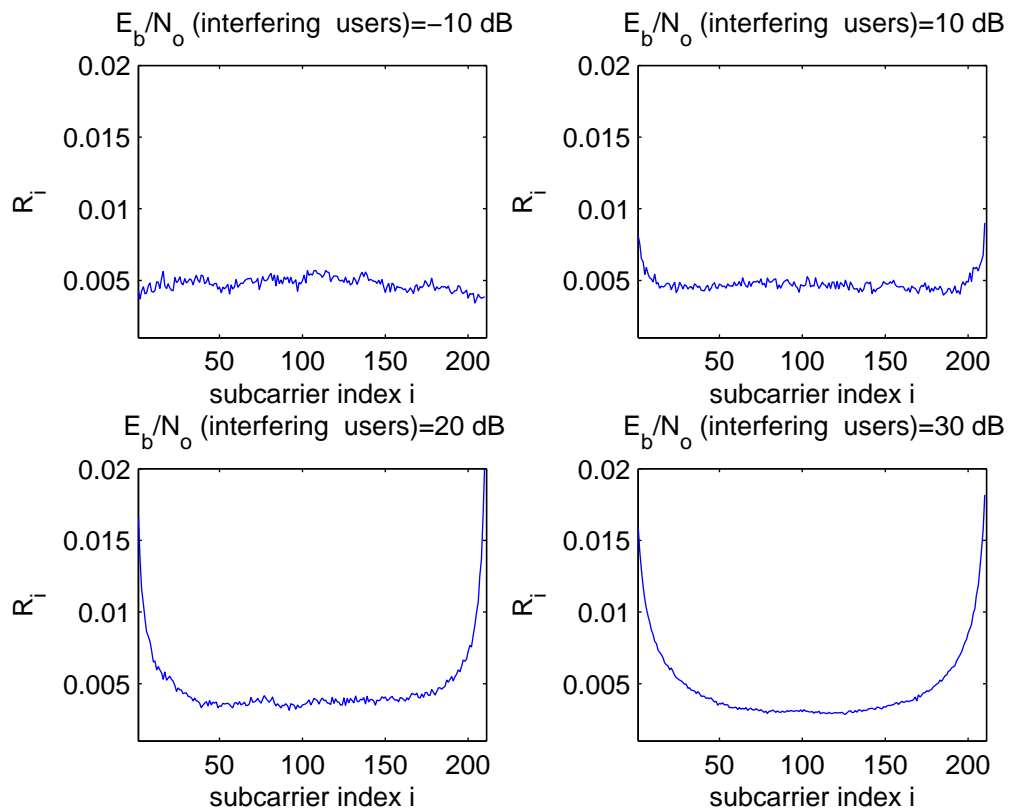


Figure 2.27: Performance of OFDM system in multipath channel with estimated synchronization parameters versus the subcarrier index for different values of the SNR of the interfering users and, for $M = 1024$ subcarriers, $SNR = 26$ dB and 64-QAM constellation.

synchronization for the user of interest has been performed by exploiting the joint ST and CFO algorithm reported in the deliverables D2.1 and D2.2 while a similar synchronization procedure has been described for CP-OFDM systems. The results have shown that the OFDM system is more sensible to the errors in the estimation of the synchronization parameters than FBMC. Moreover, this sensitivity to the errors in the estimation of the synchronization parameters increases in the case of the higher-dimensional 64-QAM constellation. Also the sensitivity of both systems to the near-far effect has been investigated. The results have shown that the BER is nearly independent of the SNR of the interfering users in the case of the FBMC system while it is significantly worsened by the increase of interfering user powers for CP-OFDM. Finally, the impact of multiple-access interference on different subcarriers has been evaluated. The results have shown that in the case of the FBMC system all the subcarriers exhibit nearly the same BER while in OFDM the subcarriers more subject to interferences of the other users exhibit much poorer performance as long as the SNR of the interfering users increases. Therefore, the results have confirmed that, when equipped with the considered synchronization procedure, multiple-access FBMC systems can work correctly without timing advance procedures and, moreover, they can result quite insensitive to the near-far effect.

Chapter 3

Cross Layer Aspects

3.1 Introduction

Resource allocation in multi-carrier systems such as FBMC, refers mainly to the allocation of time and frequency per user, in order to transmit an amount of data which will maintain the required QoS level per case. A resource allocation method in wireless multi-user systems consists of two main components, namely the Scheduler and the Resource Allocator. The Scheduler decides on the order of packet transmissions for all transmitting users, while the Resource Allocator makes the real allocation of exact time slots and frequencies for each transmission. In this chapter, the two proposed approaches of the general resource allocation problem in the last deliverable are further described and discussed, that aim to take advantage of the good frequency selectivity of FBMC to result in considerably improved performance compared to CP-OFDMA. The first approach considers separated scheduling and resource allocation procedures, where the Scheduler provides the Resource Allocator with a prioritized list of packets for transmission. In the second approach the two procedures are operating jointly to investigate if this case improve performance.

3.2 Separated resource allocation and scheduling approach

In this part the separated resource allocation and scheduling approach is described, where the addressed scheduling and resource allocation problem at the downlink of a multiuser multicarrier system is solved by two separate, yet interactive modules, *i.e.*, the *resource allocator* (RA) working across the physical layer (PHY) and the medium access control layer (MAC), and the *scheduler* which works on top of RA. The basic system structure and operation are briefly reviewed in the first section, then the algorithms of the two modules are explained in detail respectively, where the updates and improvements in comparison with the last deliverable are emphasized. Simulations on the RA alone are shown in section 3.2.2.5, which demonstrate the performance advantage of FBMC over CP-OFDM. We will

leave the simulations of applying the whole model and algorithms to CP-OFDM and FBMC systems to the next deliverable, and describe here only the simulation model at the end of 3.2.3.5.

3.2.1 Basic Procedure and System Structure

We consider the base station employing a multicarrier system as the downlink transmitter in an isolated cell. There are a number of users, say U users in the cell, each having one service flow to be served out of the five service flow types as defined in IEEE 802.16, namely Unsolicited grant service (UGS), Real-time polling service (rtPS), Extended real-time polling service (ertPS), Non-real-time polling service (nrtPS) and Best effort service (BE). Determined by the characteristics of the service flow, the traffic from each user has its own density and delay tolerance. Thus at the data link layer of the BS arrive different amount of packets with various latency requirements from the U users. The problem we explore now is how to serve as many packets as possible, by using the available bandwidth and transmit power.

The scheduling and resource allocation procedure is performed for each *Transmission Time Interval* (TTI), during which the wireless channel is assumed to stay constant. For every TTI, the scheduler receives a number of packets passed down from higher layers. Depending on the *quality of service* (QoS) requirements and previous statistics, the scheduler decides which packets are to be served and in which priority order, and provides the prioritized list of packets to the RA. The RA then looks for the specific subchannel assignment, power allocation and modulation and coding schemes (MCS) that could serve the list of packets best, under the current channel realization.

From the procedure description above, it can be seen that beside the two central components scheduler and RA, there are three auxiliary components needed in the system to make simulations and evaluations possible: a traffic modeler, a channel generator, and a statistics module. Moreover, a control unit is necessary for scenario setup and system initialization. The basic structure of the system and the interconnections between the components are shown in Figure 3.1, and explained in the following.

- Control unit

As the initialization step, the control unit creates U user objects, the properties of each describe the physical status (*e.g.*, distance from the BS) as well as the QoS requirements (*e.g.*, service flow type, minimum sustainable data rate, maximum latency) of the particular user. These user objects are assumed to be static over a large number of TTI's.

- Traffic modeler

The traffic modeler simulates the data traffic of the users as various numbers of packets with different lengths and latency requirements, such that each user gets satisfactory QoS, and then passes these packet objects to the scheduler.

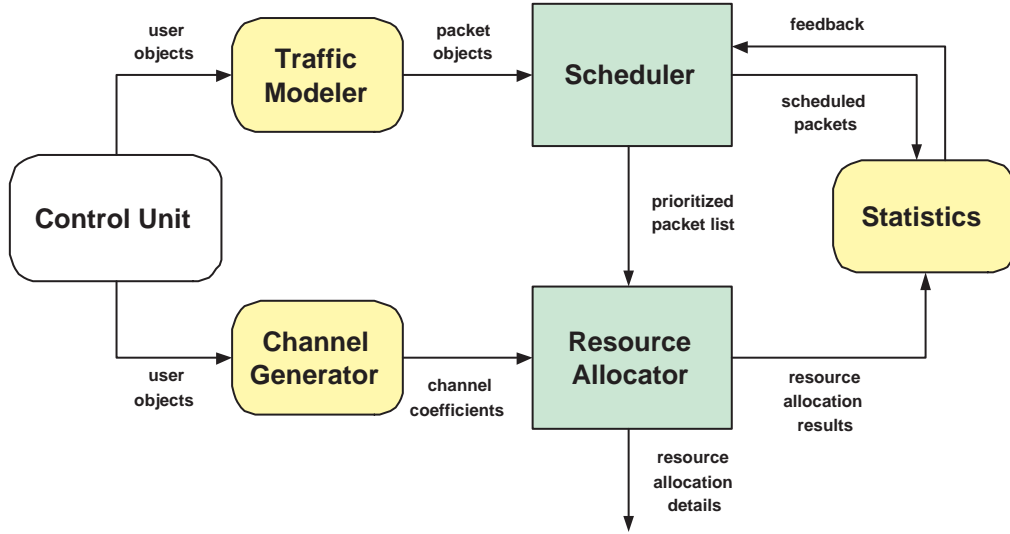


Figure 3.1: System Structure

- Scheduler
The input packets are scheduled and put into a prioritized list. The decision is informed to the statistics component.
- Channel generator
The channel generator randomly generates the channel coefficients of the users.
- Resource allocator
With a prioritized packet list as input for every TTI, the RA outputs the resource allocation details such as a specific subchannel assignment and power allocation strategy, as well as the servabilities of the packets from the original list.
- Statistics
The resource allocation results for consecutive TTI's are stored and processed at the statistics component, which helps the scheduler in providing the packet list and the evaluation of the system performance.

3.2.2 The Resource Allocator Design

Recall that for each TTI of length T_I , the scheduler provides the RA with a prioritized list of K_{tot} packets, each in the format of

User ID u_k	Latency requirement $\tau_k^{(\text{rq})}$	Length in bytes b_k
---------------	--	-----------------------

The main task of the RA is then to find the resource allocation that could serve the maximum number of packets from the list. We have proposed in D6.1 to solve this optimization by iteratively solving a series of transmit power minimization problems with

given subsets of packets, and comparing the minimal resources required with the amount available. Since the packet list is prioritized by the scheduler, the generation of subsets of packets is straightforward and systematic. The basic RA algorithm is summarized in Algorithm 1, where P_{tot} denotes the total transmit power that is available in the system.

Algorithm 1 Resource Allocation Procedure by RA

Require: a prioritized list of K_{tot} packets with QoS requirements

Ensure: largest set of packets \mathcal{P}_S that could be served

```

 $\mathcal{P}_S \leftarrow \{1, \dots, K_{\text{tot}}\}, K \leftarrow K_{\text{tot}}$ 
 $P_{\min} \leftarrow$  minimum transmit power to serve  $\mathcal{P}_S$ 
while  $P_{\min} > P_{\text{tot}}$  do
     $\mathcal{P}_S \leftarrow \mathcal{P}_S \setminus \{K\}$ 
     $K \leftarrow K - 1$ 
     $P_{\min} \leftarrow$  minimum transmit power to serve  $\mathcal{P}_S$ 
end while
if  $K < K_{\text{tot}} - 1$  then
     $K \leftarrow K + 2$ 
    while  $K \leq K_{\text{tot}}$  do
         $P_{\min} \leftarrow$  minimum transmit power to serve  $\mathcal{P}_S \cup \{K\}$ 
        if  $P_{\min} \leq P_{\text{tot}}$  then
             $\mathcal{P}_S \leftarrow \mathcal{P}_S \cup \{K\}$ 
        end if
         $K \leftarrow K + 1$ 
    end while
end if

```

In the following we will briefly review the cross-layer system model and the three-step approach proposed to solve the transmit power minimization problem (details can be found in D6.1), and then introduce the adaptive subchannel size mechanism and the carrier frequency offset (CFO) models, where the former improves the efficiency of resource allocation and the latter evaluates the sensitivity of the specific multicarrier system against CFO.

3.2.2.1 System Model

We define the QoS parameter *latency* of a packet as:

Definition The latency τ is the delay a packet experiences until it is received correctly with an outage probability of no more than the predefined value $\pi^{(\text{out})}$. Let $f[m]$ be the probability that it takes exactly m TTI's to transmit the packet error-free, and M be the minimum number of transmissions needed to guarantee that in a fraction of $1 - \pi^{(\text{out})}$ out of all cases the packet transmission is successful, *i.e.*,

$$M = \min_{M'} M' \quad \text{s.t.} \quad \sum_{m=1}^{M'} f[m] \geq 1 - \pi^{(\text{out})}. \quad (3.1)$$

Then $\tau = (M - 1)(T_R + T_I) + T_I$ where T_R represents *round trip delay*.

In the following, the mathematical descriptions of the regarded system components are derived which lay the basis for cross-layer optimization.

Channel Model The downlink broadcast channel is modeled as frequency-selective fading over the total system bandwidth and frequency-flat fading over each *subchannel*, which is consist of N_c adjacent subcarriers. FDMA is employed meaning the assignment of every subchannel is exclusive to one user.

Let $H_{k,n}$ and $\sigma_{k,n}^2$ be the channel coefficient and Gaussian noise variance of user k on the n th subchannel, and p_n be the power allocated on subchannel n . When assigned to user k and neglecting the influence of CFO, the *signal-to-noise-ratio* (SNR) on subchannel n can be computed as

$$\gamma_{k,n} = \frac{|H_{k,n}|^2}{\sigma_{k,n}^2} \cdot p_n. \quad (3.2)$$

Assuming that one TTI contains N_s symbols for data transmission, we define the minimum allocation unit (MAU) as an allocation region of one subchannel in the frequency dimension by one TTI in the time dimension, which contains $N_c N_s$ symbols.

FEC coding and modulation We assume that modulation and coding is done on a per subchannel basis, and with reference to the WiMAX standard 8 modulation and coding schemes (MCS) are chosen as candidates, which are listed in Table 3.1.

Table 3.1: Modulation and Coding Schemes (MCS)

Index	Modulation Type	Alphabet Size A	Code Rate R	$R \log_2 A$
1	BPSK	2	1/2	0.5
2	QPSK	4	1/2	1
3	QPSK	4	3/4	1.5
4	16-QAM	16	1/2	2
5	16-QAM	16	3/4	3
6	64-QAM	64	2/3	4
7	64-QAM	64	3/4	4.5
8	64-QAM	64	5/6	5

We apply the *noisy channel coding theorem* [10] over each subchannel to compute the packet error probability given any particular MCS. Let the modulation alphabet and the coding rate on the n th subchannel be $\mathcal{A}_n = \{a_1, \dots, a_{A_n}\}$ and R_n respectively. The *cutoff*

rate of subchannel n with SNR $\gamma_{k,n}$ can be expressed as

$$R_0(\gamma_{k,n}, A_n) = \log_2 A_n - \log_2 \left[1 + \frac{2}{A_n} \sum_{m=1}^{A_n-1} \sum_{l=m+1}^{A_n} e^{-\frac{1}{4}|a_l - a_m|^2 \gamma_{k,n}} \right]. \quad (3.3)$$

Note that the cutoff rate is monotonically increasing with SNR when the modulation alphabet is fixed.

According to the noisy channel coding theorem, there always exists a block code with block length l and binary code rate $R_n \log_2 A_n \leq R_0(\gamma_{k,n}, A_n)$ in bits per subchannel use, such that with maximum likelihood decoding the error probability $\tilde{\pi}_{k,n}$ of a code word satisfies

$$\tilde{\pi}_{k,n} \leq 2^{-l(R_0(\gamma_{k,n}, A_n) - R_n \log_2 A_n)}. \quad (3.4)$$

In order to apply this upper bound on code word error probability to the extensively used turbo decoded convolutional code, quantitative investigations have been done in [11] and an expression for the *equivalent block length* is derived based on link level simulations. The result from [11] shows that the performance of a turbo decoded convolutional code of rate R_n applied to B_n information bits in a very good approximation equals the performance of a block code with block length

$$n_{\text{eq}} = \beta_{n_{\text{eq}}} \ln L_n, \quad (3.5)$$

where $L_n = B_n/R_n$ and parameter $\beta_{n_{\text{eq}}}$ is used to adapt this model to the specifics of the employed turbo code. In our situation L_n can be plugged in with the number of bits contained in one TTI on subchannel n , *i.e.*, $L_n = N_s N_c \log_2 A_n$. Consequently, the transmission of L_n bits is equivalent to the sequential transmission of L_n/n_{eq} blocks of length n_{eq} and has an error rate of

$$\begin{aligned} \pi_{k,n} &= 1 - (1 - \tilde{\pi}_{k,n})^{\frac{L_n}{n_{\text{eq}}}} \\ &\leq 1 - \left(1 - 2^{-n_{\text{eq}}(R_0(\gamma_{k,n}, A_n) - R_n \log_2 A_n)} \right)^{\frac{L_n}{n_{\text{eq}}}}. \end{aligned} \quad (3.6)$$

Protocol At the MAC layer an *automatic repeat request* (ARQ) protocol is employed. The data sequence transmitted in one MAU, which will be referred to as a *subpacket*, is used as the retransmission unit since it is independently decodable. We set no limit on the maximum number of retransmissions and consider the case where the corrupted subpackets are simply abandoned at the receiver, *i.e.*, no Hybrid ARQ.

Denote the set of subchannels assigned to packet k as \mathcal{S}_k , and the number of information bits from packet k loaded on subchannel n as $b_{k,n}$. The completeness of the transmission of packet k requires

$$\sum_{n \in \mathcal{S}_k} b_{k,n} = b_k. \quad (3.7)$$

On the other hand, the latency time τ_k is obviously determined by the largest subpacket error rate of packet k , denoted by $\pi_k = \max_{n \in \mathcal{S}_k} \pi_{k,n}$. Assuming that the subpacket error

probability of a retransmitted subpacket is the same as that of its original transmission, then $f_k[m] = \pi_k^{m-1}(1 - \pi_k)$ becomes a geometric series with ratio π_k , and

$$\sum_{m=1}^M f_k[m] = 1 - \pi_k^M \geq 1 - \pi^{(\text{out})} \quad (3.8)$$

implies that for packet k , the number of transmissions needed to keep the outage probability below $\pi^{(\text{out})}$ is

$$M_k = \left\lceil \frac{\ln \pi^{(\text{out})}}{\ln \pi_k} \right\rceil. \quad (3.9)$$

The latency time τ_k then follows from its definition.

3.2.2.2 Resource Allocation Algorithm

Due to the exclusive assignment of subchannels and the discrete MCS levels that are available, the transmit power minimization problem is combinatorial and computationally intractable when the number of subchannels and the number of users are large. Therefore we proposed a suboptimal algorithm of low complexity in D6.1, which first looks for the optimal subchannel assignment with fixed MCS on each subchannel, and then chooses the MCS combination that leads to the minimum transmit power required with the obtained subchannel assignment. The algorithm allows for an adjustment phase in which the subchannel assignment could be amended.

3.2.2.3 Adaptive subchannel size

As one subchannel can be assigned to at most one packet, the number of subchannels is practically a hard limit on the number of packets that the system could serve. However, the MAU's may be under utilized if the loaded packets are small. In other words, to fix the number of subchannels, or equivalently, to fix the size of each subchannel is inefficient, especially when the lengths of input packets vary greatly. Consequently, in order to better adapt to diverse traffic situations resulting in different number and different lengths of input packets, we make the number of subcarriers that make up one subchannel, *i.e.*, N_c , also an optimization variable.

Beside the possibility to serve more packets, the advantages of a small subchannel size also include having a finer frequency granularity and benefiting from multiuser diversity. On the other hand, a large subchannel size leads to more data symbols in one MAU which potentially provides a larger coding gain, as well as reduces the computations required to find a suboptimal resource allocation strategy. Based on these analysis, the optimal N_c should depend on the frequency selectivity of the channel and the input packet list. Note that in addition to the computational effort to find the optimal N_c , the performance gain of having N_c adaptive comes also at the cost of an extra overhead of a few bits to inform the receiver the value of N_c .

Since the channel should be assumed constant over each MAU, the bandwidth of one subchannel can not exceed the coherence bandwidth of the multipath channel, *i.e.*,

$\Delta f \cdot N_c \leq B^{(\text{coh})}$, where Δf and $B^{(\text{coh})}$ denote the subcarrier spacing and the coherence bandwidth of the channel respectively. Hence $\lceil \frac{B^{(\text{coh})}}{\Delta f} \rceil$ provides an upper bound for N_c . On the other hand, it is usually unnecessary and impractical to have a very high frequency resolution which requires more iterations to find the optimum N_c . As a result, an appropriate interval for two consecutive candidate N_c values should be set, which mainly depends on the ratio between pilot subcarriers and data subcarriers. Denote this interval as $N^{(l)}$, and determine the largest and smallest candidate values for N_c as \bar{N}_c and \underline{N}_c . The search for optimum N_c for a given packet list is summarized in Algorithm 2.

Algorithm 2 Search for optimum N_c given a packet list

```

Initialize  $N_c \leftarrow \bar{N}_c$ ,  $P_{\min} \leftarrow \infty$ 
 $P \leftarrow$  minimum transmit power to serve the list given ( $N_c$ )
while  $P < P_{\min}$  and  $N_c > \underline{N}_c$  do
     $P_{\min} \leftarrow P$ ,  $N_c \leftarrow N_c - N^{(l)}$ 
     $P \leftarrow$  minimum transmit power to serve the list given ( $N_c$ )
end while

```

3.2.2.4 CFO models and Compensation for interference

Despite their well-known advantages such as the ability to support high data rates and robustness, one of the main drawbacks of multicarrier systems is their sensitivity to synchronization errors in the frequency domain, *i.e.*, the existence of a carrier frequency offset (CFO), which can be caused by Doppler shift, the inherent difference between the oscillators at the transmitter and receiver side, *etc.* In this section we first summarize and derive the CFO models in both CP-OFDM and FBMC systems, which include formulating and computing the interference and SNR degradation caused by the CFO, and then discuss the method to compensate for this degradation in the resource allocation procedure.

Since we are investigating the interference situation at one receiver in the downlink, the user index k is dropped in this section. Also, the subscript n in this section indicates the subcarrier index instead of the subchannel index as in the previous sections. For both systems, we denote the normalized CFO as ε which is the CFO between the transmitter and the receiver with respect to the subcarrier spacing, *i.e.*,

$$\varepsilon \triangleq \frac{f_T - f_R}{1/NT} = (f_T - f_R)NT, \quad (3.10)$$

where f_T and f_R are the carrier frequencies of the transmitter and receiver respectively, N is the number of subcarriers and T is the sampling period. In addition, we assume that there is also a phase offset ϕ between the transmitter and the receiver, and the system is perfectly synchronized in the time domain. Further more, we restrict ε to be in the range $(-0.5, 0.5]$, as the integer part of the frequency offset does not affect the SINR.

CP-OFDM System Due to the insertion of cyclic prefix (CP), data transmission in

OFDM system is independent from block to block which consists of N samples and the CP. Let the modulated data symbols in the k th block be $\mathbf{x}[k] \in \mathbb{C}^N$. The transmitted vector before the insertion of the CP is given by

$$\mathbf{y}[k] = \mathbf{F}^H \mathbf{x}[k], \quad (3.11)$$

where $\mathbf{F} \in \mathbb{C}^{N \times N}$ is the DFT matrix. Let the length of the CP be N_p . The distortion introduced by the CFO to the m th sample in the block is [12]

$$e^{j[2\pi(f_T - f_R)[m+k(N+N_p)]T + \phi]} = e^{j\phi} \cdot e^{j2\pi\epsilon k(1 + \frac{N_p}{N})} \cdot e^{j2\pi\frac{\epsilon m}{N}}. \quad (3.12)$$

As a result, the effect of CFO can be formulated into a diagonal matrix as

$$\mathbf{C}[k] = e^{j\phi} \cdot e^{j2\pi\epsilon k(1 + \frac{N_p}{N})} \cdot \text{diag}\{1, e^{j2\pi\frac{\epsilon}{N}}, \dots, e^{j2\pi\frac{\epsilon(N-1)}{N}}\}, \quad (3.13)$$

and the received signal after the removal of the CP is given by

$$\hat{\mathbf{y}}[k] = \mathbf{C}[k] \mathbf{H}[k] \mathbf{y}[k] + \boldsymbol{\eta}[k], \quad (3.14)$$

where $\mathbf{H}[k] \in \mathbb{C}^{N \times N}$ contains the channel impulse response of the block and is a circulant matrix due to the CP, and $\boldsymbol{\eta}[k]$ represents the additive white Gaussian noise at the receiver.

If no compensation of the CFO is considered before the DFT at the receiver, the received symbols in the frequency domain are given by

$$\begin{aligned} \hat{\mathbf{x}}[k] &= \mathbf{F} \mathbf{C}[k] \mathbf{H}[k] \mathbf{F}^H \mathbf{x}[k] + \mathbf{F} \boldsymbol{\eta}[k] \\ &= \mathbf{F} \mathbf{C}[k] \mathbf{F}^H \boldsymbol{\Lambda}[k] \mathbf{F} \mathbf{F}^H \mathbf{x}[k] + \mathbf{F} \boldsymbol{\eta}[k] \\ &= \mathbf{U}[k] \boldsymbol{\Lambda}[k] \mathbf{x}[k] + \mathbf{F} \boldsymbol{\eta}[k], \end{aligned}$$

where $\boldsymbol{\Lambda}[k] \in \mathbb{C}^{N \times N}$ is a diagonal matrix containing the DFT of the channel impulse response and $\mathbf{U}[k] \in \mathbb{C}^{N \times N}$ is a circulant matrix defined by

$$\mathbf{U}[k] = e^{j\phi} e^{j2\pi\epsilon k(1 + \frac{N_p}{N})} \begin{bmatrix} \nu_N(\epsilon, 0) & \nu_N(\epsilon, N-1) & \cdots & \nu_N(\epsilon, 1) \\ \nu_N(\epsilon, 1) & \nu_N(\epsilon, 0) & \cdots & \nu_N(\epsilon, 2) \\ \vdots & \vdots & \ddots & \vdots \\ \nu_N(\epsilon, N-1) & \nu_N(\epsilon, N-2) & \cdots & \nu_N(\epsilon, 0) \end{bmatrix}, \quad (3.15)$$

where $\nu_N(\epsilon, n) = \frac{1}{N} \frac{\sin(\pi(\epsilon - n))}{\sin \frac{\pi(\epsilon - n)}{N}} e^{j\pi \frac{(\epsilon - n)(N-1)}{N}}$.

From (3.15) it can be seen that the symbol detected on subcarrier n is scaled in magnitude by $|\nu_N(\epsilon, 0)|$, rotated by $e^{j(\phi + \arg H_n)} e^{j2\pi\epsilon k(1 + \frac{N_p}{N})} e^{j\pi \frac{\epsilon(N-1)}{N}}$, and further interfered by received symbols on the other subcarriers scaled by the corresponding off-diagonal elements of $\boldsymbol{\Lambda}[k] \mathbf{U}[k]$. Since the phase rotation does not affect any signal power, we will from now

on drop the rotation term as well as the block index k . The expectation of intercarrier interference (ICI) power on the n th subcarrier can be computed as

$$\begin{aligned} I_n &= \mathbf{E} \left[\left| \sum_{\substack{n'=0 \\ n' \neq n}}^{N-1} \nu_N(\varepsilon, n' - n) H_{n'} x_{n'} \right|^2 \right] \\ &= \sum_{\substack{n'=0 \\ n' \neq n}}^{N-1} |\nu_N(\varepsilon, n' - n)|^2 |H_{n'}|^2 \mathbf{E}[|x_{n'}|^2] = \sum_{\substack{n'=0 \\ n' \neq n}}^{N-1} |\nu_N(\varepsilon, n' - n)|^2 |H_{n'}|^2 p_{n'}, \end{aligned}$$

where the second equality follows as the data symbols on each subcarrier are assumed independent from each other, and here $p_{n'}$ denotes the power allocated on the n' th subcarrier, which equals $\frac{1}{N_c}$ of the power allocated to that subchannel. The signal-to-interference-plus-noise ratio (SINR) on the n th subcarrier can therefore be expressed as

$$\gamma_n = \frac{|\nu_N(\varepsilon, 0)|^2 |H_n|^2 \mathbf{E}[|x_n|^2]}{I_n + \mathbf{E}[|\mathbf{F}\boldsymbol{\eta}|^2]} = \frac{|\nu_N(\varepsilon, 0)|^2 |H_n|^2 p_n}{I_n + \sigma_n^2}, \quad (3.16)$$

where the second equality holds as the DFT operation does not change the power of the noise.

FBMC System For the ease of computation and comparison with CP-OFDM system, we use here the root-raise cosine (RRC) filter $p(t)$ of roll-off factor 1 as the prototype filter, which has the frequency response

$$H_{\text{RRC}}(f) = \begin{cases} \sqrt{T} \cos \frac{\pi T f}{2}, & 0 \leq |f| \leq \frac{1}{T}, \\ 0, & |f| > \frac{1}{T}. \end{cases}$$

With offset QAM (OQAM), the transmit signal $s(t)$ is given by

$$\begin{aligned} s(t) &= \sum_{n'=0}^{N-1} \sum_{l'=-\infty}^{+\infty} d_{n',l'} \theta_{n',l'} p(t - l' \frac{T}{2}) e^{j2\pi \frac{n'}{T} (t - l' \frac{T}{2})} \\ &= \sum_{n'=0}^{N-1} \sum_{l'=-\infty}^{+\infty} d_{n',l'} \lambda_{n',l'} p(t - l' \frac{T}{2}) e^{j2\pi \frac{n'}{T} t}, \end{aligned} \quad (3.17)$$

where n' is the subcarrier index, l' is the symbol index in the data sequence, $\theta_{n',l'} = j^{n'+l'}$, $\lambda_{n',l'} = \theta_{n',l'} e^{-j\pi n' l'}$, and $d_{n',l'} \in \mathbb{R}$ is alternatively the real or imaginary part of the QAM symbol loaded on the n' th subcarrier.

The received signal, $r(t)$, is the transmit signal convolved with the channel impulse response $h(t)$, corrupted by the AWGN $\eta(t)$ at the front end of the receiver, and then effected by the CFO ε and the phase offset ϕ , *i.e.*,

$$r(t) = (h(t) \otimes s(t) + \eta(t)) \cdot e^{j(2\pi \frac{\varepsilon}{T} t + \phi)}. \quad (3.18)$$

It is then passed through the AFB and sampled at each output at sampling rate $\frac{2}{T}$. The detected symbol on the n th subcarrier at time index l , namely $\hat{d}_{n,l}$, is therefore expressed as

$$\begin{aligned}\hat{d}_{n,l} &= \Re \left\{ \lambda_{n,l}^* \cdot (r(t) \cdot e^{-j2\pi \frac{n}{T}t}) \otimes \tilde{p}(t) \Big|_{t=l \cdot \frac{T}{2}} \right\} \\ &= \Re \left\{ \lambda_{n,l}^* \cdot \left((h(t) \otimes s(t) + \eta(t)) \cdot e^{j(2\pi \frac{\varepsilon-n}{T}t + \phi)} \right) \otimes \tilde{p}(t) \Big|_{t=l \cdot \frac{T}{2}} \right\} \\ &= \Re \left\{ \lambda_{n,l}^* \cdot e^{j\phi} \left(x(t) \cdot e^{j2\pi \frac{\varepsilon-n}{T}t} \right) \otimes \tilde{p}(t) \Big|_{t=l \cdot \frac{T}{2}} \right\} + \\ &\quad \Re \left\{ \lambda_{n,l}^* \cdot e^{j\phi} \left(\eta(t) \cdot e^{j2\pi \frac{\varepsilon-n}{T}t} \right) \otimes \tilde{p}(t) \Big|_{t=l \cdot \frac{T}{2}} \right\},\end{aligned}$$

where $x(t) = h(t) \otimes s(t)$ and $\tilde{p}(t)$ is the matched filter of $p(t)$ which is known to be $p(t)$ itself. Note that we use \otimes to denote the convolution operation and $*$ to denote the complex conjugate operation.

The frequency response of $x(t)$ reads

$$X(f) = \sum_{n'=0}^{N-1} \sum_{l'=-\infty}^{+\infty} d_{n',l'} \lambda_{n',l'} H(f) e^{-j2\pi l' \frac{T}{2} f} H_{\text{RRC}}(f - \frac{n'}{T}), \quad (3.19)$$

where $H(f)$ represents the frequency response of the wireless channel, and we have

$$\begin{aligned}\left(x(t) \cdot e^{j2\pi \frac{\varepsilon-n}{T}t} \right) \otimes \tilde{p}(t) \Big|_{t=l \cdot \frac{T}{2}} &= \int_{-\infty}^{+\infty} e^{j2\pi l \frac{T}{2} f} X(f - \frac{\varepsilon-n}{T}) H_{\text{RRC}}(f) df \\ &= \sum_{n'=0}^{N-1} \sum_{l'=-\infty}^{+\infty} d_{n',l'} \lambda_{n',l'} w_n(\varepsilon, \Delta n, \Delta l),\end{aligned} \quad (3.20)$$

where $\Delta n = n - n'$, $\Delta l = l - l'$, and $w_n(\varepsilon, \Delta n, \Delta l)$ is defined as

$$w_n(\varepsilon, \Delta n, \Delta l) \stackrel{!}{=} \int_{-\infty}^{+\infty} e^{j\pi \Delta l T f} H(f - \frac{\varepsilon-n}{T}) H_{\text{RRC}}(f - \frac{\varepsilon-\Delta n}{T}) H_{\text{RRC}}(f) df.$$

Note that $H_{\text{RRC}}(f)$ is only nonzero for $f \in [-\frac{1}{T}, \frac{1}{T}]$, and $H_{\text{RRC}}(f - \frac{\varepsilon-\Delta n}{T})$ is a shifted version of $H_{\text{RRC}}(f)$. As a result, $w_n(0, \Delta n, \Delta l) = 0$ when $|\Delta n| > 1$, *i.e.*, only the immediately adjacent subcarriers contribute to the interference when there is no CFO. With a nonzero ε , one of the secondly adjacent subcarriers also interferes.

In the following we assume that the channel is flat over each subcarrier due to equalization. Consequently, within the bandwidth of one subcarrier the channel frequency response is a constant and can be taken out of the integral operation. Let the channel coefficient on subcarrier n be H_n . Given normalized CFO ε , subcarrier offset Δn and symbol offset Δl ,

the defined integral $I(b_1, b_2)$ has the following analytical expression

$$\begin{aligned}
 I(b_1, b_2) &\stackrel{!}{=} \int_{\frac{b_2}{T}}^{\frac{b_1}{T}} e^{j\pi\Delta l T f} H_{\text{RRC}}(f - \frac{\varepsilon - \Delta n}{T}) \cdot H_{\text{RRC}}(f) df \\
 &= \frac{b_1 - b_2}{2} \cdot e^{j\pi\Delta l \frac{b_1+b_2}{2}} \cdot \left[\cos \pi \frac{\varepsilon - \Delta n}{2} \cdot \text{sinc} \left(\Delta l \cdot \frac{b_1 - b_2}{2} \right) \right. \\
 &\quad + \frac{1}{2} e^{j\pi(\frac{b_1+b_2}{2} - \frac{\varepsilon - \Delta n}{2})} \cdot \text{sinc} \left((\Delta l + 1) \cdot \frac{b_1 - b_2}{2} \right) \\
 &\quad \left. + \frac{1}{2} e^{-j\pi(\frac{b_1+b_2}{2} - \frac{\varepsilon - \Delta n}{2})} \cdot \text{sinc} \left((\Delta l - 1) \cdot \frac{b_1 - b_2}{2} \right) \right].
 \end{aligned}$$

As a result, the unbounded integral w_n can be expressed and conveniently computed as the sum of several bounded integrals, *i.e.*, when $\varepsilon > 0$,

$$\begin{aligned}
 w_n(\varepsilon, 0, \Delta l) &= H_{n-1}I(\varepsilon - \frac{1}{2}, \varepsilon - 1) + H_n I(\varepsilon + \frac{1}{2}, \varepsilon - \frac{1}{2}) + H_{n+1}I(1, \varepsilon + \frac{1}{2}) \\
 w_n(\varepsilon, -1, \Delta l) &= H_n I(\varepsilon + \frac{1}{2}, \varepsilon) + H_{n+1}I(1, \varepsilon + \frac{1}{2}) \\
 w_n(\varepsilon, 1, \Delta l) &= H_{n-1}I(\varepsilon - \frac{1}{2}, -1) + H_n I(\varepsilon, \varepsilon - \frac{1}{2}) \\
 w_n(\varepsilon, 2, \Delta l) &= H_{n-1}I(\varepsilon - 1, -1),
 \end{aligned}$$

and when $\varepsilon < 0$,

$$\begin{aligned}
 w_n(\varepsilon, 0, \Delta l) &= H_{n-1}I(\varepsilon - \frac{1}{2}, -1) + H_n I(\varepsilon + \frac{1}{2}, \varepsilon - \frac{1}{2}) + H_{n+1}I(\varepsilon + 1, \varepsilon + \frac{1}{2}) \\
 w_n(\varepsilon, 1, \Delta l) &= H_{n-1}I(\varepsilon - \frac{1}{2}, -1) + H_n I(\varepsilon, \varepsilon - \frac{1}{2}) \\
 w_n(\varepsilon, -1, \Delta l) &= H_n I(\varepsilon + \frac{1}{2}, \varepsilon) + H_{n+1}I(1, \varepsilon + \frac{1}{2}) \\
 w_n(\varepsilon, -2, \Delta l) &= H_{n+1}I(1, \varepsilon + 1),
 \end{aligned}$$

where in each equation, the parameters $\varepsilon, \Delta n$ and Δl from w_n apply to the integrals I .

Consequently, the detected symbol $\hat{d}_{n,l}$ can be expressed as

$$\begin{aligned}
\hat{d}_{n,l} &= \Re \left\{ \lambda_{n,l}^* e^{j\phi} \sum_{n'=0}^{N-1} \sum_{l'=-\infty}^{+\infty} d_{n',l'} \lambda_{n',l'} w_n(\varepsilon, \Delta n, \Delta l) \right\} + \\
&\quad \Re \left\{ \lambda_{n,l}^* \cdot e^{j\phi} \left(\eta(t) \cdot e^{j2\pi \frac{\varepsilon-n}{T} t} \right) \otimes \tilde{p}(t) \Big|_{t=l \cdot \frac{T}{2}} \right\} \\
&= d_{n,l} \cdot \Re \{ e^{j\phi} w_n(\varepsilon, 0, 0) \} + \\
&\quad \sum_{\substack{l'=-\infty \\ l' \neq l}}^{+\infty} d_{n,l'} \cdot \Re \{ \lambda_{n,l}^* \lambda_{n,l'} e^{j\phi} w_n(\varepsilon, 0, l-l') \} + \\
&\quad \sum_{\substack{n'=0 \\ n' \neq n}}^{N-1} \sum_{l'=-\infty}^{+\infty} d_{n',l'} \cdot \Re \{ \lambda_{n,l}^* \lambda_{n',l'} e^{j\phi} w_n(\varepsilon, n-n', l-l') \} + \\
&\quad \Re \left\{ \lambda_{n,l}^* \cdot e^{j\phi} \left(\eta(t) \cdot e^{j2\pi \frac{\varepsilon-n}{T} t} \right) \otimes \tilde{p}(t) \Big|_{t=l \cdot \frac{T}{2}} \right\},
\end{aligned}$$

where after the second equality, the first term indicates the desired signal, the second term represents the intersymbol interference (ISI) on the same subcarrier, the third term represents the ICI + ISI from all symbols on the other subcarriers, and the last term indicates the effect of noise to the detected symbol.

From the equations it can be seen that unlike in CP-OFDM system, the phase offset has an influence on the signal power due to the real operation. Yet via detecting the pilot symbols the receiver should be able to estimate ϕ , and therefore in the following we assume that ϕ is perfectly corrected at the receiver. The expected interference power to

$d_{n,l}$, denoted as $I_{n,l}$, and the SINR for the symbol are given by

$$\begin{aligned}
I_{n,l} &= \mathbf{E} \left[\left| \sum_{\substack{l'=-\infty \\ l' \neq l}}^{+\infty} d_{n,l'} \cdot \Re \{ \lambda_{n,l}^* \lambda_{n,l'} w_n(\varepsilon, 0, l - l') \} + \right. \right. \\
&\quad \left. \left. \sum_{\substack{n'=0 \\ n' \neq n}}^{N-1} \sum_{l'=-\infty}^{+\infty} d_{n',l'} \cdot \Re \{ \lambda_{n,l}^* \lambda_{n',l'} w_n(\varepsilon, n - n', l - l') \} \right|^2 \right] \\
&= \sum_{\substack{l'=-\infty \\ l' \neq l}}^{+\infty} \mathbf{E} [|d_{n,l'}|^2] |\Re \{ \lambda_{n,l}^* \lambda_{n,l'} w_n(\varepsilon, 0, l - l') \}|^2 + \\
&\quad \sum_{\substack{n'=0 \\ n' \neq n}}^{N-1} \sum_{l'=-\infty}^{+\infty} \mathbf{E} [|d_{n',l'}|^2] |\Re \{ \lambda_{n,l}^* \lambda_{n',l'} w_n(\varepsilon, n - n', l - l') \}|^2 \\
&= \sum_{\substack{l'=-\infty \\ l' \neq l}}^{+\infty} \frac{p_n}{2} |\Re \{ \lambda_{n,l}^* \lambda_{n,l'} w_n(\varepsilon, 0, l - l') \}|^2 + \\
&\quad \sum_{\substack{n'=0 \\ n' \neq n}}^{N-1} \sum_{l'=-\infty}^{+\infty} \frac{p_{n'}}{2} |\Re \{ \lambda_{n,l}^* \lambda_{n',l'} w_n(\varepsilon, n - n', l - l') \}|^2, \\
\gamma_{n,l} &= \frac{\mathbf{E} [|d_{n,l}|^2] |w_n(\varepsilon, 0, 0)|^2}{I_{n,l} + \mathbf{E} \left[\left| \Re \left\{ \lambda_{n,l}^* \left(\eta(t) \cdot e^{j2\pi \frac{\varepsilon-n}{T} t} \right) \otimes \tilde{p}(t) \Big|_{t=l \cdot \frac{T}{2}} \right\} \right|^2 \right]} \\
&= \frac{p_n}{2I_{n,l} + \sigma_n^2},
\end{aligned} \tag{3.21}$$

$$\begin{aligned}
\gamma_{n,l} &= \frac{\mathbf{E} [|d_{n,l}|^2] |w_n(\varepsilon, 0, 0)|^2}{I_{n,l} + \mathbf{E} \left[\left| \Re \left\{ \lambda_{n,l}^* \left(\eta(t) \cdot e^{j2\pi \frac{\varepsilon-n}{T} t} \right) \otimes \tilde{p}(t) \Big|_{t=l \cdot \frac{T}{2}} \right\} \right|^2 \right]} \\
&= \frac{p_n}{2I_{n,l} + \sigma_n^2},
\end{aligned} \tag{3.22}$$

where again the independence between the data symbols is applied, and it is assumed that the power allocated to the subcarrier stays the same. This assumption of course does not always hold true, but a closer study on $|w_n(\varepsilon, \Delta n, \Delta l)|^2$ shows that when ε is very small, the function value becomes negligible quite fast with increasing Δl . For example, when $\varepsilon = 0.02$, only the two immediately adjacent symbols, *i.e.*, $\Delta l = \pm 1$, contribute a nontrivial interference to the detected symbol. Therefore the assumption is in general valid which simplifies the calculation of the power allocation.

Compensation of residual CFO With the aid of pilot symbols, the receiver estimates and compensates for the CFO. However, this compensation could be imperfect even in the downlink, and the system should be able to live with the residual CFO. From the resource allocation point of view, what is obtained from subchannel assignment and MCS selection

is now a required SINR instead of a required SNR, which has a general form of

$$\gamma_n^{(\text{rq})} = \frac{a_{n,n}p_n}{\sum_{n' \neq n} a_{n,n'}p_{n'} + \sigma^2}.$$

Stacking all N equations together, we have a set of linear equations the solution of which gives the power allocation that is able to achieve all required SINR values on every sub-carrier, *i.e.*,

$$\mathbf{p} = \begin{bmatrix} a_{0,0} & -a_{0,1} & \cdots & -a_{0,N-1} \\ -a_{1,0} & a_{1,1} & \cdots & -a_{1,N-1} \\ \vdots & \vdots & \ddots & \vdots \\ -a_{N-1,0} & -a_{N-1,1} & \cdots & a_{N-1,N-1} \end{bmatrix}^{-1} \cdot \sigma^2 \begin{bmatrix} \gamma_0^{(\text{rq})} \\ \gamma_1^{(\text{rq})} \\ \vdots \\ \gamma_{N-1}^{(\text{rq})} \end{bmatrix}.$$

Note that at the transmitter, the worst case residual CFO is assumed for compensation, yet in the subchannel assignment and MCS selection phase the impact of a residual CFO is neglected.

3.2.2.5 Simulation Results

The system parameters used in simulations are listed in Tab. 3.2. It should be noted that due to the less out-of-band emission it generates and the absence of CP, the FBMC system can employ more subcarriers (5% more than CP-OFDM is assumed) and more symbols per TTI (12.5% more than CP-OFDM is assumed which is a common fraction of CP to the number of data samples) for data transmission. Moreover, we model the wireless channel as a frequency-selective fading channel consisting of 6 independent Rayleigh multipaths with an exponentially decaying power profile. The delay spreads are uniformly distributed within $1 \mu\text{s}$, resulting in a rms delay spread of about $0.3 \mu\text{s}$ which is consistent with the assumed channel coherence bandwidth. The path loss in dB is computed as $PL(d) = 140.6 + 35.0 \log_{10} d$ following the COST-Hata model, where d is the distance between MS and BS in km, and the receiver noise level is -174 dBm/Hz .

To test the RA and compare the performances of CP-OFDM and FBMC systems, we design two lists of packets, one list of 40 small packets and the other of 20 larger packets with details given in Tab. 3.3 and Tab. 3.4, and use them as input to the RA. We assume that each packet comes from a different user, where the users are uniformly located in a cell of radius 2 km. The case that there are users with more than one packet to transmit can be easily accommodated.

The two upper figures in Fig. 3.2 show the cumulative distributions of the minimum transmit power of both CP-OFDM and FBMC systems to serve the lists of large and small packets, while the lower figures illustrate the histograms of optimum subchannel size in the corresponding cases. For both packet lists, the FBMC system requires around 1 dBm less transmit power than the CP-OFDM system, which is the result of having more data

Table 3.2: System Parameters

Total bandwidth		10 MHz
Center frequency	f_c	2.5 GHz
FFT size		1024
Transmission Time Interval (TTI)	T_I	2 ms
Round Trip Delay (RTD)	T_R	10 ms
Maximum number of transmissions allowed	\tilde{m}	5
Turbo code dependent parameter	β	32
Outage probability	$\pi^{(\text{out})}$	0.01
Number of data subcarriers in OFDM	N	720
Number of data subcarriers in FBMC	N	756
Number of data symbols per TTI in OFDM	N_s	16
Number of data symbols per TTI in FBMC	N_s	16

Table 3.3: List of small packets

Packet k	b_k / bytes	$\tau_k^{(\text{rq})}$ / ms	Packet k	b_k / bytes	$\tau_k^{(\text{rq})}$ / ms
1 – 20	64	20	21 – 40	128	40

Table 3.4: List of large packets

Packet k	b_k / bytes	$\tau_k^{(\text{rq})}$ / ms	Packet k	b_k / bytes	$\tau_k^{(\text{rq})}$ / ms
1 – 20	64	20	21 – 40	128	40

subcarriers and more data symbols in each TTI. On the other hand, the necessity of having adaptive subchannel size can be shown in the lower figures, where the preference for a larger subchannel size is evident when serving the list of large packets, and when serving the list of small packets, the minimum subchannel size is almost always the optimum.

In Fig. 3.3, the CDF's of the minimum transmit power required for serving the list of large packets after the compensation of residual CFO are drawn, where two maximum residual CFO values $\varepsilon = 0.02$ and $\varepsilon = 0.05$ have been tested and the curves with no

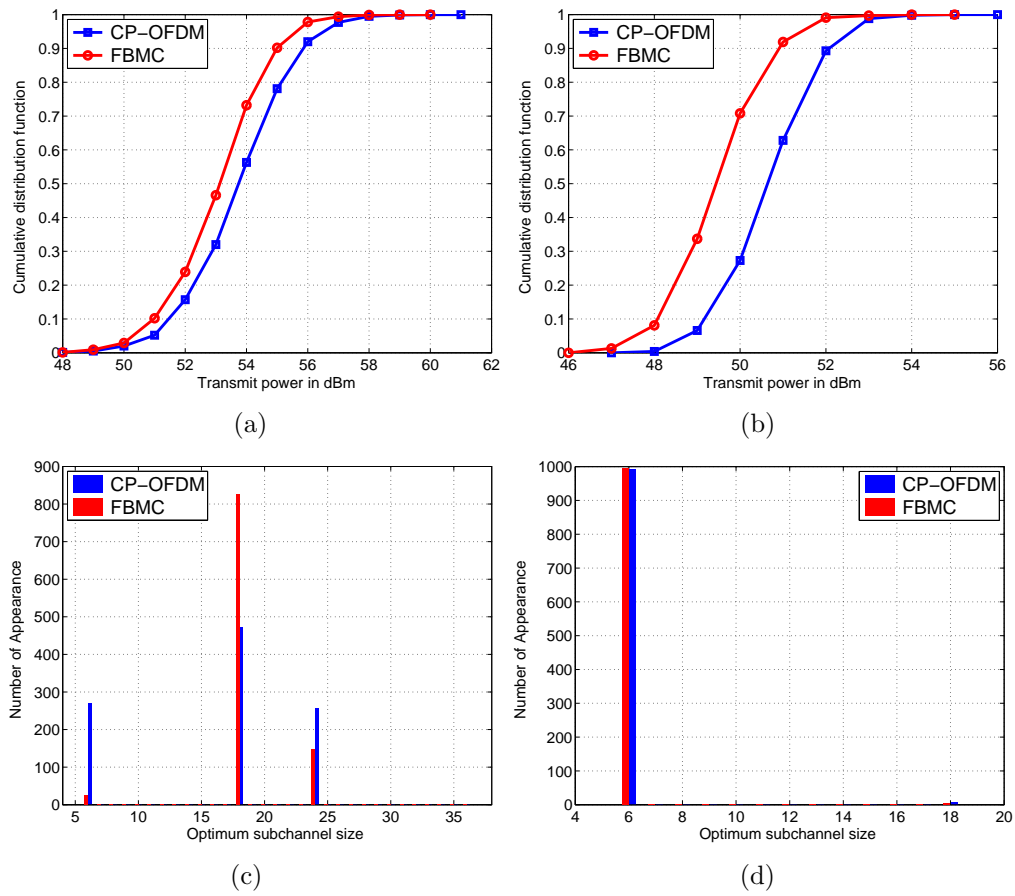


Figure 3.2: CDF of minimum transmit power and histogram of optimum subchannel size for lists of large(left) and small(right) packets from 1000 simulations, without CFO

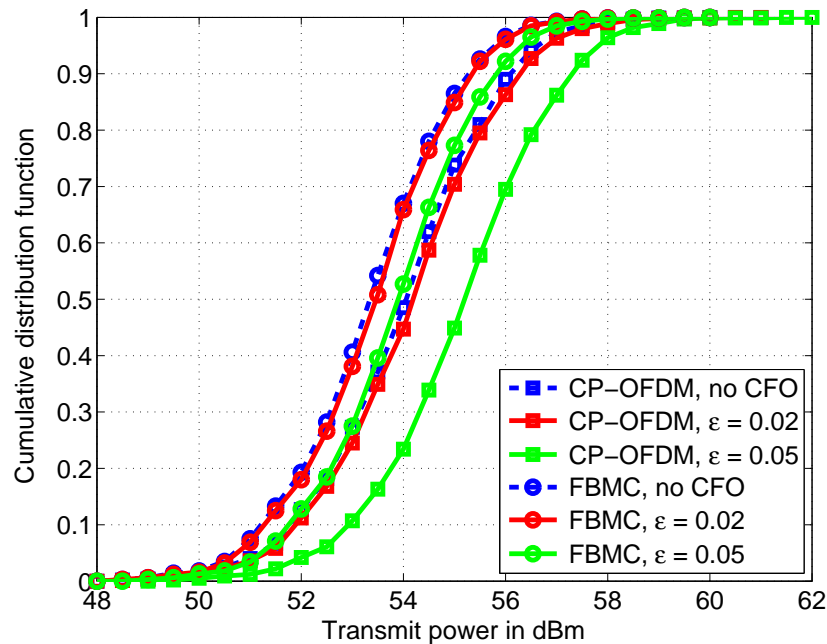


Figure 3.3: CDF of minimum transmit power for the list of large packets

residual CFO are also drawn as a reference. On average, to compensate for the two residual CFO, the CP-OFDM system requires 0.1521 dBm and 1.1612 dBm more transmit power, while the FBMC system requires 0.0794 dBm and 0.5459 dBm more, respectively. **This demonstrates from a QoS provisioning and resource allocation point of view, that the FBMC system is less sensitive to CFO and outperforms the CP-OFDM system, and its advantage is even larger when the CFO increases.**

We would also like to point out that, due to the sufficient frequency granularity the FBMC system provides and the overlapping in time domain during transmission, in our approach we do not consider further partitioning the MAU in time. Another important reason of not doing this is the considerable signalling overhead that could be saved.

3.2.3 Scheduler Design

3.2.3.1 Introduction

Legacy wireless communication systems were providing very few or no adaptation capabilities at all, as a result of the limited transmission requirements they were asked to fulfill. Nowadays, the efficient support of a wide set of network applications under a variety of conditions is considered as one of the most important requirements for modern wireless communication systems. To address this complex issue, different performance improvement mechanisms are introduced in almost all layers of a typical wireless protocol stack. Such mechanisms include the multi-encoding rate functionality at the Application

layer, the adaptive Automatic Repeat Request (ARQ) mechanisms at the Transport layer, the adaptive routing at the Network layer, the adaptive Forward Error Correction (FEC) and appropriate resource allocation at the Medium Access Control (MAC) layer, and the adaptive modulation, coding and power control mechanisms at the Physical (PHY) layer. Although these mechanisms have been initially designed to work independently, there is an increasing need for the development of a scheme that will allow for their efficient co-operation towards optimized system performance. This need emerges from the fact that their independent parallel operation may result in inefficiencies caused mainly by possible conflicting actions.

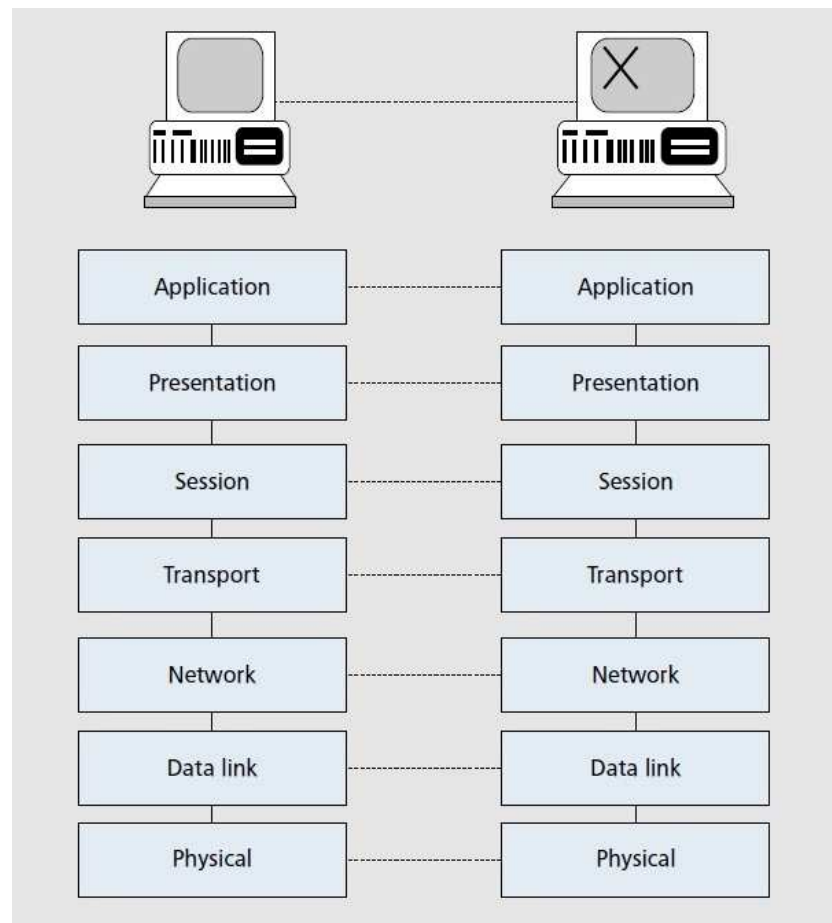


Figure 3.4: The layered OSI architecture

A typical example of inefficient operation is the case of a TCP connection in a path that contains one or more wireless links. In this case, TCP may misinterpret packet errors on the wireless links as indications of congestion and reduce the transmission rate in an attempt to solve the problem. However, in this case, a data rate reduction is not considered as the most appropriate action as it reduces the throughput without facing the actual problem of errors on the wireless link. To overcome this situation, a cross-

layer cooperative mechanism between the MAC and the Transport layers could provide the TCP protocol with the necessary information regarding the nature of the packet losses as either transmission errors on the wireless link or packet losses due to congestion. This way, unnecessary transmission rate reductions could be avoided.

3.2.3.2 Cross-layer for real-time traffic in the recent bibliography

In the recent bibliography we can find a great variety of proposals on cross-layer schemes designed for numerous kinds of wireless networks and applications. In this section cross-layer schemes focusing on Quality of Service (QoS) and throughput improvement and Radio Resource Management (RRM) for real-time traffic are presented.

3.2.3.2.1 Quality of service and throughput improvement A large number of recent proposals on cross-layer design aim at improving the QoS provision and the overall performance of the system they are applied to. Such proposals include rate control algorithms based on the experienced channel conditions that aim to normalize the unpleasant variations of the wireless medium quality. Other mechanisms introduce efficient schemes to avoid unnecessary retransmissions and improve the system throughput. Adaptive coding schemes that take into account both the QoS requirements of the applications and the conditions of the wireless medium are also suggested.

More specifically, the authors in [13] present a general cross-layer feedback architecture for mobile wireless environments. This design uses a “tuning layer” for every layer of the wireless protocol stack. Each tuning layer provides an interface to the data structures that determine the operation of its corresponding protocol layer. The tuning layers are used by “protocol optimizers” that contain the cross-layer optimization algorithm and comprise the “optimization subsystem” that operates concurrently with the wireless protocol stack. Although the authors suggest the introduction of this functionality in all layers, the overall scheme’s purpose is the improvement of the TCP feedback mechanism’s throughput. This is achieved by a) making it aware of the channel quality and rescheduling the retransmissions until the channel conditions improve and b) adjusting the connections’ receiver window according to the applications’ requirements.

[14] presents two cross-layer algorithms, a dual based and a penalty-based one, that address the problem of rate control in a multi-hop random access network. These algorithms are implemented in a distributed manner and work both at the Data-Link layer to adjust transmission attempt probabilities, and at the Transport layer to adjust session rates. The first algorithm updates the transmission attempt probabilities at the Data-Link layer, based on information regarding the mobile node’s neighborhood, while the Transport layer adjusts the session rates based on the link rates computed by the Data-Link layer. In the second algorithm, each session computes its rate based on its contribution to the overall traffic of its path while the Data-Link layer computes the transmission attempt probabilities taking into account its effect on the neighboring nodes. The main objective of both algorithms is the provision of proportional fairness amongst end-to-end sessions.

In [15], the authors study the problem of rate optimization for multicast communications at the MAC layer. The proposed design performs joint optimization of the MAC multicast threshold, i.e., the minimum number of existing ready receivers before a sender decides to transmit packets, and the transmission rate in order to maximize the overall throughput. Additionally, the Transport layer erasure coding is introduced that provides reliable transmissions and avoids retransmissions at the MAC layer. Its use achieves throughput improvement compared to a typical MAC layer mechanism that retransmits lost packets.

3.2.3.2.2 QoS support for multimedia applications A subgroup of this category deals with the support of demanding multimedia applications. The reason for the growing interest in this area is the fact that modern multimedia applications are characterized by strict QoS requirements especially regarding bandwidth, packet loss and latency, and require special handling by the packet-based wireless communication networks that were traditionally designed to support best effort traffic. Thus, cross-layer designs in this area include a) encoding and rate adaptation algorithms for the support of real-time voice and video applications over wireless packet networks, b) adaptive packetization and scheduling algorithms that provide the best possible QoS to multimedia applications given specific wireless channel conditions, and c) algorithms for the efficient support of wireless multicast streaming applications.

For example, [16] deploys an Application layer adaptive packetization, a prioritized scheduler and a MAC layer retransmission scheme for the support of delay-sensitive multimedia over wireless data networks. The aim is to fulfill the rate and delay constraints of the applications and provide resilience against distortion. This is achieved by providing the optimal packetization and retransmission scheme that takes into account information from the Application, MAC and Physical layers. This information includes content characteristics (e.g., signal variance), video encoder features (i.e., compression levels), applications' delay characteristics and channel conditions. The described mechanism achieves performance improvement equal to 2 dB or more in terms of Peak Signal-to-Noise ratio (PSNR) in many video sequences under a variety of transmission conditions.

In [17], information from the Application, MAC and Physical layers is taken into account to propose a cross-layer architecture for adaptive video multicast streaming over multi-rate Wireless Local Area Networks (WLANs). An automatic rate selection mechanism, employed by the access point, is introduced and its mission is the selection of the most appropriate multicast data rate at the Physical and MAC layers, based on the channel conditions perceived by the mobile terminals. Hierarchical video encoders are used at the Application layer, with the ability to adapt the video transmission to the varying channel conditions. Thus, mobile terminals experiencing low channel quality receive only the base layer of the encoded video, while others experiencing favorable conditions receive video enhancement layers. The use of this mechanism achieves performance improvement in terms of video quality, delay, throughput and signaling overhead.

In [18], an architecture for video streaming over IEEE 802.11 (Wi-Fi) networks is pre-

sented. The rate adaptation is performed in the Physical, the MAC layer and the video encoder residing at the Application layer. More specifically, the transmission rate of the MAC layer and the video coding rate at the Application layer can be dynamically adjusted, using channel state and medium sharing information. An entity called channel state predictor performs an estimation of the channel state, while a medium sharing predictor performs link throughput estimation based on the throughput observed during previous transmissions. The transmission rate selected is the one that maximizes the user throughput given specific channel conditions. The use of the described architecture achieves performance improvement in terms of PSNR and packet loss rate.

[19] introduces a cross-layer mechanism for real-time traffic over IEEE 802.16 (WiMAX) networks. This mechanism uses information from the Physical and MAC layers, namely the packet error, the packet timeout rates and the mean delay of real-time applications. It coordinates the adaptive modulation capability at the Physical layer and multi-rate data-encoding capability of modern real-time applications. Its aim is to assist WiMax systems to adapt to frequent channel and traffic changes and results in reduced packet loss rates.

Finally, [20] proposes a cross-layer architecture that performs joint optimization of the Application, Data-Link and Physical layers for the efficient support of wireless video streaming. More specifically, the Physical and Data-Link layers adapt the transmission to the wireless quality variations, while the Application layer takes into consideration the video distortion information and adapts its encoding rate accordingly.

3.2.3.2.3 Radio resource management (RRM) Radio resource management is an issue of great importance in wireless communication networks. The air interface and hardware resources need to be efficiently utilized to achieve increased throughput and channel capacity and avoid unpleasant phenomena such as interference. Several proposals on cross-layer designs regarding RRM can be found in the recent bibliography. The majority of them introduce efficient schemes for power control, resource allocation, admission control and packet scheduling.

In [21] the Data-Link layer performs resource allocation taking into account its impact on the Transport layer. The importance of such a design emerges from the fact that the resource allocation strategy directly influences the performance of TCP and UDP protocols, as it affects the connections' delay and loss rates. Additionally, at the Data-Link layer, the fairness weights for the data traffic are calculated based on cross-layer information from higher layers when scheduling integrated voice/data traffic. The proposed design manages to achieve satisfactory QoS provision and effective MAC scheduling. However, it assumes perfect power control in uplink transmissions, which may be unfeasible in actual cellular networks.

[22] tackles the problem of connection admission control in Code Division Multiple Access (CDMA) networks for multi-service packet traffic. Packet traffic is modeled as a Markov Modulated Poisson Process (MMPP) and connection admission control is performed, taking into account the QoS requirements regarding the Physical layer Signal to Interference Ratio (SIR) and the Network layer blocking probability. Four cross-layer

schemes are proposed, each one providing different levels of QoS guarantees at the Physical and Network layers, network utilization for packet traffic and computational complexity. More specifically, the first algorithm is a linear programming based scheme that maximizes network utilization subject to both SIR and blocking probability constraints. The second algorithm aims at guaranteeing the SIR outage probability. Due to the fact that these algorithms are computationally demanding, two more algorithms are proposed. These algorithms are sub-optimal but computationally efficient and they differ mainly on their capability to guarantee SIR outage probability.

[23] proposes a joint MAC-Physical layer resource management algorithm that performs packet scheduling, subcarrier allocation and power control for wireless Orthogonal Frequency Division Multiplexing (OFDM) networks. The above operations are performed taking into account the interdependencies between the MAC and Physical layers, e.g., the impact of channel state information on the performance of packet scheduling and power allocation. Its aim is the maximization of the system power efficiency and overall performance, guaranteeing in parallel QoS provision and fairness. According to simulation results the described scheme achieves the improved QoS and fairness in a degree similar to the one expected by known wired fair queuing systems, while guaranteeing improved power and spectrum efficiency. However, its performance depends highly on the accuracy of the channel state estimations and QoS provision is negatively affected in cases of imperfect channel state information.

In [24], a cross-layer rate, scheduling and power control scheme for multi-hop wireless networks is considered. The joint design of these operations takes into account information such as the channel contention, physical interference and link capacities. This scheme decomposes the overall problem to the three sub-problems of congestion control, scheduling design and power control. The main goal is to improve system performance, as well as the transparent interaction of TCP congestion control algorithms, link scheduling and transmission power allocation.

3.2.3.3 The cross-layer optimization mechanism

The cross-layer mechanism for real-time traffic over WiMax networks described here is based on the architectural framework introduced in [20], which consists of N layers and a cross-layer optimizer (Figure 3.5).

According to this framework, the optimization process is performed in three steps:

- i. **Layer abstraction:** Computes an abstraction of layer-specific parameters that are processed by the optimizer. This process aims at reducing the overall data processing and communication overhead while maintaining consistency.
- ii. **Optimization:** Determines the values of layer parameters that optimize a specific objective function.
- iii. **Layer reconfiguration:** Distributes the optimal values of the abstracted parameters to the corresponding layers that in turn translate them back into layer-specific

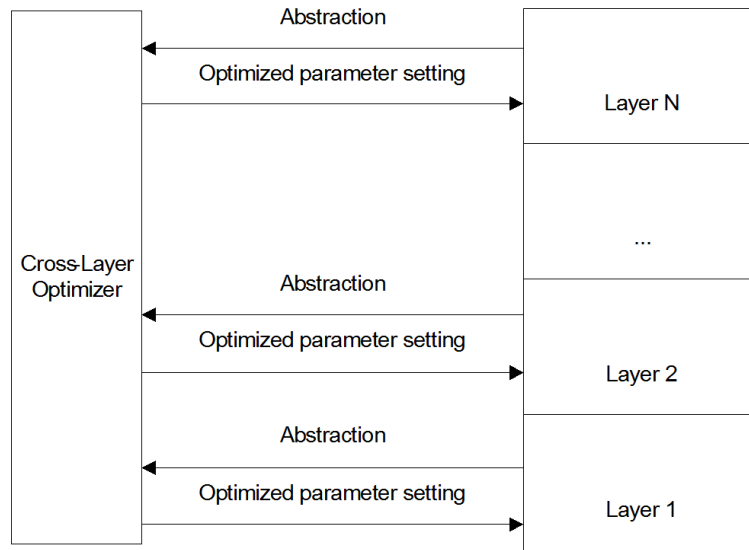


Figure 3.5: General Cross-Layer Architecture

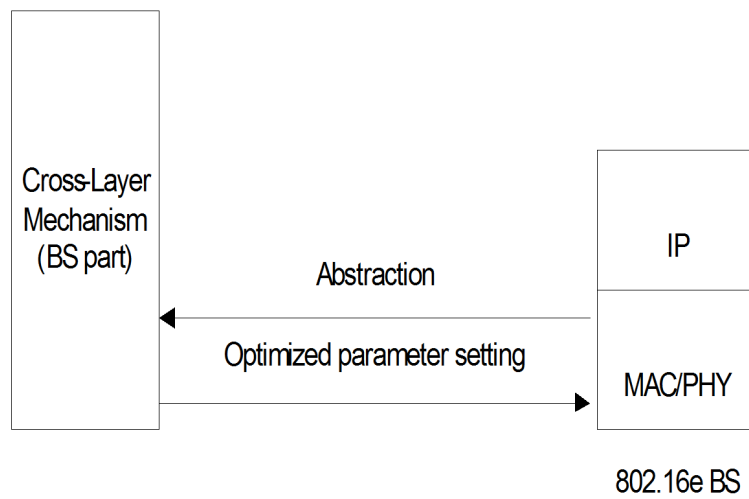
information.

The rate at which the above steps are repeated depends on the variance of the channel conditions and the applications' requirements. In general, the different parameters can be divided in four main types:

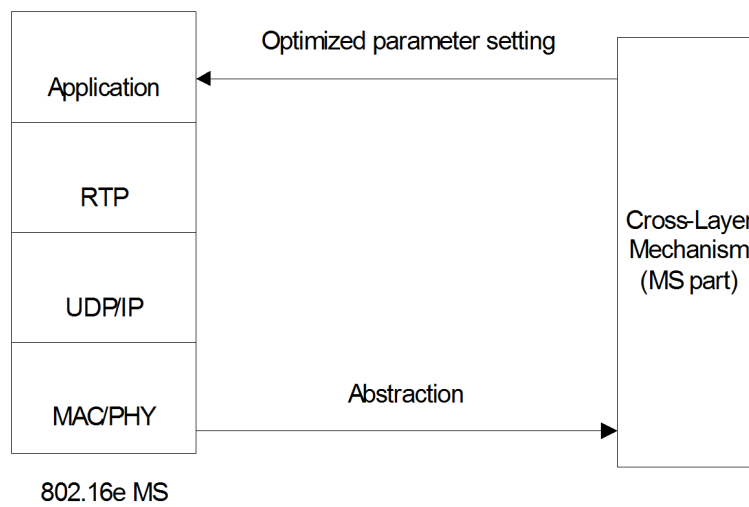
- a. Directly Tunable (DT) parameters that can be directly set as a result of the optimization process.
- b. Indirectly Tunable (IT) parameters that may be modified as a result of the setting of the Directly Tunable parameters.
- c. Descriptive (D) parameters that can only be read but not tuned by the optimizer.
- d. Abstracted (A) parameters that are abstractions of the previous types of parameters.

More details about this framework can be found in [20]. The mechanism described in this section works in three layers, namely the Physical, Data-Link (MAC) and Application layers. The cross-layer mechanism for WiMax networks is split into two parts, namely the Base Station (BS) part and the Mobile Station (MS) part, residing at the BS and the MSs of a WiMax network respectively (Figure 3.6).

The BS part accepts an abstraction of layer-specific information, namely, the channel conditions, QoS parameters and transmission power capabilities of all active connections, provided by the BS PHY and MAC layers (Step 1: Layer Abstraction). According to this information, a decision algorithm determines the desired encoding mode of each MS, separately for each direction (uplink or downlink) (Step 2: Optimization). Finally, the BS



(a)



(b)

Figure 3.6: BS (a) and MS (b) part functionality

part configures the corresponding layers with the determined parameters (Step 3: Layer Reconfiguration) (Figure 3.6a). The MS part may either accept the BS part's suggestions regarding encoding mode adjustments or refine them, based on its better knowledge of the status of the MS's active connections and instruct the MS application layer accordingly (Figure 3.6b).

The system under consideration consists of an IEEE 802.16e (mobile WiMAX) cell [25], managed by a Base Station (BS) and a number of Mobile Stations (MSs) moving within the area of coverage. The cross-layer mechanism is split into two parts, namely the BS part and the MS part, residing at the BS and each MS, respectively. The operation of the cross-layer mechanism (Figure 3.7) for both uplink and downlink directions can be divided in three main phases.

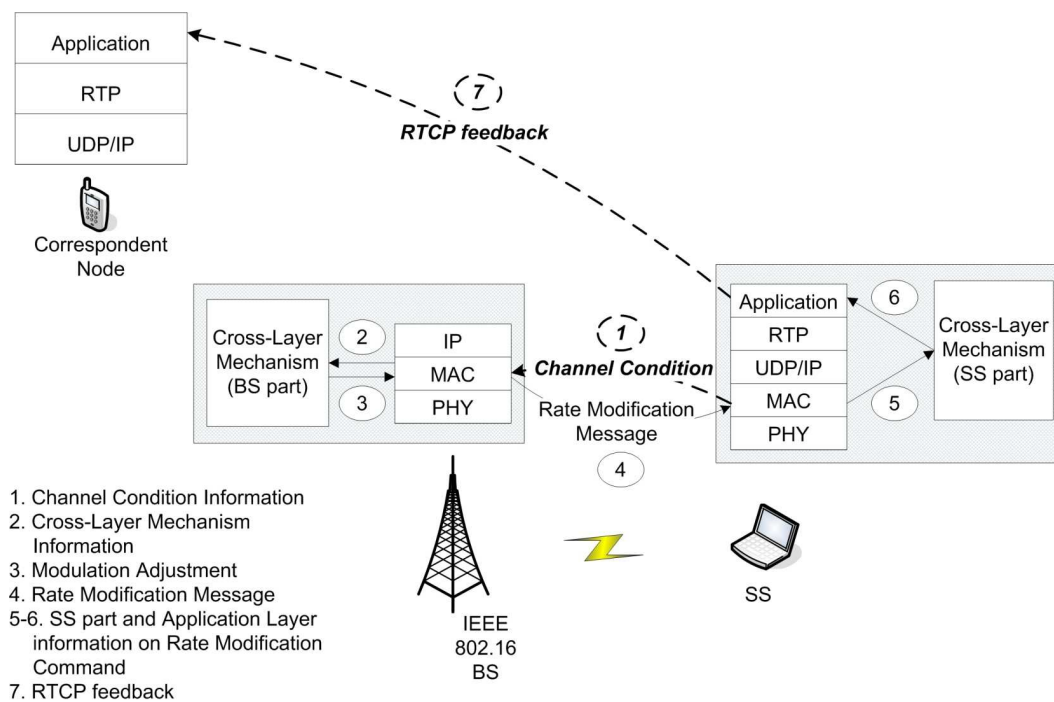


Figure 3.7: Operation Outline

In *Phase 1*, the BS part starts by collecting all the required information regarding the performance status of each of its active connections. This information includes channel state conditions on the uplink and downlink directions, packet timeout rate and mean delay and is provided to the BS as follows:

- i. Channel conditions for the uplink are known from the BS PHY layer. For the downlink, the BS receives channel quality measurements from the MSs using standard IEEE 802.16e signaling either periodically, through the Channel Quality Information Channel (CQICH), or on demand, through the Channel Measurement Report Request and Response (REP-REQ, REP-RSP) messages [REF] (see arrow (1) in Figure 3.7).

- ii. Packet timeout rate and mean delay for all active connections in both directions can be provided by the BS MAC layer (see arrow (2) in Figure 3.7).

In *Phase 2*, the BS part uses the collected information to run a decision algorithm (described below) and decide on the Application layer encoding mode used. This decision is taken separately for each MS aiming at providing an improved QoS.

In *Phase 3*, the BS MAC layer transfers to the MS MAC layer its decisions about encoding mode adjustments. These decisions are transferred using the Rate Adjustment Request (RATE-ADJ-REQ) message defined in [19] (see arrow (4) in Figure 3.7). This message contains the BS part recommendation in the form of a target overall mean media encoding rate.

The MS MAC layer transfers the received rate modification request to the MS part (see arrow (5) in Figure 3.7) that in turn decides on the connections that should be affected and sends proper cross-layer messages to the Application layer (see arrow (6) in Figure 3.7). On the uplink direction, the proper adjustments are performed at the MS Application layer while on the downlink, the traffic source is informed by the MS Application layer for media encoding rate adjustments through a standard Application Layer RTCP Receiver Report (RR) message which is part of the extensions of Real-time Transport Protocol (RTP) for RTCP-based feedback [26] (see arrow (7) in Figure 3.7).

Syntax	Size
RATE-ADJ-REQ_Message_Format() {	
Management Message Type = 67	8 bits
Direction	1 bit
Total Rate Recommended	32 bits
}	

Table 3.5: RATE-ADJ-REQ message

3.2.3.4 Decision algorithm

In this section, the operation of the decision algorithm executed during *Phase 2* in the BS part of the proposed cross-layer mechanism is described. This algorithm takes into account the packet loss rates and mean delay of each connection and decides on the adaptation of the encoding mode at the Application layer. Its aim is to improve the QoS provided to the connections in terms of packet loss rate, throughput and mean delay.

The algorithm is initiated at regular time instances and takes proper adaptation decisions based on the packet loss rate and the mean delay of each connection. The actions to be taken by the decision algorithm are as follows:

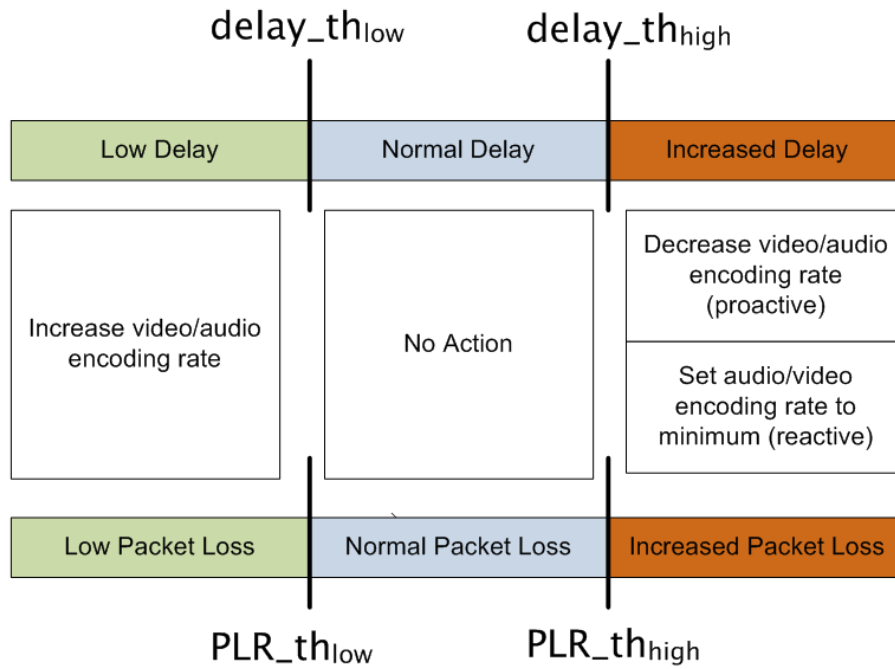


Figure 3.8: Operation of the decision algorithm.

1. In case the Packet Loss Rate (PLR) exceeds the connections maximum PLR threshold, referred to as $\text{PLR_th}_{\text{high}}$ ($\text{PLR} > \text{PLR_th}_{\text{high}}$) the connection is suffering from increased packet loss that significantly deteriorates its QoS. In that case, the BS part decides to set the Application layer encoding mode to its minimum value in order to moderate timeouts and reduce packet losses.
2. In case the mean delay exceeds the connection delay bound, referred to as $\text{delay_th}_{\text{high}}$, ($\text{delay} > \text{delay_th}_{\text{high}}$) the connection is considered to be facing increasing mean delay that may result in packet timeouts. In order to avoid further delay increase and packet timeouts, the decision algorithm instructs for an encoding rate decrease that will reduce the experienced delay.

To achieve an efficient performance under all possible conditions, the algorithm must make adaptation decisions also when the QoS for a specific connection is improved. Thus, when the loss rate and the mean delay decrease significantly, ($\text{PLR} < \text{PLR_th}_{\text{low}}$ and $\text{delay} < \text{delay_th}_{\text{low}}$), the BS part may instructs for an encoding rate increase to improve the QoS provided to the user.

It is worth noting that the performance of such a decision algorithm depends much on the selected delay and loss thresholds, as these can make the operation too sensitive (initiating changing of encodings rates too often), or too insensitive (not initiating changing of encoding rates when needed). As the channel and traffic condition are dynamic, an adaptable thresholds setting would be required for optimal performance.

3.2.3.5 Simulation model

The simulation model was implemented with Matlab 7.6 which is the object oriented version of Matlab. Thus, it is preferred to refer to all components as objects, in order to avoid confusion with modules, structures, or even matrixes used by the previous versions of Matlab. A general and more detailed illustration of the simulation model can be seen in the two figures below, respectively.

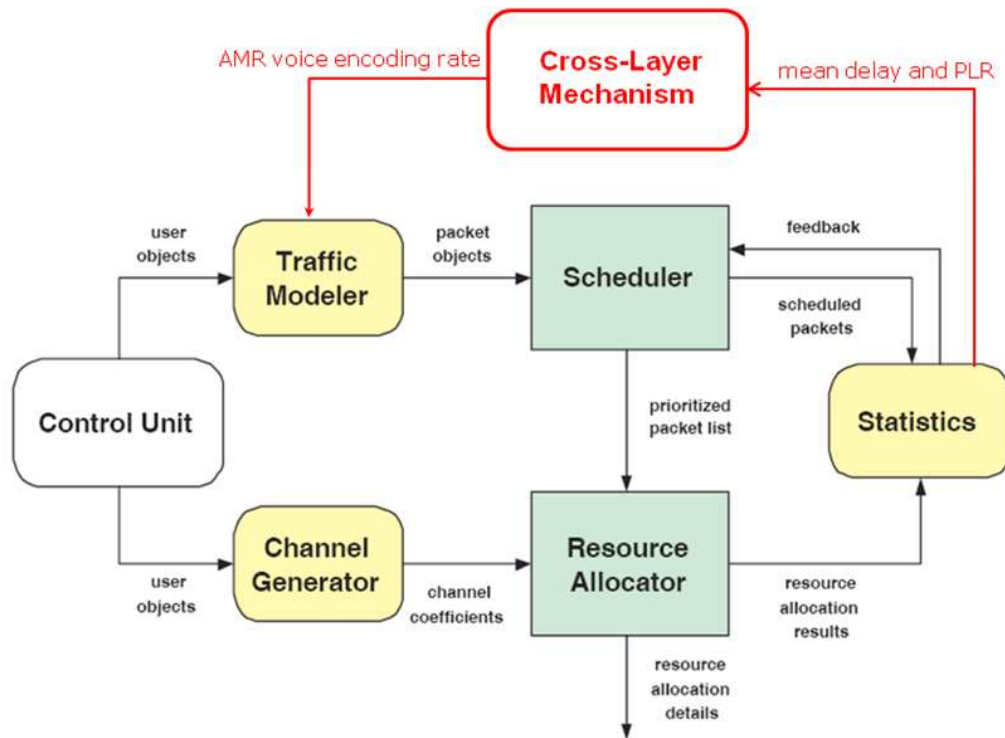


Figure 3.9: General illustration of the simulation model.

As it can be seen, the model consists of a number of components, each one implemented as a Matlab object, interconnected to each other. The “Scenario” object is a central component in the above architecture, as it acts as the coordinator aiming at three major objectives:

- i. to keep all necessary parameters of the whole system,
- ii. to initiate all other components and,
- iii. to run the simulation and coordinating all other components by keeping the clock of the simulation.

As numerous scenarios might be running, different instances of the Scenario object can be created in order to store different parameters used by different scenarios, instead

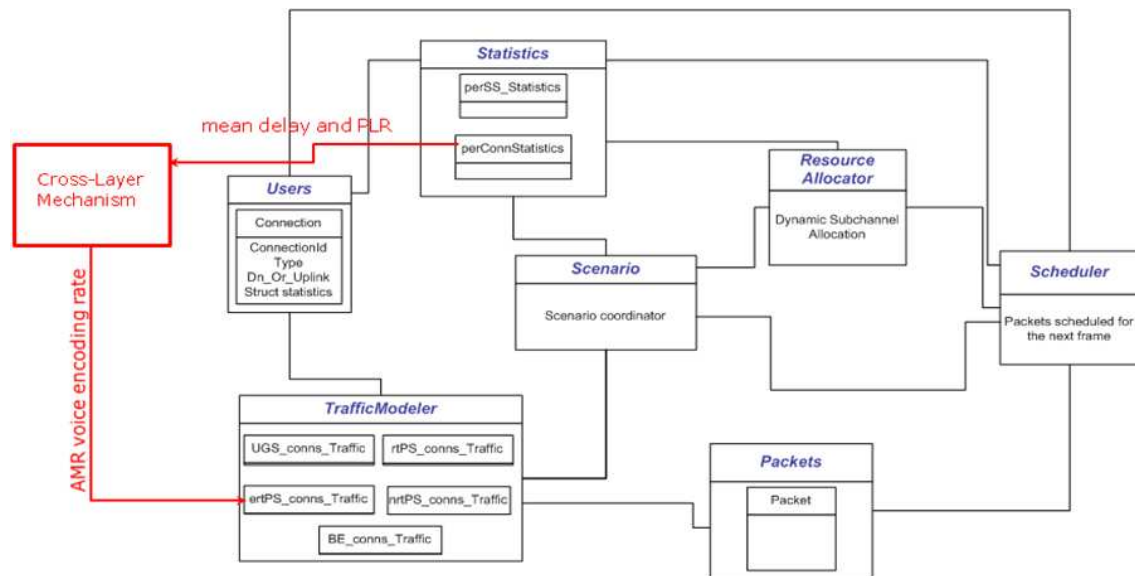


Figure 3.10: Detailed illustration of the simulation model.

of changing the parameters on the same Scenario object. In other words, the “identity” of each simulation is kept at each scenario instance, and all other objects are initiated according to this identity. The clock of the system counts frames, although for diversity reasons the arrival time of packets is counted in usecs and the data rates are counted in kbps. The variety of the metrics is necessary in order to avoid buffer overruns.

It must be clarified that all system operations are executed serially. The numbers of users as well as their traffic characteristics are defined during initialization procedure and constitute the requirements/specifications of each user, whereas any transition can happen only through the “Scenario” object. Although the implementation of all communications through the “Scenario” object is more advisable, it needs multiple redirections to specific functions and leads to unreasonably large number of iterations. Thus, a relative freedom between communications of different objects is adopted. This means that if, i.e., the RA needs a specific information from, i.e., the Users object, then it is preferable to let the RA get that information directly from the Users object, as this does not cause any problems to the procedure.

Cross-layering is implemented as described above to adjust the encoding rate of voice traffic based on the performance metrics of the MAC layer. The “Cross-Layer Mechanism” object gets the mean delay and packet loss rate information from the “Statistics” object, executes the decision algorithm, and, based on its outcome, communicates with the “TrafficModeller” to provide the new AMR (Adaptive Multi Rate) voice encoding rate. Since voice is using the ertPS traffic class of WiMax, only this traffic generator is affected.

Finally, the “Packets” object contains an ordered list of objects of type “Packet”, that hold all the information related to the packets inside the system, at any instance of time. This is the reason of placing “Packets” object in the middle of the above figure, as it is

not a functional model like e.g. the RA object.

3.3 Joint Resource Allocation and Scheduling

3.3.1 Introduction

As it was described in PHYDYAS's deliverables [5] and [9] the OFDMA and/or FBMC transmission schemes efficiently combines discrete multicarrier modulation with frequency division multiple access (FDMA). The advantages of OFDMA/FBMC access scheme include the flexibility in subcarrier allocation, the absence of multiuser interference due to subcarrier orthogonality, and the simplicity of the receiver among others. In multicarrier based schemes, the subcarriers are grouped into larger units referred to as subchannels. Then, these subchannels are grouped across the frequency and time domains into bursts, where each burst is mapped to one user (in unicast) or a group of users (in multicast). The burst allocation and the Modulation and Coding Scheme (MCS) applied to each burst are adapted on a frame basis. This allows the Base Station (BS) to dynamically adjust the bandwidth usage per user according to the users' requirements, i.e. the Quality of Service, and the users' current channel state.

Based on previous works on Cross-Layer packet scheduling and subchannel allocation scheme in 802.16e System in [27, 28, 29, 30], and following the MTBA (Mixed and Band AMC) zone proposed in [5] and [31], we define one burst as a set of continuous Minimum Resource Units (MRU) (logical or physical) in both time and frequency domains by always following a rectangular shape containing data from one Service Flow (SF). Each SF is a unidirectional flow of packets with a particular set of QoS parameters [25]. Hence as it was described in subsection 4.2.1 of deliverable D6.1, the number of MRUs required for each user can be determined a priori according to the average SNR independently of the instantaneous channel. Based on previous research works on MRU possible shape formats [32], a new dynamic radio resource management scheme considering the rectangular burst shape was proposed and described in [5, 9] which takes into account the position within the frame of the burst.

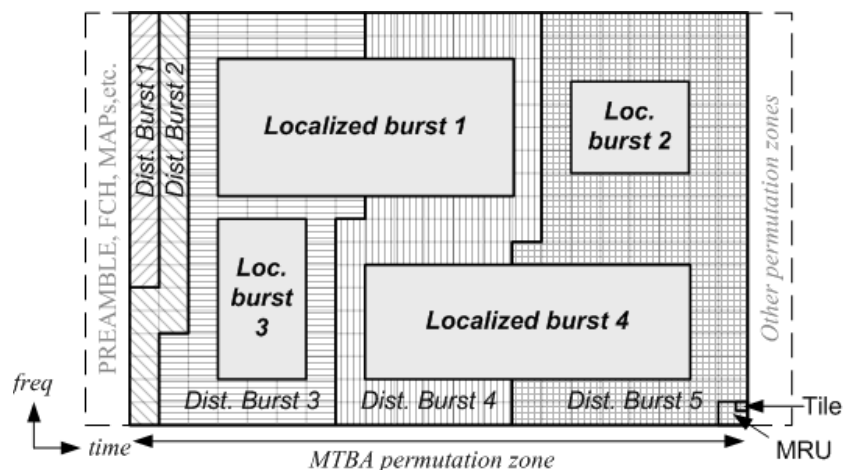


Figure 3.11: Proposed mixed TUSC and Band AMC (MTBA) zone in deliverable D6.1 [5]

Both the resource unit (RU) and the data region always follow a rectangular shape structure (see Figure 3.11). Since the MS receiver needs to know how the downlink frame is organized in order to properly decode the data, the downlink control channel includes the number of bursts transmitted as well as the signalling for each burst. In the IEEE 802.16 standard each burst is signalled by the parameters indicated in Table 3.6. Multicast transmission is addressed by mapping different Connection Identifiers (CID) to each burst, where the BS is responsible for issuing the Service Flow Identifiers (SFID) and mapping it to single CIDs. These bits signalling are transmitted at the beginning of each frame within the DL-MAP region after the synchronization preamble and the Frame Control Header (FCH) [30].

Field	Size [bits]
Number of CIDs	$J = 8$
CIDs (optional)	$J \cdot 16$
MCS	4
hline Symbol offset, t_i	8
Subchannel offset, c_i	6
Number of OFDMA symbols, w_i	7
Number of subchannels, h_i	6
Boosting	3

Table 3.6: Signalling required per transmitted burst in the DL-MAP

3.3.2 Rectangular shaped bursts allocation

The main goal of the resource allocation and scheduling mechanisms is to maximize the system throughput (i.e. the spectral efficiency) while guaranteeing the QoS constraints for each user. Nevertheless, one key issue for any resource allocation scheme is to minimize the signalling that is required to inform the receivers how the frame is structured. Following the IEEE 802.16 transmission format, since each burst requires a specific signalling, it is suitable that all the scheduled packets belonging to the same user are transmitted within the minimum number of bursts hence the signalling is minimized.

Thus the optimum shape and position of each burst (with its respective MCS) is explored while the QoS requirements are fulfilled for each user. To reduce the algorithm complexity, the optimization problem formulation considers uniform power allocation across the subcarriers and that each user is allocated a single burst per frame. According to these premises and considering that there are K active users, the resource allocation and the rate

adaptation problem that guarantees the different QoS requirements while maximizing the spectral efficiency can be mathematically expressed as follows

$$\arg \max_{\xi} \left\{ \sum_{k=1}^K \sum_{n=1}^Q \sum_{l=1}^T \varpi^{(k)} \xi^{(k)}(n, l) - K \cdot I_{CC} \right\}, \quad (3.23)$$

subject to

$$\text{C1)} \quad R^{(k)} = \sum_{n=1}^Q \sum_{l=1}^T \varpi^{(k)} \xi^{(k)}(n, l) \geq b^{(k)}, \quad (3.24)$$

$$\text{C2)} \quad \xi^{(k)}(n, l) \cdot \xi^{(k')}(n, l) = 0, \text{ for } k \neq k' \text{ and } n \in [0, Q-1], l \in [0, T-1], \quad (3.25)$$

with

$$\eta^{(k)}|_{\text{BER} \leq \mu} = \Psi(\text{ESINR}^{(k)}). \quad (3.26)$$

In Eq. (3.23) the term I_{CC} means the number of the required signalling bits transmitted within the control channel for each burst. The minimum required bits per frame $b^{(k)}$ per user is obtained by Eq.(4.28) in [5], ξ_i is a binary $Q \times T$ matrix which indicates which RUs are allocated to each user (i.e. $\xi^{(k)}(n, l) = 1$ means the (n, l) RU has been assigned to the k -th user). In order to force each burst to follows a rectangular shape, the ones in $\xi^{(k)}$ must be placed inside a rectangle. Since each k -th burst must follow a rectangular shape and considering the burst starts at n_k and l_k with h_k and w_k the number of the RUs in frequency and time respectively, the $\xi^{(k)}$ is given by

$$\xi^{(k)}(n, l) = \begin{cases} 1, & \text{if } (n_k \leq n \leq n_k + h_k - 1) \text{ and } (l_k \leq l \leq l_k + w_k - 1), \\ 0, & \text{others,} \end{cases} \quad (3.27)$$

which guarantees that the different bursts do not overlap. Finally, Eq. (3.24) and Eq. (3.26) are used to determine the actual number of bits transmitted for the k -th user $R^{(k)}$. The term ϖ represents the upper layer throughput (in bits) per RU, and it is obtained as a function of the effective signal to noise ratio (ESINR) per each burst, the available MCS and the upper bound BER.

3.3.3 System description

Same system characteristics as in section 4.3.3.2 in [5] have been used, where one single cell with a total of K MSs within its cell area with no interference sources. The Time Division Duplexing (TDD) scheme is applied, thus channel reciprocity can be assumed between uplink and downlink. The whole TDD frame is formed by a total of N_s symbols with T_{frame} duration. The whole transmission bandwidth BW is formed by a total of N_c subcarriers where only N_{used} users are active. As it is depicted in Figure 3.11, the MRUs allocated to any data stream within a frame have a two dimensional shape constructed by at least one

subchannel and two FBMC symbols. The specific size of the MRU varies according to the permutation scheme [25]. As in [5] we define a MRU as a resource unit formed by a set of $N_{sc} \times N_{st}$ symbols in frequency and time domains respectively. Once the size of the MRUs is defined, we can obtain the total number of MRUs per frame $Q \times T$, where $Q = N_c/N_{sc}$ is the number of subchannels and $T = N_s/N_{st}$ defines the number of the time slots.

Working in the sense of reducing the feedback requirements, Han et al. proposed in [33] to send the channel quality metrics (CQM) of the n -best subchannels, as well as sending the CQMs of n -listed subchannels which are requested by the BS. Moreover, selective feedbacks where only the CQM of those subchannels above a threshold are reported, is also a quite popular technique [34, 35, 36, 37]. In this case, only the index of the subchannel needs to be sent in the feedback channel.

We consider here the case that the transmitted data in each burst belongs to only one SF (i.e. to a single MS), and the MCS applied to each burst might be adapted. Since the MS receiver needs to know how the downlink frame is organized in order to properly decode the data, the downlink control channel includes the number of bursts transmitted as well as the signalling for each burst.

In the [25] each burst is signalled by the parameters indicated in Table 3.6, Multicast transmission is addressed by mapping different Connection Identifiers (CID) to each burst, where the BS is responsible for issuing the Service Flow Identifiers (SFID) and mapping it to single CIDs.

3.3.3.1 Analysing the feedback signalling limits under JRAS-RDP algorithm

Once the resources per SF have been resolved, the Packet Data Unit (PDU) block represented in Figure 3.11 prepares the data that will be mapped into each burst at the PHY layer. Thus, the PDU block and its counterpart at the MS side are responsible of the fragmentation and the reconstruction of the network layer packets. Next, the Burst Mapping block breaks the packet data units in order to map each fragment into one physical burst. Each physical burst may apply a different MCS. The MCS for each burst is obtained according to the effective SNR (SNR_{eff}) of the channel over the MRUs assigned to the burst. For low mobility scenarios we can consider the channel for each subcarrier nearly constant during the whole frame, thus the SNR_{eff} is an arbitrary function of the different post-processing SNR per subcarrier (SNR_i) such that,

$$SNR_{eff} = f(SNR_1, SNR_2, \dots, SNR_n, MCS) \quad (3.28)$$

where SNR_{eff} would be the SNR that in case of an additive white Gaussian noise (AWGN) channel it would achieve the same Bit Error Rate (BER). Several metrics as the; Exponentially Effective SNR (EESM), the Mean Instantaneous Capacity (MIC), or others based on the Mutual Information per Bit can be applied to obtain the SNR_{eff} (developed in [5] thanks to described methodology in [38] and [39]). In the presented work the harmonic mean of the channel values has been used (for more detailed information see [39]), which gives a tight lower bound of the BER and it is independent of the MCS.

From [9], it may be seen that the effective channel power attenuation in case of FBMC is given by,

$$|H_{\text{eff},n,m}|_{\text{FBMC}}^2 = \frac{|H_{n,m}|^2}{\left(1 + \frac{|H_{n,m}|^2 \sum_{(p,q) \in \Omega_{\Delta n, \Delta m}^*} w_{n+p, m+q}^2 P_{n+p, m+q}}{\sigma^2}\right)} \Rightarrow \quad (3.29)$$

$$\Rightarrow \text{SNR}_{\text{eff},n,m} = \frac{P_{n,m}}{\sigma^2} |H_{\text{eff},n,m}|_{\text{FBMC}}^2 \quad (3.30)$$

Where $P_{n+p, m+q}$ is the total power transmitted by each symbol belonging to the $\Omega_{\Delta n, \Delta m}^*$ values which surround the transmitted symbol. Note that Δn and Δm are chosen according to the coherence time (T_c) and the bandwidth (B_c). The sub-index n represent the carrier position, and m is the symbol time sub-index, the values of $w_{p,q}$ are the constant filter bank coefficients.

It has been stated that the use of localized bursts instead of distributed bursts improves the spectral efficiency of the system since selective fading can be often avoided. Consequently, localized bursts must be placed first and in case no more localized bursts can be allocated, the remainder resources are assigned to distributed bursts.

In order to obtain the SINR thresholds where each MCS gives a BER lower than a certain value, a link level simulation has been carried out where the BER has been computed through several RUs. Two types of channel models have been considered. For the distributed bursts, only the average SNR is used (as in similar open-loop adaptation mechanisms) [31]. We assume that the channel experienced by any RU (hence also by the distributed burst) is an uncorrelated Rayleigh channel. This imply that the channel transfer function $H(n, m)$ can be modelled as a random variable following a zero mean complex Gaussian distribution with unitary standard deviation. As described in table 4.6 in deliverable D6.1 (see [5]), we can observed that those MCS where high puncturing rates are applied fail to obtain a low BER for a Rayleigh channel, which indicates that the diversity order is severely affected by the puncturing.

Average SINR for BER= 10^{-4} and 10^{-6} with Z-QAM and Convolutional Coding (using a soft-decoder) in a Rayleigh channel.

In order to allocate the localized bursts, the downlink frame is first segmented into RUs of adjacent subcarriers and symbols, having $Q \times T$ available RU in frequency and time domain respectively. Next, the BS calculates the priorities associated to each user on those known subchannels as following the JRAS prioritization scheme. For the subchannels where the channel is not known an available rate $\varpi_n^{(k)} = 0$ is fixed (i.e. $\varphi_n^{(k)} = 0$). Then the RUs are iteratively allocated according to users' priority $\varphi_n^{(k)}_{-1}$ until every service flow is allocated at least $R^{(k)}$ bits or any other localized burst can be created/increased (whatever happens first). Iteratively, the user whose requirements have not been met yet claim for an unallocated RU such that its priority is the highest. A schematic of the proposed JRAS-RDP is depicted in and described in "Algorithm 1". Furthermore, the RUs are allocated to burst following rectangular shapes established within the IEEE 802.16 standard.

JRAS-RDP with limited feedback algorithm:

Start of the algorithm:

- 1:** Initialize the resource allocation matrices ξ, θ thus all the resource are unallocated and fix the number of allocated burst $B = 0$.
 - 2:** compute the users bit rate requirements $b^{(k)}$ (see Eq. (?))
 - 3:** Divide the OFDMA frame into RU in which contiguous subcarrier permutation is applied.
 - 4:** **while** there are unallocated RU where the channel is known **then**
 - 5:** apply the JRAS-RDP algorithm
 - 6:** **end while**
 - 7:** divide the remaining unallocated resource into RU in which distributed subcarrier permutation is applied
 - 8:** Update the number of transmitted bits per user per frame as well as the bit rate requirements $b^{(k)}$ according to the allocated localized bursts.
 - 9:** **if** $b^{(k)} > 0$ for any k **then**
 - 10:** update the priorities over each n -th RU in order to guarantee the QoS requirements:
 $\varphi_n^{(k)} = \varphi_n^{(k)} - 1$
 - 11:** **else**
 - 12:** update the priorities over each n -th RU thus the spectral efficiency is maximized:
 $\varphi_n^{(k)} = \varphi_n^{(k)} - 2$
 - 13:** **end if**
 - 14:** **if** there are unallocated RUs where the channel is unknown **then**
 - 15:** allocate a distributed RU to the user with higher priority $\varphi_n^{(k)}$
 - 16:** Update the number of transmitted bits per user per frame as well as the bit rate requirements $b^{(k)}$ according to the currently allocated RU.
 - 17:** go to line 9
 - 18:** **else**
 - 19:** go to line 21
 - 20:** **end if**
 - 21:** **End of the algorithm.**
-

Algorithm 1: JRAS-RDP with low rate feedback algorithm description

Then, when all $\varphi_n^{(k)}_{1)}$ (or $\varphi_n^{(k)}_{2)}$) in case the minimum resources have been satisfied) become zero, it means that the localized bursts cannot be increased any more since the BS doesn't know the channel in the remaining RUs. Those remaining resources are then divided into tiles, physically indexed and mapped over N_{dMRU} RUs. Moreover, the N_{dMRU} MRUs are logically indexed such that the tiles of two consecutive RUs are placed at distant positions within the downlink frame. Then, the unallocated RUs are iteratively assigned (irrespective of its index) to the different distributed bursts until all the RUs have been assigned or all the data in the buffers have been allocated. The priorities assigned to each user are updated every iteration considering the ESINR is equal to the average SNR and the channel is Rayleigh (hence the priorities don't depend on the RU position). The maximum number of distributed bursts (according to the signalling scheme proposed in [40, 32]) is equal to the number of users, K , in case all the buffers are non-empty. Hence, at the end of this second allocation process, each user might be allocated one distributed burst with up to N_{dMRU} consecutive (logically indexed) MRUs.

3.3.4 Simulation Results

In order to evaluate the performance of the JRAS-RDP with limited feedback algorithm the system parameters described in Table 4.5 in [5] have been used. The shape of the RUs for the localized bursts is $N_{\text{sc}} = 18$ and $N_{\text{sd}} = 3$, whereas the distributed burst are formed by 6 tiles (i.e. $N_t=6$) with 3 sub-carriers and 3 symbols each tile (i.e. $N_{\text{st}} = 9$). The loss due to pilot subcarriers in both types of RUs is a function of the pilot density $\mu_p = 8/9$. We assume that the MTBA zone spans over the whole useful downlink subframe hence $N_s = 60$ FBMC symbols. The performance of the proposal is assessed only for Best Effort traffic varying the number of active users K and the knowledge of the CSI at the BS. The main evaluated performances are the spectral efficiency in order to observe the effects of signalling reduction, and the packet delay to determine if the system is able to guarantee the different QoS requirements.

In order to take into account the loss due to the signalling (channel feedback and DL-MAP transmission), we define the system spectral efficiency ν as

$$\nu[\text{bits/s/Hz}] = \left(\frac{\sum_{d=1}^D B_d}{\sum_{d=1}^D \left(\frac{B_d}{r_d} + \frac{B_{\text{sign}}}{r_{\text{sign}}} \right) + \frac{B_{\text{CSI}} + B_{\text{SNR}}}{r_{\text{sign}}}} \right) \mu_p \quad (3.31)$$

where B_d is the data bits transmitted in the d -th burst, r_d is the spectral efficiency of the MCS applied to the proper burst, and D means the total number of bursts transmitted during the whole simulation. B_{sign} indicates the signalling bits (transmitted within the DL-MAP) required by each allocated burst, whereas B_{CSI} and B_{SNR} are the bits transmitted by the MS in the uplink for reporting its CSI and the average SNR respectively. It is considered here that the signalling bits are transmitted with a BPSK and a coding rate $1/2$, thus the term r_{sign} which means that the spectral efficiency of the MCS used to transmit the signalling is equal to $r_{\text{sign}} = 0.5$. The amount of signalling bits required for

each burst is 60 and 43 for each localized and distributed burst respectively. Since the signalling bits are transmitted following a PUSC scheme, we can also apply the Rayleigh SNR thresholds being sure that these bits are properly decoded ($\text{BER} < 10^{-6}$) for any user within a range of 1.69 km. To obtain the term B_{CSI} we have considered that the MSs feedback the SNR value of their n -best subchannels with 6 bits, thus the SNR range of 0-32dB is sampled with steps of 0.5dB. Likewise, the average SNR is fed back from all the MSs each 15ms with a codeword of 6 bits length.

In the first scenario, K different active users ($K = \{100, 125, 150\}$) are evaluated where each user's service flow is simulated under the web browsing test service. For this service class, the packet delay is unrestricted and the maximum BER for this service class is equal to 10^{-6} . The traffic is modelled such that a web browsing session is simulated (see details on this test service in [25]). In our simulation, the mean reading time between two consecutive packet calls has been reduced to 20s to increase the link activity. As in [5], the used simulation time is $T_{\text{sim}} = 125\text{s}$ in order to include different packets calls.

The system spectral efficiency (as described in (3.31)) for different combinations of n (number of fed back subchannels) and k (number of MSs) has been calculated and analysed. The effect of notifying in the downlink which MS have data pending to be transmitted is evaluated. The case where all the MS continuously feedback their CSI information are compared with the case where the BS requests the MS to feed back their CSIs only in case there are data for them in the BS queues (dashed lines). For the continuous feedback case, the spectral efficiency is highly reduced as n is increased leading to a (nearly) zero spectral efficiency for the Full-CSI knowledge case. It is then concluded that when the MS have to report their channel independently from the input buffers, the gain due to multiuser diversity is neutralized by the loss caused by the uplink signalling. On the other hand, for the BS requested feedback case, we observed a slight increase of the spectral efficiency as n is increased. Larger gains and spectral efficiencies is expected for real-time and non-real time traffic where the number of simultaneously active users is higher.

The 99-th percentile of the packets delay behaviour was also analysed. From preliminary obtained performances we can wrap-up that by combining distributed and localized bursts, the delay can be reduced more than one order of magnitude. If we compare the delay in the case where there is no CSI at the transmitter (i.e. $n = 0$) to the $n = 1$ case, the difference in delay between both schemes is very noticeable (more than one order of magnitude for $K > 50$). This is due to the fact that since the localized bursts have been prioritized over the distributed bursts, it is more than probable that every user is allocated one low rate data channel which guarantees the minimum throughput. Moreover, it is observed that if n is increased, this minimum throughput is increased reducing the packet delay. However, very slight improvements are achieved for $n > 4$.

The amount of resources required for downlink and uplink signalling (DL-MAP length and n -best subchannels feedback load) is also analyzed. Simulation results show the sum of downlink and uplink signalling in terms of number of required OFDM symbols per frame. To obtain the number of symbols occupied by the signalling we have considered that all the signalling (downlink and uplink) is transmitted with a BPSK modulation and a coding rate equal to $1/2$. Therefore, the number of signalling bits that can be fitted within two/one

FBMC/OFDM symbol (with 1728 active subcarriers) is 768 bits (i.e. $1728 \times 1/2 \times \mu_p = 768$). Then, having the maximum signalling load obtained through the whole simulation (i.e. the worst case), it is observed that as it was expected as K or n are increased the amount of signalling is increased. If we assume that at most ten FBMC symbols (which is equivalent to five OFDM symbols) can be dedicated to signalling within one frame, we can conclude that the best combination pairs of $\{K, n\}$ are $\{50, 8\}$, $\{100, 4\}$, and $\{150, 2\}$. As a result, by modifying n a tradeoff between the required signalling and the system spectral efficiency (and the fixed delay) can be achieved.

Then, two main conclusions are drawn. First, we have observed that the delay can be highly improved in case localized and distributed bursts are combined. In fact, the use of localized bursts guarantees that unless the system is very saturated every user will have at least one sub-channel assigned. This brings up the idea of adapting the number of feedback subchannels according to user requirements or certain fixed priorities. And second, we have shown that by using MTBA zones, a tradeoff between spectral efficiency, delay and load signalling requirements could be obtained by optimizing the number of sub-channels signalled in the uplink. Preliminary results showing the worst case and assuming n fixed during the whole simulation time, we expect that the system performance could be further improved by adapting n as a function of the number of users that actually have data to transmit.

Finally, it is worth mentioning that the MTBA can be also used to multiplex users with different mobility levels, i.e. the low mobility users can be assigned to the localized bursts, whereas the high mobility users can be assigned to the distributed bursts. By doing it so, the low mobility users could achieve high spectral efficiencies whereas the high mobility users would increase the transmit diversity. The advantage then of the MTBA zone comes from the fact that the whole frame could be used efficiently.

3.3.5 Conclusions from initial results

A new resource allocation and data scheduling algorithm is proposed for multicarrier communication such as OFDMA and FBMC. The scheme might be applied for Band AMC subcarrier permutation of PUSC subcarrier permutation indistinctly. Moreover, the proposed TSPS scheme has shown to handle sensitive delay applications (i.e. rtPS and nrtPS), while obtaining high spectral efficiencies by exploiting the multiuser diversity on those unallocated resources. On the other hand, the proposed algorithm, which is based on iterative burst increments, aims to decrease the number of required bursts per frame, which leads to an important reduction of the overload signalling as well as a reduction on the receiver complexity and power consumption. Finally, another observed advantage of this cross-layer structure for resource allocation is its low computational complexity compared to the case where each MRU is independently evaluated.

3.4 Conclusions

It has been demonstrated that from a resource allocation and QoS provisioning point of view, the FBMC system is more robust than the CP-OFDM system. This has been shown for the downlink and will be extended to the uplink.

Assignment of subchannels per user within one subframe should be kept constant in the FBMC system. This is due to pre- and posttails from the prototype filter length and also facilitates the associated signalling.

Intercell Interference should be made aware to the RA to avoid blindness, which may cause packet losses.

Chapter 4

Conclusions

Detailed conclusions are given at the end of the various sections, for the different topics covered in the report.

The main results are:

- FBMC is less sensitive to synchronization errors both in up- and downlink. A multi-tap equalizer not only corrects multipath induced distortion but also synchronization errors. Less multiple access interference is produced.
- Resource allocation is also more robust with respect to carrier frequency offset in FBMC systems.
- Therefore, synchronization requirements (both carrier and timing) are less stringent and less demanding with respect to hardware implementation inaccuracies.

Bibliography

- [1] M. T. Ivrlac and J. A. Nossek. On the problem of bandwidth partitioning in fdd block-fading single-user miso/simo systems. *EURASIP Journal on Advances in Signal Processing*, 2008, 2008.
- [2] D. S. Waldhauser, L. G. Baltar, and J. A. Nossek. MMSE subcarrier equalization for filter bank based multicarrier systems. In *Proc. IEEE 9th Workshop on Signal Processing Advances in Wireless Communications SPAWC 2008*, pages 525–529, 6–9 July 2008.
- [3] M. Bellanger. SC-equalization. Technical report, PHYDYAS Internal Report, May 2008.
- [4] M. Bellanger. Analytical expressions for the reference prototype filter. Technical report, PHYDYAS Internal Report, February 2009.
- [5] European project ICT-211887 PHYDYAS. Deliverable D6.1: Duplexing and multiple access techniques, software description. Technical report, <http://www.ict-phydyas.org>, January 2009.
- [6] European project ICT-211887 PHYDYAS. Deliverable D2.1: Data-aided synchronization and initialization (single antenna). Technical report, <http://www.ict-phydyas.org>, July 2008.
- [7] European project ICT-211887 PHYDYAS. Deliverable D2.2: Synchronization and initialization with single antenna. blind techniques. Technical report, <http://www.ict-phydyas.org>, January 2009.
- [8] European project ICT-211887 PHYDYAS. Deliverable D6.2: Duplexing and multiple access techniques, software description. Technical report, <http://www.ict-phydyas.org>, December 2009.
- [9] European project ICT-211887 PHYDYAS. Deliverable D3.2: Optimization of transmitter and receiver. Technical report, <http://www.ict-phydyas.org>, January 2009.
- [10] R. G. Gallager. *Information Theory and Reliable Communication*. John Wiley and Son, 1968.

- [11] B. Zerlin, M. Ivrlac, W. Utschick, J. Nossek, I. Viering, and A. Klein. Joint optimization of radio parameters in HSDPA. In *Proc. VTC 2005-Spring Vehicular Technology Conference 2005 IEEE 61st*, volume 1, pages 295–299, 30 May–1 June 2005.
- [12] J. Lee, H.-L. Lou, D. Toumpakaris, and J. M. Cioffi. Effect of carrier frequency offset on OFDM systems for multipath fading channels. In *Proc. IEEE Global Telecommunications Conference GLOBECOM '04*, volume 6, pages 3721–3725, 29 Nov.–3 Dec. 2004.
- [13] V. T. Raisinghani and S. Iyer. Cross-layer feedback architecture for mobile device protocol stacks. 44(1):85–92, Jan. 2006.
- [14] X. Wang and K. Kar. Cross-layer rate optimization for proportional fairness in multi-hop wireless networks with random access. 24(8):1548–1559, Aug. 2006.
- [15] W. Ge, J. Zhang, and S. Shen. A cross-layer design approach to multicast in wireless networks. 6(3):1063–1071, March 2007.
- [16] M. van der Schaar and D. S. Turaga. Cross-layer packetization and retransmission strategies for delay-sensitive wireless multimedia transmission. 9(1):185–197, Jan. 2007.
- [17] J. Villalon, P. Cuenca, L. Orozco-Barbosa, Yongho Seok, and T. Turetli. Cross-layer architecture for adaptive video multicast streaming over multirate wireless LANs. 25(4):699–711, May 2007.
- [18] L. Haratcherev, J. Taal, K. Langendoen, R. Lagendijk, and H. Sips. Optimized video streaming over 802.11 by cross-layer signaling. 44(1):115–121, Jan. 2006.
- [19] D. Triantafyllopoulou, N. Passas, A. Salkintzis, and A. Kaloxylos. A heuristic cross-layer mechanism for real-time traffic over IEEE 802.16 networks. *Wiley's International Journal of Network Management*, 17(5):347–361, 2007. special issue on “Management Solutions for QoS Support over the Entire Audio-Visual Service Distribution Chain”.
- [20] S. Khan, Y. Peng, E. Steinbach, M. Sgroi, and W. Kellerer. Application-driven cross-layer optimization for video streaming over wireless networks. 44(1):122–130, Jan. 2006.
- [21] H. Jiang and W. Zhuang. Cross-layer resource allocation for integrated voice/data traffic in wireless cellular networks. 5(2):457–468, Feb. 2006.
- [22] F. Yu, V. Krishnamurthy, and V. C. M. Leung. Cross-layer optimal connection admission control for variable bit rate multimedia traffic in packet wireless CDMA networks. 54(2):542–555, Feb. 2006.
- [23] Y. J. Zhang and K. B. Letaief. Cross-layer adaptive resource management for wireless packet networks with OFDM signaling. 5(11):3244–3254, November 2006.

- [24] C. Long, X. Guan, and B. Li. Cross-layer congestion control, scheduling and power control design in multihop networks with random access. In *Proc. IEEE International Conference on Multimedia and Expo*, pages 1125–1128, 9–12 July 2006.
- [25] IEEE standard for local and metropolitan area networks part 16: Air interface for fixed and mobile broadband wireless access systems amendment 2: Physical and medium access control layers for combined fixed and mobile operation in licensed bands and corrigendum 1, 2006.
- [26] Extended RTP profile for real-time transport control protocol (RTCP)-based feedback (RTP/AVPF), July 2006.
- [27] Q. Liu, X. Wang, and G. B. Giannakis. A cross-layer scheduling algorithm with QoS support in wireless networks. 55(3):839–847, May 2006.
- [28] L. Wan, W. Ma, and Z. Guo. A cross-layer packet scheduling and subchannel allocation scheme in 802.16e OFDMA system. In *Proc. IEEE Wireless Communications and Networking Conference WCNC 2007*, pages 1865–1870, 11–15 March 2007.
- [29] S. S. Jeong, D. G. Jeong, and W. S. Jeon. Cross-layer design of packet scheduling and resource allocation in OFDMA wireless multimedia networks. In *Proc. VTC 2006-Spring Vehicular Technology Conference IEEE 63rd*, volume 1, pages 309–313, 2006.
- [30] H. J. Kushner and P. A. Whiting. Convergence of proportional-fair sharing algorithms under general conditions. 3(4):1250–1259, July 2004.
- [31] X. Wang, G. B. Giannakis, and Y. Yu. Channel-adaptive optimal OFDMA scheduling. In *Proc. 41st Annual Conference on Information Sciences and Systems CISS '07*, pages 536–541, 14–16 March 2007.
- [32] Y. Sun. Asymptotic capacity of multi-carrier transmission with frequency-selective fading and limited feedback. submitted to IEEE Trans. on Information Theory.
- [33] Z.-H. Han and Y.-H. Lee. Opportunistic scheduling with partial channel information in OFDMA/FDD systems. In *Proc. VTC2004-Fall Vehicular Technology Conference 2004 IEEE 60th*, volume 1, pages 511–514, 26–29 Sept. 2004.
- [34] Y. J. Choi and S. Bahk. Selective channel feedback mechanisms for wireless multi-channel scheduling. In *Proc. International Symposium on a World of Wireless, Mobile and Multimedia Networks WoWMoM 2006*, page 10pp., 26–29 June 2006.
- [35] J. H. Kwon, D. Rhee, I. M. Byun, K. S. Kim, and K. C. Whang. Efficient adaptive transmission technique for multiuser OFDMA systems with reduced feedback rate. In *Proc. Wireless Telecommunications Symposium WTS '06*, pages 1–5, April 2006.

- [36] T. Ohseki, M. Morita, and T. Inoue. Burst construction and packet mapping scheme for OFDMA downlinks in IEEE 802.16 systems. In *Proc. IEEE Global Telecommunications Conference GLOBECOM '07*, pages 4307–4311, 26–30 Nov. 2007.
- [37] J. Chen, R. A. Berry, and M. L. Honig. Performance of limited feedback schemes for downlink OFDMA with finite coherence time. In *Proc. IEEE International Symposium on Information Theory ISIT 2007*, pages 2751–2755, 24–29 June 2007.
- [38] A. Mourad. *On the system Level Performance of MC-CDMA Systems in the Downlink*. PhD thesis, Ecole National Supérieur Des Telecommunications de Bretagne, June 2006.
- [39] R. Srinivasan and et al. IEEE 802.16m evaluation methodology document (EMD), C802.16m-08/004r5, January 2009.
- [40] K.-H. Lee, D.-H. Cho, T. Kwon, H. Lee, S. Choi, and J. Kim. Overlapped two-dimensional resource allocation scheme in OFDMA DL-MAP. *IEEE C802.16e-04/352r2*, August 2004.